

**DEVELOPMENT OF AN ULTRA-BRIGHT LASER AND AN
APPLICATION TO MULTI-PHOTON IONIZATION**

by

Donna Theo Strickland

Submitted in Partial Fulfillment
of the
Requirements for the Degree

DOCTOR OF PHILOSOPHY

Supervised by Gerard A. Mourou

Institute of Optics

and College of Engineering and Applied Science of

University of Rochester

Rochester, New York

1988

CURRICULUM VITAE

Donna Theo Strickland was born on May 27, 1959 in Guelph Ontario, Canada. She attended McMaster University from 1977 until 1981 and received the B.Eng. degree, with Honours in Engineering Physics. In the fall of 1981 she entered the Ph.D. program in Optics at the University of Rochester.

During her first year of study, Ms. Strickland was a Fellow of the Institute of Optics. Since that time she has been a Fellow of the Laboratory for Laser Energetics. Ms. Strickland was the recipient of a scholarship from the Natural Sciences and Engineering Research Council of Canada from 1981 to 1985.

Ms. Strickland's research in Optics was performed under the guidance of Professor Gerard A. Mourou.

ACKNOWLEDGEMENTS

It is a pleasure to acknowledge the invaluable advice of my supervisor Dr. Gerard Mourou. The development of the CPA laser is due in a great part to his inspiration. I am indebted to Dr. See Leang Chin, who suggested studying multi-photon ionization and supervised the MPI experiments. I would also like to thank Dr. David Meyerhofer and Dr. Joseph Eberly for many helpful discussions and assistance in the writing of this thesis.

I consider it a privilege to have been a member of one of the leading ultra-fast groups. My studies here were enriched by the expertise (not to mention the off-beat sense of humour) of all the members of the group. In particular, I would like to thank Patrick Maine who worked with me in developing the existing TTT laser. I am also grateful to Steve Augst for his assistance with the multi-photon experiments and Bill Donaldson and Chris Moore for doing all my computer work. Special thanks to Doug Dykaar who did such a nice job on the figures in my thesis and kept me calm and kept me going through the final weeks.

The assistance I received from the staff and faculty of the Laboratory for Laser Energetics was greatly appreciated. In particular, I am grateful to the optics group and DEL for lending me equipment for very extended periods of time.

I would like to acknowledge Dr. Abraham Szöke of LLNL and Qi-chang Su, who supplied me with theoretical curves for the multi-photon experiments.

I am especially grateful to my family. My sister and parents have continually supported and encouraged me through all my years of education and my brother always pushed me (although not in his direction) with his competitive spirit.

ABSTRACT

Conventional amplifiers have not been able to amplify short pulses to high energies either because the stored energy of the gain medium was too low or the high peak powers in the amplifier would cause nonlinear effects and eventually damage to occur. Chirped radar was developed over forty years ago to solve a similar problem in the radar field. The optical analog to chirped radar, Chirped Pulse Amplification (CPA) has been studied here and a prototype laser system has been developed.

The CPA technique uses fibre and grating pulse compression techniques. Short pulses are stretched several times their initial duration by group velocity dispersion, either in an optical fibre or a pair of gratings. The long pulses are then amplified in a high energy gain medium, without reaching the peak power limitation. The high energy pulse can be recompressed to its original pulse duration by a second dispersive delay line, with the opposite dispersion.

The prototype system focuses 50 ps pulses from a cw mode-locked Nd:YLF oscillator into an optical fibre. The bandwidth is stretched to ~ 4 nm and the pulse width is stretched to 150 ps. The duration is further stretched by a grating pair to 500 ps. The long pulses are amplified in three stages to an energy of 0.5 J. The amplified pulses are compressed to a 1 ps duration by a second pair of gratings. The entire system sits on two 4x8 foot optical benches. With the CPA technique Terawatt powers can be achieved with a very compact and simple system. The technique can also be scaled to very high energies to give power levels in the petawatt (10^{15} W) level. These power levels should open new fields of research in such areas as multi-photon and plasma physics.

The prototype system was used to study multi-photon multiple ionization at intensities in the 10^{16} to 10^{17} W/cm² range. The experiments produced the highest charge state, Xe¹²⁺, observed to date. The experiments showed that the higher charge states are produced at lower intensities for longer wavelengths. It was also shown that the ionization process is independent of pulse duration if the bandwidth is constant.

TABLE OF CONTENTS

CURRICULUM VITAE	ii
ACKNOWLEDGEMENTS	iii
ABSTRACT	iv
TABLE OF CONTENTS	vi
LIST OF TABLES	ix
LIST OF FIGURES	x
CHAPTER	
I. INTRODUCTION	1
A. Review of Intense Laser Sources	3
1. Nd:glass Systems	3
2. CO ₂ Lasers	4
3. Dye Lasers	5
4. Excimer Amplifiers	6
B. Review of Multi-photon Multiple Ionization Experiments	8
1. Historical Overview	8
2. Saclay MPI Experiments	12
3. Recent Non-resonant MPI Results	14
C. Outline	17
References	19
II. STUDY OF THE CPA TECHNIQUE	23
A. Introduction	23
1. Pulse Compression	24

1. IR Wavelength Interaction	97
2. Green Wavelength Interaction	103
3. Long Pulse Interactions	109
References	112
IV. DISCUSSION OF MPI RESULTS	113
A. Ion Yield Curves	113
B. Z Dependence	119
C. Wavelength Dependence	122
D. Comparison with Saclay Results	124
E. Comparison with Modified Keldysh Theory	126
References	137
V. CONCLUSIONS	139
A. Summary	139
B. New Laser Developments	140
1. Towards Shorter Pulse Durations	140
2. Towards Petawatt Power Levels	141
C. Future Multi-photon Experiments	143
References	145
Appendix	146

LIST OF TABLES

3 - 1	Identification of peaks of TOF spectrum of Fig. 3 - 9	96
4 - 1	Comparison of the CPA and Saclay saturation intensities of the first charge states.	125

LIST OF FIGURES

1 - 1	Graph of energy extracted as a function of pulse duration for GDL laser. The horizontal line is the stored energy of the system.	4
1 - 2	Schematic depicting direct and sequential ionization processes for Sr	11
1 - 3	Plot of ionization yield as a function of peak intensity for xenon for 0.532 μm radiation (from Ref. 25)	13
1 - 4	Plot of appearance intensity for Xe, Kr, and Ar as a function of ionization potential for the picosecond dye laser MPI experiments (from Ref. 32)	15
2 - 1	CS ₂ compression system configuration	29
2 - 2	Measurement of broadened spectral bandwidth	31
2 - 3	Streak camera measurement (a) focus spot, (b) compressed pulse	33
2 - 4	Two-photon fluorescence measurement	34
2 - 5	Two-photon fluorescence measurement of central portion of beam	35
2 - 6	Experimental configuration of mJ CPA system	40
2 - 7	Frequency spectra where (a) just SPM is present and (b) Raman generation takes place	42
2 - 8	Autocorrelation measurement of stretched pulse	43
2 - 9	Autocorrelation measurement of compressed pulse	45
2 - 10	Streak camera trace of amplified and compressed pulse	50
2 - 11	Laser pulse energy as a function of lamp energy	51
2 - 12	Pulse energy histogram of 2000 shots (a) before, (b) after grating	

	compressor	53
2 - 13	Frequency spectrum (a) before and (b) after amplification	54
2 - 14	(a) Block diagram of 40mJ CPA system, (b) amplifier configuration	55
2 - 15	Streak camera traces of frequency doubled pulses at the (a) input and (b) output of the fibre	57
2 - 16	SPM and Raman pulse at output of fibre	58
2 - 17	Streak camera traces of IR pulses at the (a) input and (b) output of the 2.4 km fibre	59
2 - 18	Streak camera trace of compressed 40mJ pulse	62
2 - 19	Regenerative amplifier and four pass system configuration	63
2 - 20	Streak camera trace of compressed 1.3J, 2 ps pulse	65
2 - 21	(a) Block diagram of 0.6 J CPA system, (b) amplifier configuration	67
2 - 22	Autocorrelation of 0.5 J compressed pulse - Correlation width = 1.4 ps	69
2 - 23	Four pass grating expansion configuration	72
3 - 1	Schematic of experimental system	79
3 - 2	Interaction chamber configuration	80
3 - 3	Plot of green energy as a function of IR energy	83
3 - 4	Autocorrelation of pulse profile. The solid line is a best fit Lorentzian profile	85
3 - 5	Third order correlation of temporal profile	86
3 - 6	Streak camera trace of two pulses at the output of the compressor	87
3 - 7	Densitometer trace of (a) uncompressed and (b) compressed pulses. Lines show contours of constant intensity	89

3 - 8	TOF spectra of Helium at (a) low pressure and (b) high pressure	92
3 - 8	TOF spectra of (c) Neon and (d) Argon	93
3 - 8	TOF spectra of (e) Krypton and (f) Xenon	94
3 - 9	TOF spectrum of xenon showing the maximum charge state, Xe^{12+}	95
3 - 10a	Ion yield as a function of IR intensity for xenon. Low and high pressure data overlaid	98
3 - 10b	Ion yield as a function of IR intensity for krypton	99
3 - 10c	Ion yield as a function of IR intensity for argon	100
3 - 10d	Ion yield as a function of IR intensity for neon	101
3 - 10e	Ion yield as a function of IR intensity for helium	102
3 - 11a	Ion yield as a function of green intensity for xenon	104
3 - 11b	Ion yield as a function of green intensity for krypton	105
3 - 11c	Ion yield as a function of green intensity for argon	106
3 - 11d	Ion yield as a function of green intensity for neon	107
3 - 11e	Ion yield as a function of green intensity for helium	108
3 - 12	Streak camera trace of uncompressed pulse	109
3 - 13	Ion yield as a function of 200 ps pulse intensity	111
4 - 1	Ion yield curves of Kr with IR radiation. The data points are represented by best fit lines.	116
4 - 2	Plot of ionization rate of of Xe as determined by Keldysh formula	118
4 - 3	Appearance intensity as a function of ionization potential of the charge state	120
4 - 4	Plot of appearance intensities for Ar and Kr as a function of sum of ionization potentials	121

4 - 5	Maximum charge states observed at 6×10^{16} W/cm ² at 1.05 μm as a function of total absorbed energy	122
4 - 6	Plot of appearance intensity for Ar with green and IR radiation	123
4 - 7a	Comparison of theoretical and experimental results for xenon with IR radiation	132
4 - 7b	Comparison of theoretical and experimental results for xenon with green radiation	133
4 - 7c	Comparison of theoretical and experimental results for helium with IR radiation	134
4 - 7d	Comparison of theoretical and experimental results for helium with green radiation	135

CHAPTER I

INTRODUCTION

The ability to produce laser intensities greater than 10^{18} W/cm² would open up new physical regimes in such fields as plasma, relativistic and multi-photon physics. The electric field generated at this intensity is on the order of 10^{11} V/cm, which is ~ 20 times the atomic field strength ($e/a_0^2 = 5 \times 10^9$ V/cm). This field should be sufficient to excite inner shell electrons by multi-photon ionization, leading to a new understanding of atomic physics and possible new X-ray laser schemes.¹ The quiver energy or ponderomotive potential of a charged particle, for these intensities and a 1 μ m wavelength, would be on the order of 1 MeV. Under such a potential, the electron would be accelerated to relativistic speeds.² It is believed that at intensities of $\sim 10^{19}$ W/cm², positron-electron pairs would be created.³

Conventional laser sources either cannot be scaled to reach these intensities because the saturation fluence is too low or the systems become too large with too low a repetition rate to be useful for these experiments. Increasing the power of a laser system can be accomplished in one of two ways. The first is to increase the energy of the system and the second is to decrease the pulse duration. Almost without exception, the two processes are mutually exclusive. Short pulse systems are limited in energy to the millijoule level and the large energy systems must operate with long pulses, typically on the nanosecond time scale.

Conventional short pulse systems use dye amplifiers because of the large

bandwidth and high gains of these media. However, the large gain means that the saturation fluence level of the dye amplifiers is low, approximately 1 mJ/cm^2 , and so the energy of these systems is limited to a few millijoules.⁴ The energy of dye systems has been increased using excimer amplifiers, which also have low saturation levels, but can be made with very large apertures.^{5,6} Presently, these systems are being expanded to amplify the pulses to the Joule level. However, because of the low saturation fluence levels, these systems will have to be very large. Scaling these systems to higher energies seems infeasible.

The alternative is to use a system that has a large energy storage capability, such as Nd:glass which has a saturation fluence of $\sim 5 \text{ J/cm}^2$. Nd:glass systems have been developed which produce 10 kJ pulses, but, at a pulse width of 1 ns giving a peak power of 10^{13} W .⁷ The power in the amplifier must be kept below a level where nonlinear effects would occur and eventually lead to damage. These intense Nd:glass lasers are very large filling entire buildings. The repetition rate is only 1 shot per hour making it impractical for multi-photon experiments.

The ideal laser for these new experiments should be very intense, compact, have a reasonable repetition rate and be scalable to allow even higher intensities. As part of this thesis work a novel laser technique, which at present produces terawatt powers and in the future could be scaled to generate petawatt (10^{15} W) powers is studied.^{8,9} The prototype system, which produces a 1 ps pulse with 0.5 J of energy, was designed and constructed. The entire system fits on a 4×16 foot optical bench. The technique uses optical pulse compression. With the Chirped Pulse Amplification (CPA) scheme a pulse from an oscillator is injected into an optical fibre, where both the bandwidth and pulse duration are stretched due to the combined action of self-phase modulation and group velocity dispersion. The long pulse can then be amplified to the saturation level, without reaching the prohibited peak power level.

The amplified pulse is then compressed to approximately the inverse of the broadened bandwidth by passing the pulse through a negatively dispersive delay line, comprised of a pair of parallel gratings.

To demonstrate its usefulness, the CPA laser was used to investigate multi-photon multiple ionization of noble gases. The ionization process was studied at intensities that were previously not achievable in the infra red region of the spectrum. These experiments generated the highest charge state (Xe^{12+}) that has been observed to date.

I. A Review of Intense Laser Sources

I. A. 1 Nd:glass Systems

The most powerful laser system in the world is a Nd:glass laser system. The NOVA system generates 10 kJ pulses at a pulse duration of 1 ns generating powers in the 10^{13} W/cm² range.⁷ The system is extremely large filling an entire building. The final amplifier in the chain is a disc, 46 cm in diameter. Nd:glass amplifiers have very large saturation fluences of ~ 5 J/cm², but, this energy can only be extracted for long pulses. The intensity in the amplifier must be kept below a level where nonlinear effects occur. These nonlinear effects would lead to self-focusing, filamentation and eventually damage. The maximum intensity that can be handled by a Nd:glass amplifier is on the order of 10 GW/cm². Although Nd:glass amplifiers have a large bandwidth of ~ 20 nm, and can therefore support pulse durations as short as 100 fs, they are very inefficient short pulse amplifiers. This point is illustrated in Fig. 1-1, which shows the maximum energy that can be extracted from the Glass Development Laser at LLE, as a function of pulse duration. The horizontal curve shows the stored

energy of the system, which is ~ 1 kJ. The graph shows that the stored energy is efficiently extracted for pulse durations greater than 1 ns, but, for a pulse duration of 1 ps, the extracted energy is reduced by three orders of magnitude.

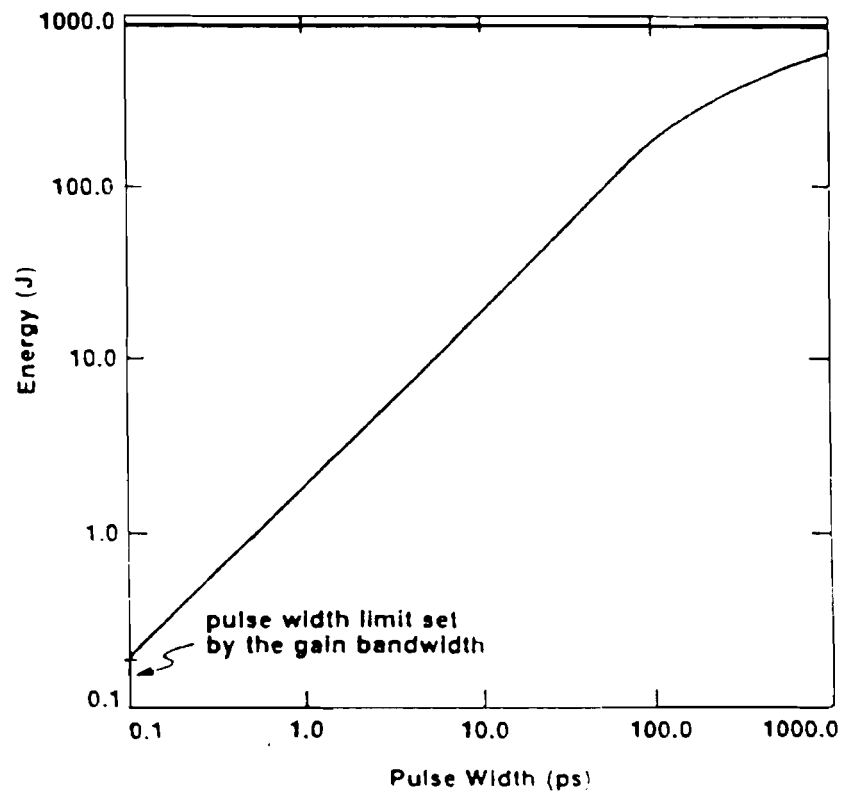


Figure 1 - 1. Graph of energy extracted as a function of pulse duration for GDL laser.

The horizontal line is the stored energy of the system.

I. A. 2 CO₂ Lasers

A second type of large energy laser is the CO₂ laser. CO₂ can generate kJ energy pulses with a duration of 1 ns. Unlike Nd:glass, CO₂ does not have a bandwidth broad enough to support pulse durations shorter than 1 ns. The gain

bandwidth can be pressure broadened, but, the aperture of the high pressure systems is limited by the present technology. At present, the energy of short pulse CO₂ lasers is limited to the ten millijoule level.

Corkum has generated 2 ps pulses which are then amplified to an energy of 15 mJ in a 1 x 1 x 40 cm TE CO₂ laser.¹⁰ The 2 ps pulse was generated by reflecting a single longitudinal-mode output of CO₂ oscillator, from two CdTe slabs. The slabs will normally transmit the 10 μm radiation, but, will become metallic and reflective when driven by an intense radiation field. The slabs can therefore be used as switches and in this case, were driven by a 2 ps amplified dye laser pulse. The resulting short, CO₂ laser pulses are then amplified to the energy of 15 mJ in a CO₂ gain module, operated in a regenerative amplifier configuration.

One advantage of a CO₂ laser for multi-photon experiments is its long wavelength. The ponderomotive potential produced by a laser pulse is proportional to $I\lambda^2$, where I is the laser intensity and λ is the wavelength. Therefore, CO₂ lasers, which lase at 10 μm, generate the same ponderomotive potentials as Nd:glass lasers, with two orders of magnitude less intensity.

I. A. 3 Dye Lasers

The most common short pulse systems are based on dye lasers because of their large spectral bandwidths and large gains. There are several different dye laser configurations to generate and amplify sub-picosecond pulses.⁴ Pulse durations as short as 27 fs have been generated directly by a Colliding-Pulse Mode locking (CPM) dye laser¹¹ and pulse durations as short as 6 fs have been achieved by optically compressing the CPM laser pulses.¹² The saturation fluence is on the order of 1 mJ/cm² and this level can easily be achieved for sub-picosecond pulses, making dye

amplifiers very efficient systems, but, they cannot be scaled to generate higher energies than ~ 1 mJ.

I. A. 4 Excimer Amplifiers

Excimer amplifiers have been used to increase the energy of the short pulses produced by dye laser systems. The saturation fluence is approximately the same for excimer amplifiers as that for dye lasers, but, excimer lasers can operate with much larger apertures. For single picosecond pulse durations, the saturation fluence has been measured to be $1.8\text{-}2$ mJ/cm²¹³ and ~ 1 mJ/cm²¹⁴, for XeCl and KrF amplifiers, respectively. 160 fs pulses have been amplified to 12 mJ in XeCl amplifiers.¹⁵ The short pulse was generated by a CPM laser that was made to operate at a wavelength of 616 nm, which corresponds to double the wavelength of a XeCl laser. The laser pulses were amplified in a series of four dye amplifiers, which were pumped by a frequency doubled, Q-switched Nd:YAG laser. The amplified pulse energy was 0.6 mJ, with negligible Amplified Spontaneous Emission (ASE) and the pulse duration was 200 fs. The frequency of the pulses was doubled in a KDP crystal, to match the XeCl line. The pulse was then amplified in a single pass of two XeCl gain modules to an energy of 12 mJ, with 5 mJ of ASE present.

KrF amplifiers have a larger gain bandwidth of 3.4 nm and can therefore amplify shorter pulses than XeCl, but, achieving short pulse durations at the KrF lasing wavelength of 248 nm is more difficult. The Chicago group has generated 20 mJ pulses with durations of 500 fs, at a wavelength of 248 nm.⁵ 1.5 ps pulses were generated by a dye laser, synchronously pumped by the second harmonic of a CW mode-locked Nd:YAG laser. The dye laser is tuned to 745 nm by a two-plate birefringent filter. The pulses were shortened to 150 fs by a fibre-grating compressor

and then amplified in a series of two dye amplifiers to an energy of 130 μJ . The wavelength of 248 nm was achieved by frequency doubling the 745 nm radiation in a KDP crystal and then sum-frequency mixing the second harmonic with the fundamental in a second KDP crystal. The energy of the 248 nm seed pulse was 300 nJ. This pulse then is amplified in two KrF modules to an energy of ~ 20 mJ with 5% of the energy being ASE. The laser pulses can be focused to intensities in the 10^{16} - 10^{17} W/cm^2 range.

Szatmari and co-workers have amplified 80 fs pulses to 75 mJ in a KrF gain medium.⁶ A dye oscillator and amplifier were used to generate 8 ps pulses at a wavelength of 365 nm and a pulse energy of 5 μJ . These laser pulses pumped a distributed-feedback dye laser (DFDL), which lases at half the frequency of the KrF amplifier. The DFDL pulses are amplified in three stages to an energy of 60 μJ , with saturable absorbers between each stage. The laser frequency was doubled in a 0.2 mm thick ADP crystal. The UV pulse is amplified in a double pass of KrF gain module to an energy of 15 mJ, with less than 5% being ASE. The pulse duration after amplification is 350 fs, which does not correspond to the transform limit of the frequency bandwidth. This indicates that the pulse has been frequency chirped. The amplified pulse is further stretched to a duration of 500 fs, by passing the beam through a quartz plate. The pulse is then compressed by passing it through a pair of 45° quartz prisms, separated by 25 cm. The compressed pulse duration is 81 fs. The uncompressed pulses were further amplified in $4.5 \times 3.5 \times 45$ cm^3 KrF amplifier to an energy of 75 mJ, which sits on a pedestal of 85 mJ of ASE. At the time a proper saturable absorber was not available to reduce the ASE. Also, compression of the 75 mJ pulse was not tried and no discussion of the pulse duration of the amplified pulse was given.

I. B Review of Multi-photon Multiple Ionization Experiments

I. B. 1 Historical Overview

Prior to the advent of the laser, all absorptive interactions between optical radiation and atoms were linear in nature, that is a single photon was absorbed. However, it was predicted as early as 1931, by Goepfert-Mayer,¹⁶ that an atom could simultaneously absorb two photons, if the radiation field was strong enough. The process required extremely high field intensities, that were not possible with existing light sources. It was not until after the invention of the laser in 1960, that the required optical field strengths could be generated and her theory verified experimentally. In 1961 Kaiser and Garret were the first to observe the excitation of an atom to an energy level corresponding to the energy of the sum of the two photons.¹⁷

The continual development of brighter laser sources propelled the investigation of higher order nonlinear processes. The intensities produced in the focus of a Q-switched laser are high enough to observe the ionization breakdown of air. One of the mechanisms for the dielectric breakdown that was considered was Multi-Photon Ionization (MPI). The absorption of more than two photons is required to ionize nitrogen and so the existing two photon theories had to be extended to account for the following N photon process:



where A is the atomic species, $h\nu$ is the photon energy, e^- is the electron and N is the first integer that satisfies the condition that $Nh\nu$ is greater than the ionization potential.

Bebb and Gold¹⁸ extended the theory of Goepfert-Mayer and provided an approximate simplified theory for the absorption of N photons, where N can be any

integer. For the process of multi-photon ionization, lowest order perturbation theory (LOPT) predicts that the N-photon ionization rate, $W^{(N)}$, follows the relation:

$$W^{(N)} = \sigma_N \Phi^N, \quad (1 - 2)$$

where σ_N is the generalized N-photon cross section and Φ is the radiation flux. Ionization experiments at intensities below $\sim 10^{10}$ W/cm² follow this relation. However, as intensities have increased beyond 10^{12} W/cm² the rates no longer can be described by LOPT.

In ionization, the final state is a continuum state of the atom. Keldysh developed a semiclassical theory which considered the final state to be that of a free electron in an electro-magnetic radiation field.¹⁹ For optical wavelengths and intensities below about 10^{13} W/cm² the Keldysh approach can be called a non-perturbative multi-photon theory, whereas for very long wavelengths or very intense fields, this theory treats the electron as tunnelling out of a potential well.

Voronov and Delone were the first to study MPI experimentally.^{20,21} A Q-switched ruby laser was focused into xenon or krypton gas at a low pressure of $\sim 10^{-2}$ Torr. The electric field at focus was $\sim 10^7$ V/cm. At a pressure of 10^{-2} Torr, the mean free path of the electrons is ~ 1 cm, which is two orders of magnitude larger than the focal spot size. The ionization is then a collision-free process and can only be attributed to multi-photon ionization. The number of generated ions was plotted as a function of peak laser intensity, on a logarithmic scale. According to perturbation theory, the slope gives the number of photons required to surpass the ionization potential. In these experiments, the experimentally determined nonlinear orders were always smaller than that predicted by perturbation theory. Voronov and Delone attributed these discrepancies to the fact that the atomic bound levels that were nearly resonant to an integral number of photons would act to enhance the ionization process.

Chin et al.²² showed that at the highest intensities available with a Q-switched

ruby laser, saturation of the ionization rate occurred because of the depletion of neutral atoms in the focal region. The logarithmic plots of the ion yield versus intensity, for these experiments had the expected slope, predicted by LOPT at low intensities, but the slope decreased at higher intensities. The number of generated ions continues to increase in the saturation region as a result of the expanding volume of ionization. Cervenán and Isenor²³ determined the ion yield as a function of intensity for the case of a Gaussian beam focused by either a spherical or cylindrical lens at large intensities. After the number of neutral atoms is depleted in the interaction region, the number of generated ions increases as the volume encompassed by a constant intensity increases. The volume of constant intensity and therefore the ion yield increases as $I^{3/2}$ and I^2 for a Gaussian beam, focused by a spherical and cylindrical lens, respectively.

The early MPI experiments studied the ionization of noble gas atoms, which have ionization potentials greater than 10 eV. Aleksakhin and co-workers studied MPI of strontium and barium which have much lower ionization potentials.²⁴ A Sr atom will be ionized with the absorption of 5.7 eV and a second electron can be removed if an additional 11 eV of energy is absorbed. The second charge states of both Sr and Ba were generated by MPI with the interaction of 1 μm radiation at an electric field strength 6×10^6 V/cm. The observation of multiple ionization stages led to the question of whether the second ionization state is a result of direct or sequential ionization. That is, there are two possible schemes to ionize the neutral atom to the second ionization state. By the sequential process, the neutral atoms are ionized to the first ionization state by simultaneous absorption of P photons, where P times the photon energy is greater than the ionization potential. When the neutral atoms are depleted in the focal volume, the ions are further ionized to the second level by the absorption of Q photons, which is the minimum number of photons required to ionize the first charge state. By the second process, the neutral atom simultaneously absorbs

R photons, where R times the photon energy is greater than the sum of the two ionization potentials. These two processes are shown schematically in Fig. 1-2, for the ionization of Sr atoms to the second ionization state. The experimental results showed that significant numbers of Sr^{2+} were generated before the production of Sr^{1+} was saturated, indicating that direct ionization occurred.

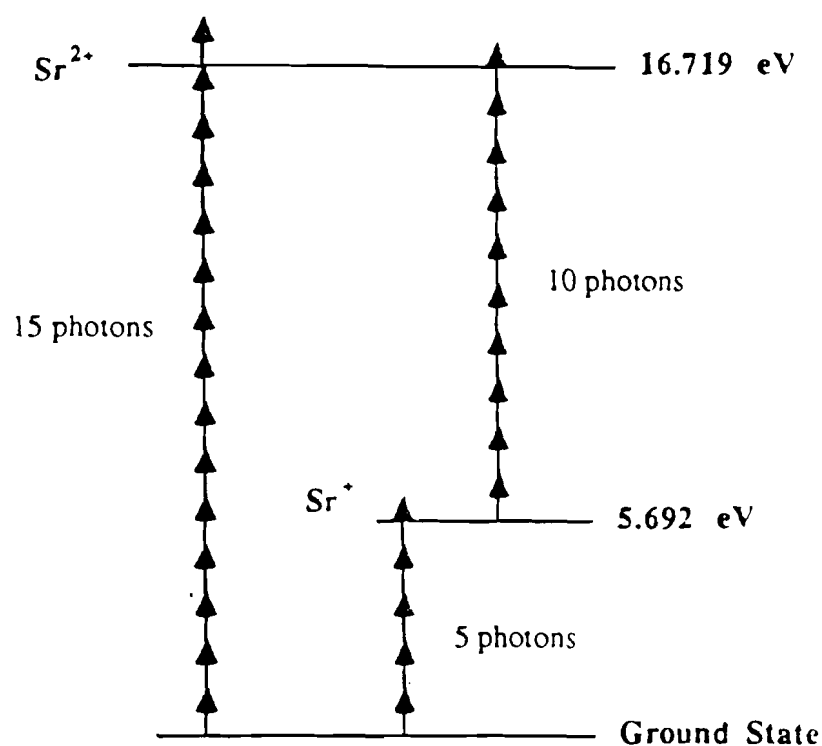


Figure 1-2. Schematic depicting direct and sequential ionization processes for Sr

Multi-photon multiple ionization has been studied in the intensity range of 10^{11} to 10^{16} W/cm^2 , at different wavelengths and pulse durations. The results of the various experiments are discussed in the next two sections.

I. B. 2 Saclay MPI Experiments

The Saclay group has extensively studied MPI with near IR radiation. L'Huillier et al.²⁵ used a mode-locked Nd:YAG oscillator and Nd:glass amplifiers to generate 50 ps pulses, at intensities in the 10^{13} - 10^{14} W/cm² range. At these intensities, ionization states up to Kr⁴⁺ and Xe⁴⁺ were observed. The plots of ionization yield versus intensity showed that double ionization states were produced before the saturation of the first ionization state. The saturation of the ion production of the first and second ion states occurred at the same intensity. Also the intensity dependence of the production of the doubly charged ions was measured to be equal, within experimental accuracy, to the predicted values for direct ionization from the ground states. It was concluded that doubly charged ions were most probably due to the direct ionization of the neutral atom.

This group then studied the multi-photon ionization of Xe, Ne²⁶ and He²⁷ by interaction with the second harmonic of the Nd:glass radiation. By doubling the photon frequency, the number of photons required to ionize the atom is halved. Ionization occurred at significantly lower intensities for green radiation than had been observed at 1.06 μ m. The plot of the ionization rate of Xe²⁺ had an inflection point at the saturation intensity of the first charge state. The ionization yield of Xe as a function of peak intensity is shown in Fig. 1-3. It was concluded that the ionization to the second charge state, occurred at low intensities by a direct process to the point of depletion of neutral atoms and then by a sequential process which ionized the singly charged ions.

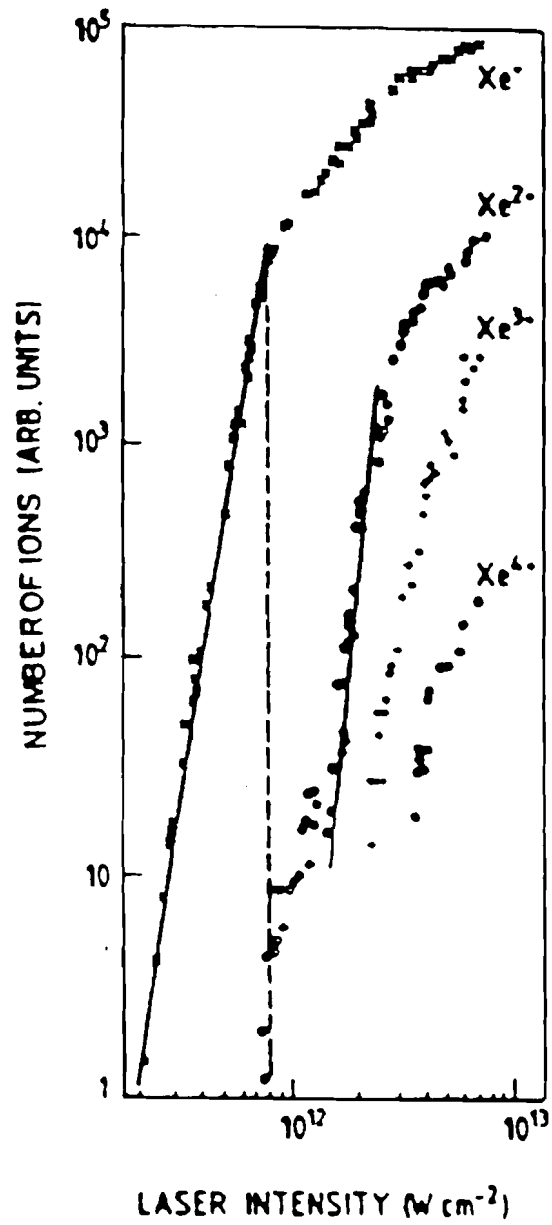


Figure 1 - 3. Plot of ionization yield as a function of peak intensity for xenon for 0.532 μm radiation (from Ref. 25)

The Saclay group also used a Nd:glass oscillator and amplifier system which generated pulse durations from 5 to 200 ps, to study the effect of pulse duration on the creation of the Xe^{2+} charge state.²⁸ With the short 5 ps pulses, Xe^{2+} was generated before Xe^+ production was saturated and both charge states had comparable saturation intensities. When the Xe atoms were ionized by a 30 ps pulse, the Xe^{2+} ionization rate again had two saturation intensity levels. Only sequential ionization occurred, that is Xe^{2+} only appeared at intensities above the saturation intensity of Xe^+ , for the 200 ps pulse durations.

I. B. 3 Recent Non-resonant MPI Results

Luk et al.²⁹ have performed multi-photon ionization experiments with a picosecond ultraviolet laser system at intensities in the 10^{16} W/cm² range. The Xe^{8+} charge state, which requires an energy of 171 eV, assuming sequential ionization, was created, but He^{2+} which would require only 54 eV of absorbed energy was not observed. The maximum charge states produced for Ar, Kr and Xe corresponded to the removal of entire subshells, indicating that some form of electron coupling was responsible for the ionization process in these species. The Z dependence of the ionization process was studied by ionizing the different elements of the lanthanide sequence, where 4f electrons are being added to an inner shell. Little difference in the total energy absorbed for the different elements was observed. The charge state spectra produced by the UV laser was compared to the IR results of the Saclay group, to determine the frequency dependence. The charge states were more abundant for short wavelengths, at an intensity of 10^{14} W/cm². This comparison did not take into account that the pulse duration was also different for the two experiments. Rhodes³⁰ has recently reported the creation of charge states: Xe^{9+} , Kr^{8+} , Ar^{8+} , Ne^{4+} and

He^{2+} at an intensity of 10^{16} W/cm^2 and a wavelength of 248 nm.

Perry et al.³¹ have used a tunable picosecond laser system to investigate the multi-photon ionization of the noble gases. With the laser tuned to be non-resonant with the atomic levels, the threshold intensity required to create the different charge states of the various noble gases was measured, and plotted as a function of absorbed energy, assuming sequential ionization. The plot is shown in Fig. 1-4. The threshold intensities for all the charge states fell on a smooth curve, indicating that the ionization process is independent of the specific atomic structure. The authors consider the smooth curve to be an indication that the ionization process is sequential rather than direct.

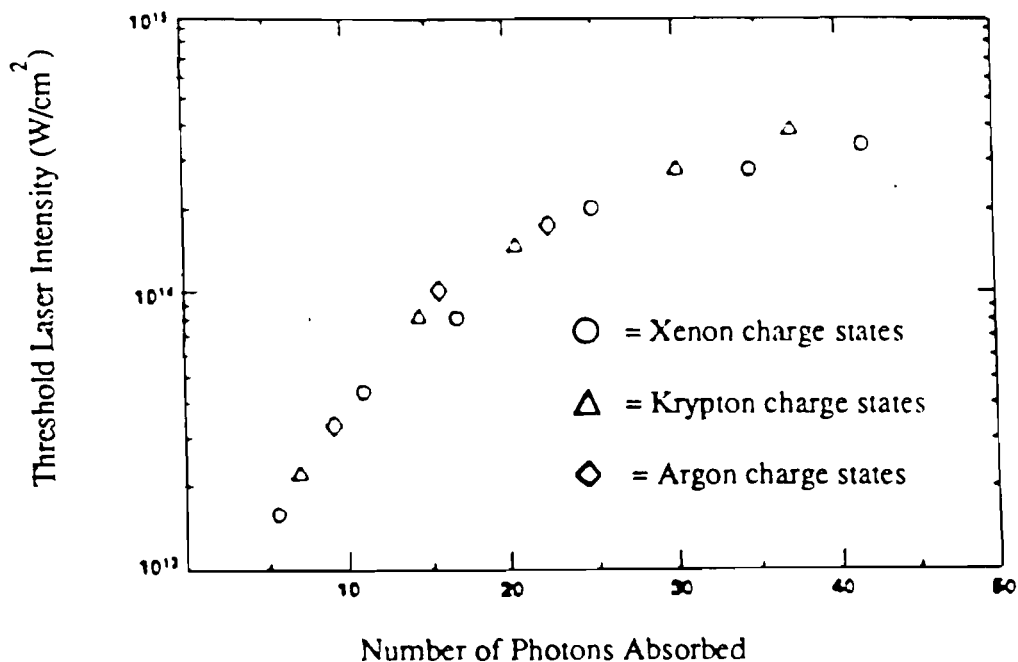


Figure 1 - 4. Plot of appearance intensity for Xe, Kr, and Ar as a function of ionization potential for the picosecond dye laser MPI experiments (from Ref. 32).

Inflection points occurred in the curves of ion yield as a function of peak intensity, as with the Saclay results. The explanation of direct ionization was ruled out in this paper, because of the much smaller cross sections of the direct processes. One explanation of the inflection points was that they are due to a small modulation on the beam profile, which leads to higher local intensities, which saturate before the entire beam saturates. The second explanation that is offered for the inflection points is a process known as channel closing. At high intensities, it has been shown that the ionization potential is increased by the "quiver" energy or the ponderomotive potential of the electric field.^{32,33} The ponderomotive potential, V , is given by;

$$V \equiv \frac{e^2 E^2}{4 m \omega^2}, \quad (1 - 3)$$

where e is the electron charge, E is the electric field, m is the electron mass and ω is the angular frequency of the radiation. When the intensity increases such that the ponderomotive potential increases by one photon of energy, the ionization process switches from an N to an $N + 1$ photon process. The higher order ionization rate is smaller until the intensity is increased to where the $N+1$ photon rate equals the N photon rate.

Yergeau et al.³⁴ have studied multi-photon ionization with a CO_2 laser. The ponderomotive potential scales as the square of the wavelength and so very large potentials can be achieved with the $10 \mu\text{m}$ radiation of a CO_2 laser. The laser intensity used in these experiments ranged from 10^{13} to $2 \times 10^{14} \text{ W/cm}^2$, which gives a ponderomotive potential of 100 to 1000 eV. These potentials are higher than the ionization potential of the atoms and therefore should affect the ionization process. The ionization rates were found to still correspond to the perturbative results. Charge states of Xe^{3+} , Kr^{2+} , Ar^{2+} , Ne^+ and He^+ were observed.

Very recently, Chin et al.³⁵ have studied multi-photon ionization for pulse durations of 900, 90 and 22 fs to study the importance of dynamic resonances and shifting ionization potentials. They observed little effect from the high lying states being shifted by the intense radiation.

1. C Outline

Following the introduction, Chapter II describes the study of the CPA technique and the development of the Table Top Terawatt laser system. The technique of optical pulse compression is discussed and the results of an initial experiment, which studied the compression of Nd:YAG pulses in CS₂ are given. The technique of Chirped Pulse Amplification is then discussed. The different compression systems are described. The first uses fibre expansion and a double grating compressor and the second technique uses both a fibre and a grating pair to extend the pulse duration and again a grating pair to compress the pulse. Two different oscillator/amplifier configurations were developed, one used a Nd:YAG oscillator and silicate glass amplifiers and the second used a Nd:YLF oscillator, with phosphate glass amplifiers. A description and results from the various CPA configurations are given. The limitation of the system to date is the damage threshold of the gratings used for the amplified compression. A description of the damage tests performed on two different types of grating are given.

Chapter III describes the MPI experiments and results obtained. A discussion of the determination of the laser intensity is given, for both long and short pulses. Time-of-Flight spectra are shown for the five noble gases at the highest intensities at 1.053 μm . The intensity dependence of the ion yields are plotted for both pulse durations and for both wavelengths measured for the five noble gases.

A discussion of these results and a comparison with other published results is

given in Chapter IV. A comparison of the charge states achieved with the infra red and green photons show that the higher charge states are produced at lower intensities with longer wavelength radiation. Possible explanations for these results will be discussed. A discussion of the effect of the 200 ps pedestal of the pulse, on the ionization process will also be given. A comparison of the experimental results and a modified Keldysh theory is also discussed.

The thesis is concluded in Chapter V, by summarizing the results of the present experiments and discussing future multi-photon experiments that can be done with the CPA laser. Also the CPA laser can be scaled to give higher peak powers by increasing the energy or decreasing the pulse width. As the work in this thesis points out, short pulse bright laser sources will have to be developed which produce short pulses with a contrast to the background radiation of over a million to one. Various new CPA laser schemes that accomplish these goals will be discussed, including a proposal by Lawrence Livermore National Laboratory to construct a Petawatt (10^{15} W) system.

References

1. O. P. Wood, W. T. Silfvast, J. Macklin and P. J. Maloney, *Opt. Lett.* 11, 198 (1986)
2. E. S. Sarachik and G. T. Schappert, *Phys. Rev. D* 1, 2738 (1970)
3. M. J. Feldman and R. Y. Chiao, *Phys. Rev. A* 4, 352 (1971)
4. Wayne H. Knox, *IEEE J. Quantum Electron.* QE-24, 388 (1988)
5. H. Egger, T. S. Luk, K. Boyer, D. F. Muller, H. Pummer, T. Srinivasan, and C. K. Rhodes, *Appl. Phys. Lett.* 41, 1032 (1982)
6. S. Szatmari, F. P. Schafer, E. Muller-Horsche, and W. Muckenheim, presented at the IQEC Conf., Baltimore MD, 1987, postdeadline paper PD20
7. Lawrence Livermore National Laboratory 1982 Laser Program Annual Report
8. Donna Strickland and Gerard Mourou, *Opt. Commun.* 56, 219 (1985)
9. P. Maine, D. Strickland, P. Bado, M. Pessot, and G. Mourou, *IEEE J.*

Quantum Electron. QE-24, 398 (1988)

10. P. B. Corkum, Opt. Lett. 8, 514 (1983)
11. J. A. Valdmanis, R. L. Fork and J. P. Gordon, Opt. Lett. 10, 131 (1985)
12. R. L. Fork, C. H. Brito Cruz, P. C. Becker, and C. V. Shank, Opt.Lett. 12, 483 (1987)
13. Paul B. Corkum and Roderick S. Taylor, IEEE J. Quantum Electron. QE-18, 1962 (1982)
14. A. J. Taylor, R. B. Gibson, and J. P. Roberts, Appl. Phys. Lett. 52, 773 (1987)
15. J. H. Glowina, J. Misewich, and P.P. Sorokin, J. Opt. Soc. Am. B 4, 1061 (1987)
16. M. Goepfert-Mayer, Ann. Physik 9, 273 (1931)
17. W. Kaiser and C. G. B. Garrett, Phys. Rev. Lett. 7, 229 (1961)
18. H. Barry Bebb and Albert Gold, Phys. Rev. 143, 1 (1966)
19. L. V. Keldysh, Sov. Phys.-JETP 20 , 1307 (1965)

20. G. S. Voronov and N. B. Delone, *Sov. Phys.-JETP* 23, 54 (1966)
21. G. S. Voronov, G. A. Delone, and N. B. Delone, *Sov. Phys.-JETP* 24, 1122 (1967)
22. S. L. Chin, N. R. Isenor, and M. Young, *Phys. Rev.* 188, 7 (1969)
23. M. R. Cervenak and N. R. Isenor, *Opt. Commun.* 13, 175 (1974)
24. I. S. Aleksakhin, I. P. Zapesochnyi, and V. V. Suran, *JETP Lett.* 26, 11 (1977)
25. A. L'Huillier, L. A. Lompré, G. Mainfray and C. Manus, *J. Phys. B: At. Mol. Phys.* 16, 1363 (1983)
26. A. L'Huillier, L. A. Lompré, G. Mainfray and C. Manus, *Phys. Rev. A* 27, 2503 (1983)
27. A. L'Huillier, L. A. Lompré, G. Mainfray and C. Manus, *Phys. Lett. A* 112, 319 (1985)
28. L. A. Lompré, A. L'Huillier, G. Mainfray and C. Manus, *J. Physique* 44, 1247 (1983)
29. T. S. Luk, U. Johann, H. Egger, H. Pummer, and C. K. Rhodes, *Phys. Rev. A* 32, 214 (1985)

30. Charles K. Rhodes, *Physica Scripta*. T17, 193 (1987)
31. M. D. Perry, O. L. Landen, A. Szoke, and E. M. Campbell, *Phys. Rev. A* 37, 747 (1987)
32. P. Kruit, J. Kimman, H. G. Muller, and M. J. van der Wiel, *Phys. Rev A* 28, 248 (1983)
33. P. H. Bucksbaum, R. R. Freeman, M. Bashkansky, and T. J. McIlrath, *J. Opt. Soc. Am. B* 4, 760 (1987)
34. F Yergeau, S L Chin and P Lavigne, *J. Phys. B: At. Mol. Phys.* 20, 723 (1987)
35. S. L. Chin, Claude Rolland, P. B. Corkum and Paul Kelly, *Phys. Rev. Lett.* 61, 153 (1988)

CHAPTER II

STUDY OF THE CPA TECHNIQUE

II. A Introduction

Numerous applications exist for ultra-bright laser sources. The power of a laser can be increased either by increasing the energy or by decreasing the pulse duration. Increasing the energy means the system must become larger and typically the repetition rate is reduced. Conventional short pulse amplifiers such as dye lasers can be amplified at kilohertz repetition rates, but, have low saturation fluence levels of $\sim 1 \text{ mJ/cm}^2$ which limits the energy to the mJ range. The ideal solution would be to amplify short pulses in a gain medium that has a large energy storage capability. The problem is that these lasers are typically solid state and therefore cannot handle high peak powers.

As part of this thesis work, a novel laser technique has been developed which circumvents this peak power limitation of solid state amplifiers.¹ The Chirped Pulse Amplification (CPA) system uses a pulse compression technique which produces long pulses that have broad bandwidths. These long pulses can be amplified to the saturation energy without reaching the peak power limit. After amplification, the high energy pulses can then be compressed to approximately the inverse of the bandwidth. The prototype was designed and constructed to show the feasibility of the CPA technique. The system produces pulses with energies of 0.5 J and pulse durations of 1 ps. The CPA laser system should scale to the petawatt (10^{15} W) power level.

When focused, these high power pulses would generate intensities in the 10^{21} W/cm² range.

II. A. 1. Pulse Compression

Optical pulse compression can be used to shorten laser pulses and thereby increase the peak power of the pulses. The pulse compression technique was first developed in the radar field over forty years ago in order to decrease the peak power in the transmitting tubes, yet, increase the radar range and resolution.² This technique, uses a linear dispersion element to stretch a short pulse several times its original length and thereby decrease the peak power, by the same magnitude. This long pulse can then be amplified to extremely large energies, without reaching prohibitively high peak powers. After amplification, the pulse is transmitted and the echo that is received is compressed back to the original pulsewidth, by passing it through a second dispersive element, which has the opposite dispersion. The resolution is identical to that of broadcasting the short pulse, but, the energy and therefore the range is increased several orders of magnitude.

This technology of chirping and recompressing a pulse was transferred to the optical regime by Gires and Tournois³ and Giordmaine, Duguay and Hansen⁴. Giordmaine et. al. linearly frequency chirped the pulse by applying an RF modulation to an electro-optic crystal and compressed the pulses with the interferometer of Gires and Tournois. Treacy showed that pulses exhibiting positive frequency chirp, ie. the frequency increases with time, could be compressed by a pair of parallel gratings.⁵ The variation of the group delay, $\delta\tau$, with respect to wavelength of two parallel gratings is given by:

$$\delta\tau = \frac{b \left(\frac{\lambda}{d}\right) \delta\lambda}{cd \left[1 - \left(\frac{\lambda}{d} - \sin\gamma\right)^2 \right]} \quad (2 - 1)$$

where b is the separation of the gratings, λ is the central wavelength, d is the groove spacing, c is the speed of light and γ is the angle of incidence. By adjusting the grating parameters, a positive linear frequency chirp can be compensated by the negative dispersion of the grating pair. As will be discussed later, the total group delay can be expressed as a Taylor series and under certain conditions, the higher order terms can become significant, which would leave the resulting compressed pulse with a non-linear phase distortion.

II. A. 2. Self-Phase Modulation (SPM)

Fisher and co-workers⁶ showed, that even shorter compressed pulses could be achieved, by using self - phase modulation, (SPM), to broaden the pulse spectrum as well as frequency chirp the pulse. Self-phase modulation is a result of the Kerr effect. At large pulse intensities, the non-linear refractive index, n_2 , becomes significant and therefore the index of refraction, n , is no longer constant, but, rather a linear function of the intensity and so for pulsed signals, it varies with time, t , as:

$$n(z,t) = n_0 + n_2 I(z, t) \quad (2 - 2)$$

where n_0 is the linear index, and $I(t)$ is the time dependent intensity. The phase of the signal, $\phi(z,t)$, can then be determined by solving the following:

$$\frac{\partial \phi(z,t)}{\partial z} = \frac{2\pi}{\lambda} n(z,t) = \frac{2\pi}{\lambda} [n_0 + n_2 I(z,t)] . \quad (2-3)$$

The total phase delay experienced by the pulse, at the output of the nonlinear medium, can be determined by integrating Eqn. 2 - 3, to give:

$$\phi(t) = \phi_0 + \frac{2\pi}{\lambda} \int_0^L n_2 I(z,t) dz , \quad (2-4)$$

where L is the length of the nonlinear medium. The second term of Eqn. 2 - 4 is known as the B integral. The phase of the signal therefore continually changes as the intensity varies resulting in the input frequency, ω_0 , being modulated. The instantaneous frequency shift from the central frequency, $\omega(t)$, is determined by differentiating the phase with respect to time:

$$\omega(t) = -\frac{d\phi(t)}{dt} = -\frac{2\pi}{\lambda} \frac{d}{dt} \int_0^L n_2 I(z,t) dz . \quad (2-5)$$

If the intensity is assumed to be independent of distance, then $\omega(t)$ can be written as:

$$\omega(t) = -\frac{2\pi}{\lambda} n_2 L \frac{dI(t)}{dt} . \quad (2-6)$$

For most optical media, n_2 is positive in the optical region of the spectrum and therefore the pulse becomes positively chirped; that is the instantaneous frequency is decreased on the rising edge of the pulse and increased on the falling edge. For a

The Fourier transform limited pulsewidth, τ_{lim} , for a Gaussian pulse is given by:

$$2\pi \Delta\nu \tau_{lim} = \Delta\omega \tau_{lim} = 4\ln 2 \quad (2 - 13)$$

By using the value of ω_{max} , given in Eqn. 2-11, the maximum compression ratio is determined to be:

$$\frac{\Delta\tau}{\tau_{lim}} = 1.03 B(0) \quad (2 - 14)$$

Therefore, the maximum compression ratio that can be achieved, using this type of compression scheme, is the value of the B integral.

II. B CS₂ Experiment

Kerr liquids were first used as the non-linear media for self-phase modulation because of their high non-linear indices. In 1975, Lehmborg and McMahon⁷ compressed 100 ps pulses from a Nd:YAG laser system to 7 ps, using CS₂ as the non-linear medium. For our first attempt at generating high energy, short pulses, we repeated their experiment.

II. B. 1. Experimental System

A diagram of the experimental system is shown in Fig. 2-1. The oscillator was a pulsed Q-switched and mode-locked Nd:YAG laser which produced pulse trains of 35 ps pulses, separated by 10 ns, with a wavelength of 1.064 μm , at a 1 Hz repetition rate.

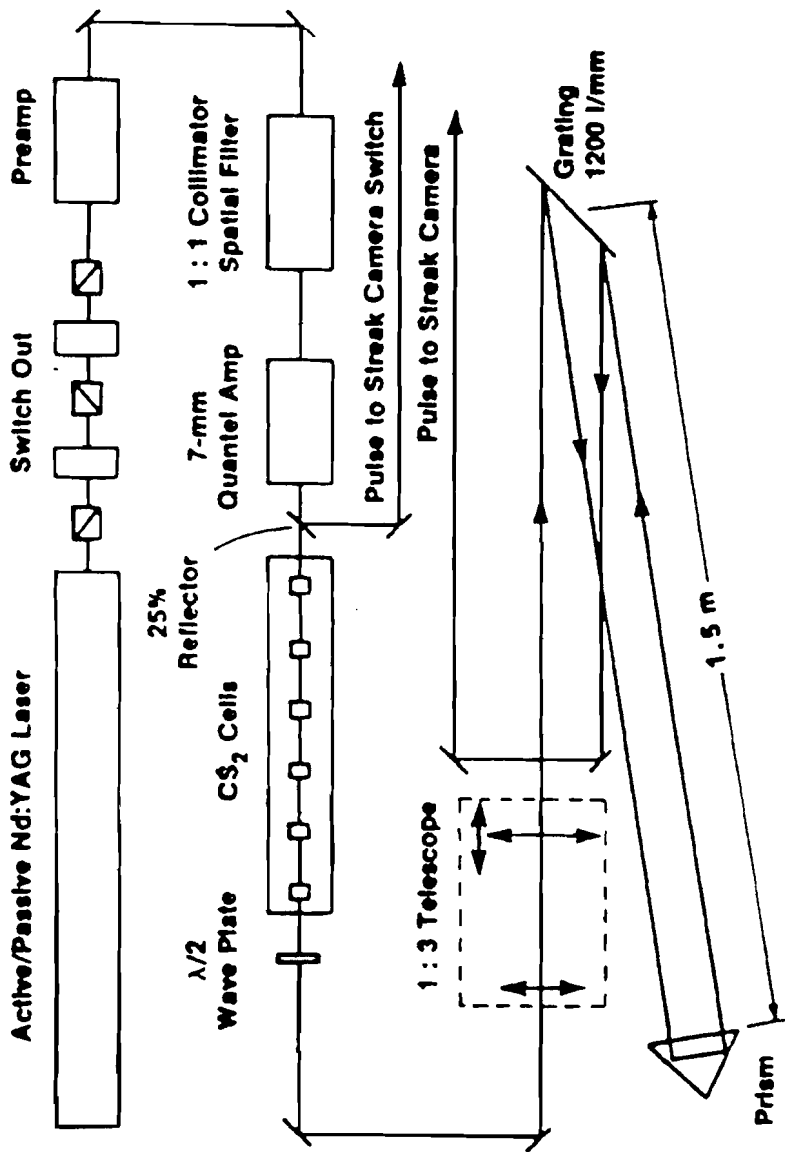


Figure 2 - 1. CS₂ compression system configuration

A series of two Pockels cell switch-outs were used, to switch out the peak pulse of the train, with a contrast of main pulse to pre-pulses of $10^6:1$. The pulse was then amplified in two successive single pass amplifiers to an energy of 7 mJ. The beam was spatially filtered between the amplifiers to clean up the wavefront. The pinhole diameter was about five times the Airy disc in order to avoid damage.

The spatial filter also collimated the beam, which had a diameter of approximately 2.5 mm. At the output of the second amplifier, the beam was split such that a 2 mJ pulse was used to drive the streak camera switch⁸ and a 5 mJ pulse was passed through a series of CS₂ cells. The peak intensity of the pulses was approximately 3.5×10^9 W/cm², at the input to the CS₂. The same nonlinear effect that causes SPM in time, also causes beam front distortion spatially across the beam. In order to minimize filamentation and beam break-up, the length of the CS₂ was divided into six cells, each 1 cm long and separated by 10 cm.

The value of B for the peak intensity of the pulse can be calculated using Eqn. 2-4. For CS₂, the values of n_0 and n_2 are 1.594 and 2.89×10^{-14} (cm²/W), respectively. The value of B, for our experimental conditions is then 36.0. Using the calculated value of B in Eqn. 2-11 gives a bandwidth of 1.7 nm, for a 35 ps pulse duration. The bandwidth was measured using a visible spectrometer. The radiation therefore had to be frequency doubled. The bandwidth of the green radiation was measured to be 1.8 nm., as shown in Fig. 2-2. This corresponds to the calculated value to within the accuracy of the intensity measurement.

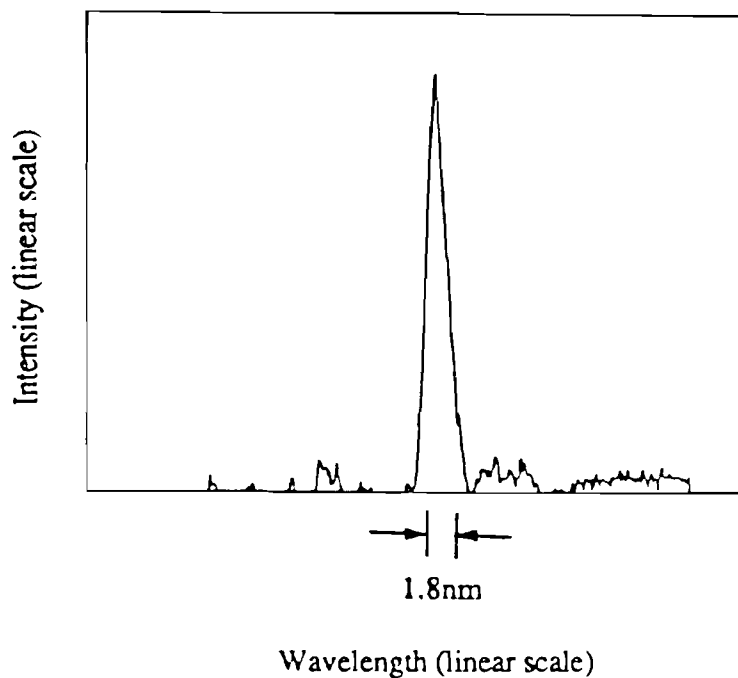


Figure 2 - 2. Measurement of broadened spectral bandwidth

The phase of the electric field is modulated through the nonlinear index by steep intensity gradients. This is true for spatial as well as temporal gradients, and so for intensities sufficient to cause self-phase modulation, the beam will also be self-focused. In order to isolate the modulated portion of the beam, a telescope was used to collimate the self-focused part and spatially filter out the wings that appear at the edge of the profile. The beam was expanded using the telescope, by a factor of three.

To compensate for the frequency chirp created by the SPM in the CS_2 cells, the pulses were transmitted along a dispersion line comprised of one grating, with a groove spacing of 1200 1/mm and a right angle prism. The angle of incidence was approximately 60° . Using equation 2-1, the separation between two gratings that is

required to compress a pulse exhibiting a frequency chirp of 1.8 nm over a 35 ps pulse duration, is calculated to be 3.2 m. The distance required can be halved by replacing the grating with a right angle prism, which rotates the beam 180°, through an axis parallel to the grooves of the grating, and then reflects the beam back to the first grating. The prism was placed on a variable delay line approximately 1.5 m from the grating. The distance was optimized for the shortest compressed pulsewidth.

II. B. 2. Results

The compressed pulses were measured using a streak camera and Two-Photon Fluorescence, (TPF). In order to be detected by the streak camera, the pulses were frequency doubled. The compressed pulsewidths were typically 6 ps, but, some pulse durations were streak camera limited at 4.5 ps, as shown in Fig. 2-3. The streak camera traces show that the duration of the streaked pulse is equal to the spot size. The best focus of the spot size was 4 pixels, which corresponds to 4.5 ps for the streak speed of the camera. The streak camera was calibrated using a 125 ps etalon. The shots could not be averaged because there was an apparent timing jitter of 20-30 ps between the 30 ps pulse driving the switch, which triggered the camera, and the detected compressed pulse.

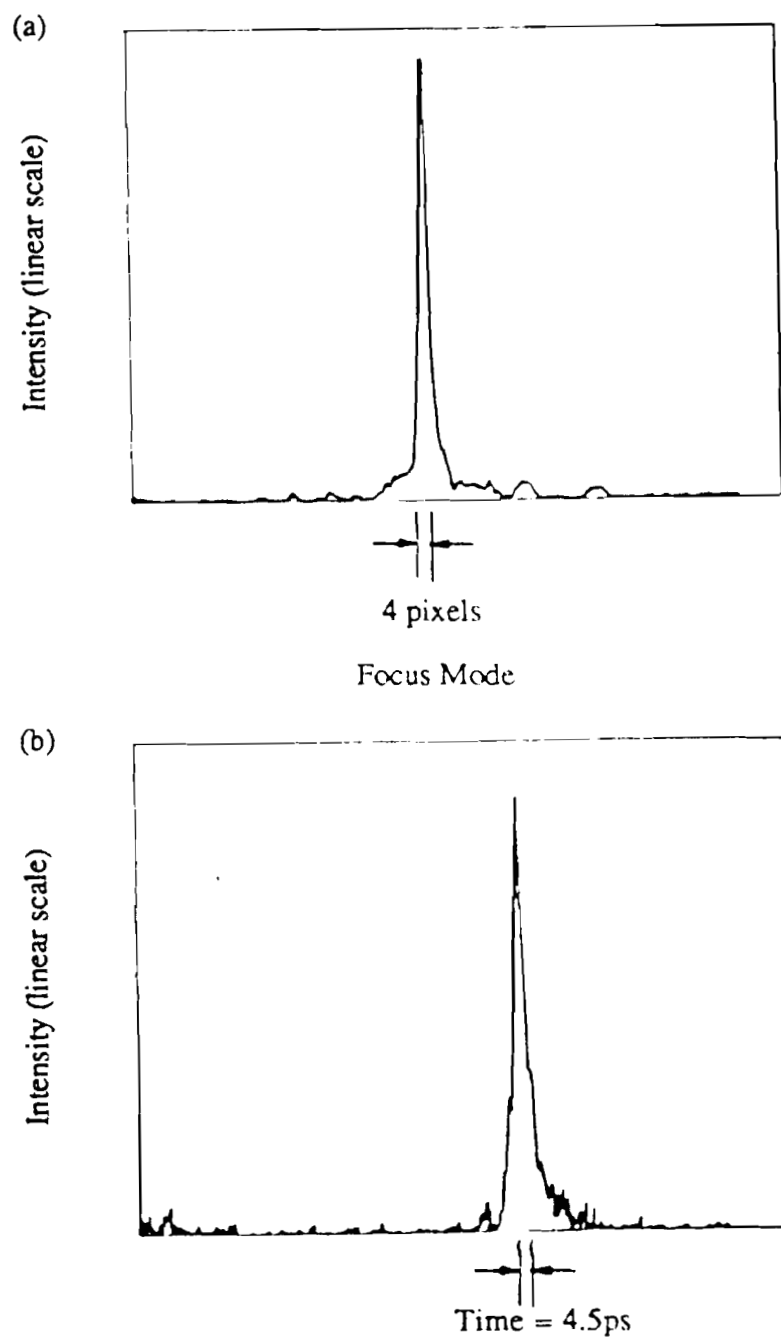


Figure 2 - 3. Steak camera measurement (a) focus spot, (b) compressed pulse

TPF was used to measure the autocorrelation of the IR temporal profiles. The first measurement shown in Fig. 2-4, indicates that the pulse was quite broad, approximately 30 ps, with large wings. An iris was placed in the beam and adjusted so that just the central portion, about 20% of the energy, was transmitted. The TPF measurement of the central part of the beam show a clean 6 ps pulsewidth in Fig. 2-5. The iris was not needed for the streak camera measurements because the light was frequency doubled, so that only the most intense part of the beam was converted. This shows that the uncompressed wings of the pulse were not successfully eliminated by spatial filtering.

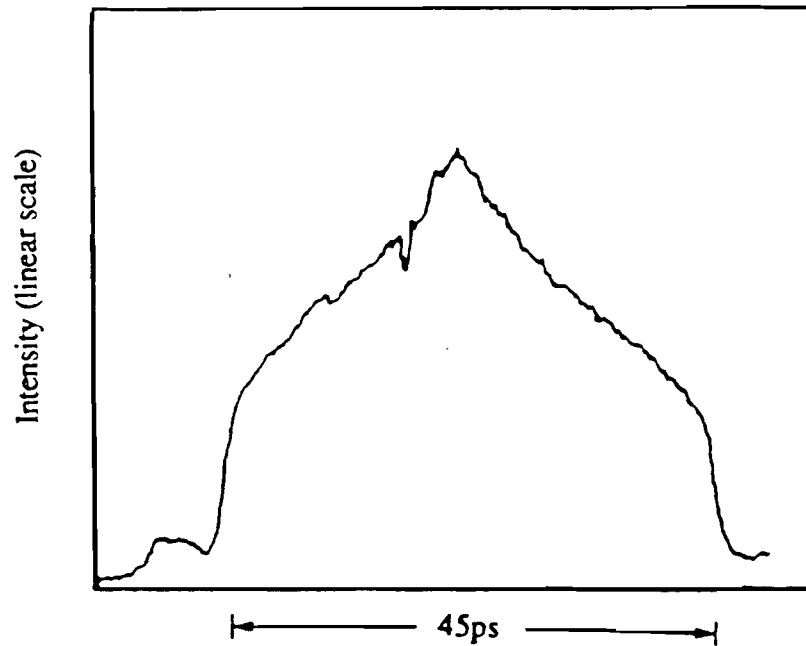


Figure 2 - 4. Two-photon fluorescence measurement

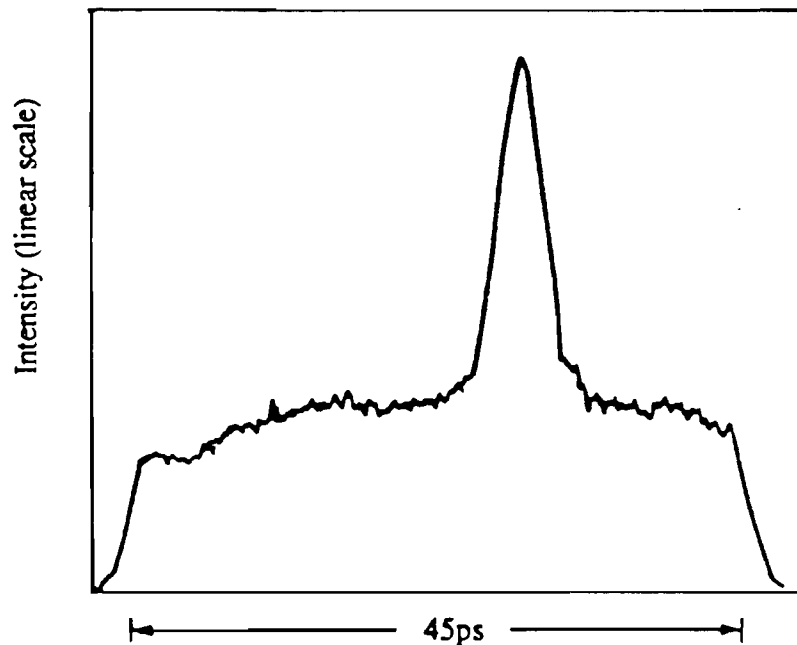


Figure 2 - 5. Two-photon fluorescence measurement of central portion of beam

This compression scheme was very lossy. The CS_2 absorbed 40% of the laser energy and the grating compressor was just 50% energy efficient. After the iris, the pulse energy was just 200 μJ , compared to 5 mJ of energy at the input of the CS_2 cells. The pulsewidth was compressed by only a factor of 5 or 6, so that the peak power was actually decreased by this compression system.

This type of compression technique also results in extremely poor beam quality. Just as the nonlinear index modulates the temporal frequency, the spatial frequencies will be modulated by a spatial intensity gradient. This spatial modulation leads to both whole beam and small scale self-focusing. Whole beam self-focusing is caused by the index of refraction being increased by the maximum amount at the centre of the beam where the intensity is the largest and unchanged at the edge of the beam profile. The severity of self-focusing increases with the intensity gradient. An intensity ripple

superimposed on the beam leads to small scale self-focusing. The small scale self-focusing will cause the ripple intensity to grow until the beam breaks up into small filaments. It can be shown that a one-dimensional intensity modulation, of spatial wave number K , superimposed upon a uniform intensity profile will grow exponentially with a gain coefficient, g , which is given by:⁹

$$g = K \left[\frac{n_2 I}{n_0} - \frac{K^2 \lambda^2}{16\pi^2} \right]^{1/2} \quad (2 - 15)$$

The first term in the bracket is the dominant term and is related to the B integral so that the ripple intensity grows exponentially with the value of the B integral. Also from Eqn. 2-15, it can be seen the gain increases with spatial frequency, and so the sharpest modulations grow the fastest, leading eventually to filamentation and beam break up.

Equation 2-15 indicates that in order to maintain a good beam quality, the value of the B integral must be kept small. A typical rule of thumb used in designing laser systems is that the B integral be kept below five. It is shown in Eqn. 2-14, however, that the maximum compression ratio that can be achieved was approximately the value of the B integral. Therefore, the maximum compression ratio that can be obtained with this type of compression scheme without distorting the beam is five. In order to achieve better compression, the pulse must be guided through the nonlinear medium, such that higher order modes cannot propagate. In this manner, large B integral values can be used to give large compression ratios and the self-phase modulated pulse can still have a clean beam profile.

II. C Fibre Pulse Compression

In 1981, pulse compression using an optical fibre, as the non-linear medium was developed at IBM¹⁰. Fibre pulse compression offers two significant advantages over the Kerr liquid technique. The first being, that the pulse propagates through a single mode fibre as essentially a plane wave. The induced phase delay is therefore, constant across the entire beam, allowing the entire beam to be equally compressed, and the wavefront to remain undistorted. The second advantage is that the fibre exhibits Group-Velocity Dispersion (GVD). The combined action of SPM and GVD broadens both the frequency spectrum and the pulse shape, resulting in almost the entire bandwidth being linearly chirped. The resulting compressed pulse has much less energy in the wings.

Originally, fibre pulse compression was used to make short pulses even shorter. The shortest pulsewidth achieved using this technique, to date, is 6 fs, by compressing a 50 fs pulse.¹¹ The compression ratio is just a factor of eight. The compression ratio, however, increases with increasing initial pulsewidth. Fibre pulse compression of 80 ps, CW mode-locked Nd:YAG laser pulses was developed at Spectra Physics and Stanford University.¹² They achieved a compression ratio of approximately 40, to reach a pulsewidth of 2 ps. The energy efficiency of the system was 25%, yielding an increase in peak power of an order of magnitude.

Fibre pulse compression has become a very valuable technique for low peak power, high repetition rate applications, but, cannot be used for high power pulses. The peak power in the fibre must be kept below a level where Raman generation takes place. The threshold power, P_{th} , for Raman generation is given theoretically by:

$$P_{th} = 30 A/GL, \quad (2 - 16)$$

where A is the effective core area of the fibre, G is the Raman gain and L is the length of the fibre.¹³ For 1.06 μm radiation, the Raman gain is 9.2×10^{-12} cm/W . Single-mode fibre, for this wavelength, typically, has a core diameter of 7 μm , which corresponds to an effective area of approximately 4×10^{-7} cm^2 . For a fibre length of 100 m, the threshold peak power would be 130 W. When Raman pulses are produced in the fibre, the energy of the SPM pulses is reduced and the pulses become unstable.

II. D CPA Technique

Fibre pulse compression cannot be used to compress high energy pulses because the fibre cannot support large energies and as in the radar field, short compressed pulses cannot be amplified efficiently in a solid state medium, without reaching prohibitively high peak powers in the amplifiers. It is shown in the Appendix that the energy in an amplifier can only be efficiently extracted if the input fluence is on the order of the saturation fluence. However, as was discussed in Section I. A. 1, only long pulses can be amplified to the saturation fluence level and keep the beam undistorted.

The solution to the problem of generating high energy, short pulses is the optical analog of chirped radar. Optical pulse compression was originally developed to simply shorten pulses, whereas pulse compression in the radar field was developed in order to amplify a long pulse, but, have the resolution of a short pulse. We have developed a similar technique, in the optical regime. The CPA technique stretches a short pulse several times its original length, in order that it can be amplified to the saturation level without reaching the prohibited peak powers in the amplifying medium. Short single picosecond pulses can be stretched to the nanosecond time scale

and can therefore be amplified by conventional techniques to the highest energies presently achieved. After amplification, the high energy pulses can be recompressed to the initial pulse durations, to generate ultra-high peak powers.

The prototype system that was built to demonstrate the CPA technique uses a CW mode-locked Nd:YLF oscillator, which generates 50 ps pulses at a wavelength of 1.053 μm . The 50 ps pulses are injected into an optical fibre to increase the bandwidth and stretch the pulse as in conventional optical pulse compression. Before the pulse is compressed, however, the long pulse is amplified in a Nd:phosphate glass system to an energy of 0.5 J. After amplification, the pulse is compressed by a pair of parallel gratings to a duration of 1 ps to generate a power of 0.5 TW. The CPA system is scalable to the petawatt level by amplifying the long pulse to the kJ level, which is presently achievable with Nd:glass laser systems.

II. D. 1. Fibre Expansion

To demonstrate the CPA concept, a laser system, which produced mJ level pulses with a 2 ps pulse duration, was built.¹ A schematic diagram of this system is shown in Fig. 2-6. A CW mode-locked, Nd:YAG laser (Spectra-Physics Series 3000) was used to produce 150 ps pulses, at an 82 MHz repetition rate. A 1.4 km length of fibre was used, as the nonlinear medium, to increase the bandwidth and stretch the pulse, by the combined effects of SPM and GVD. Five watts of average power were coupled into the single-mode, non-polarization-preserving optical fibre, with a 10x microscope objective. An identical microscope objective was used to collimate the beam at the output of the fibre. A variable attenuator comprised of two crossed polarizers and a half-wave plate was used to vary the input power to the fibre.

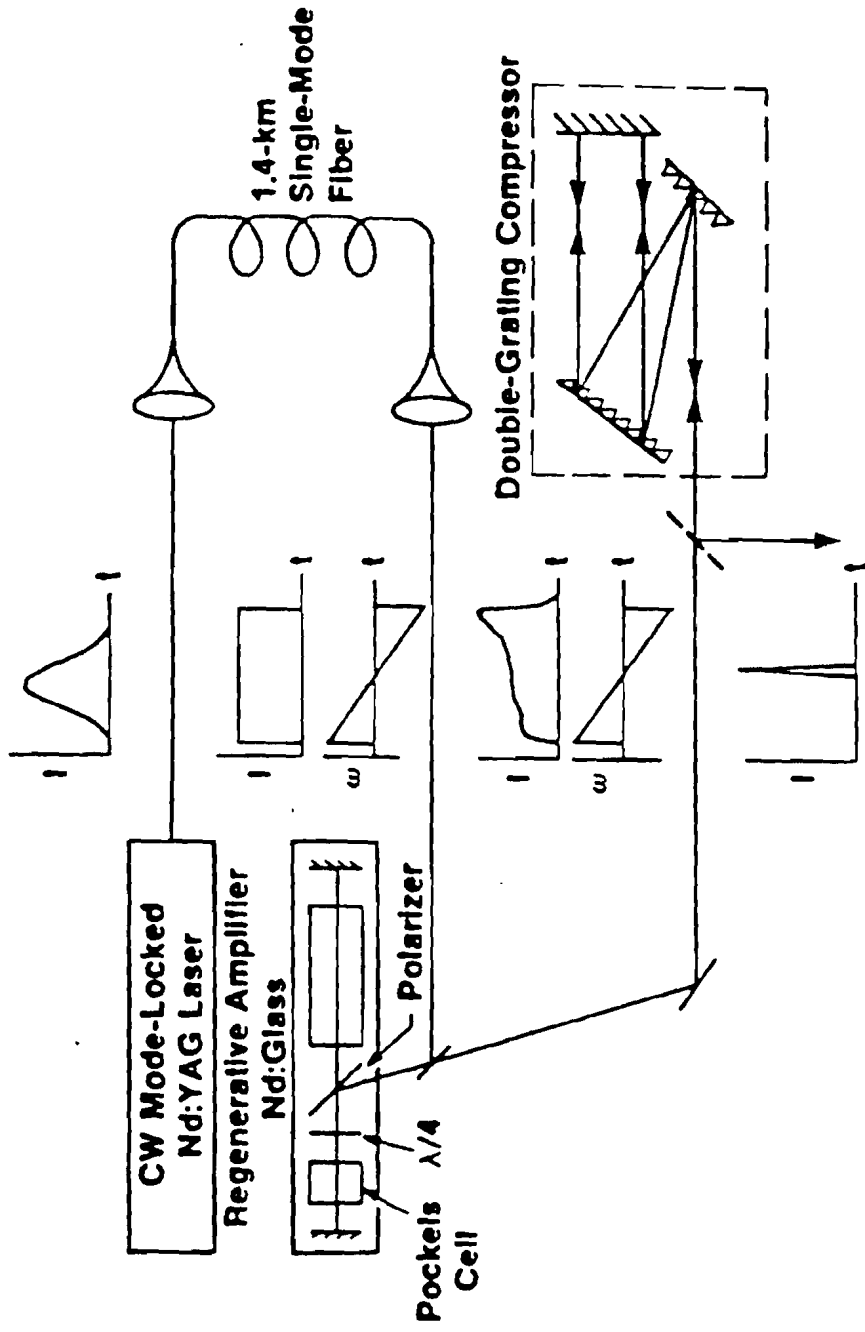


Figure 2 - 6. Experimental configuration of mJ CPA system

A quarter-wave plate was placed between the second polarizer and microscope objective in order to isolate the oscillator from back reflections off of the front surface of the fibre. The polarization would be rotated by 180° , by reflection from the surface and by another 90° , from the double pass of the $\lambda/4$ plate. The reflected light would therefore be deflected by the second polarizer. No attempt was made at isolating the oscillator from the light, that was reflected back by Rayleigh scattering, in the fibre. There seemed to be no effect of Rayleigh scattered light with this oscillator, although as will be discussed later, a Faraday rotator had to be placed between the fibre and a different oscillator.

The fibre (Corning Experimental SMF/DSTM) has a core diameter of $9\ \mu\text{m}$. The average power at the output of the fibre was $2.3\ \text{W}$ with most of the loss due to imperfect coupling. The amount of power coupled into the fibre was chosen for best energy stability of the compressed pulses. The CW pulse train, at the output of the gratings was detected with a PIN diode and displayed on an oscilloscope. At a particular power level, the pulse train would have the best stability as well as the maximum energy. This power level corresponded to the point where Raman generation could just be detected. If the input power was further increased, the energy of the compressed pulses remained constant, but, became unstable. The excess energy was converted to Raman light. This could be seen in a number of ways. The spectrum changed from a symmetric to an asymmetric spectrum at this power level. Figure 2-7 shows two spectra for different power levels in the fibre. Figure 2-7a shows the frequency spectrum produced by just SPM in the fibre, at an output power of $2.3\ \text{W}$. The spectral bandwidth was $4.0\ \text{nm}$. Figure 2-7b shows the spectrum for an output power of $3\ \text{W}$, where Raman generation is depleting the red region of the spectrum, which corresponds to the front end of the pulse.

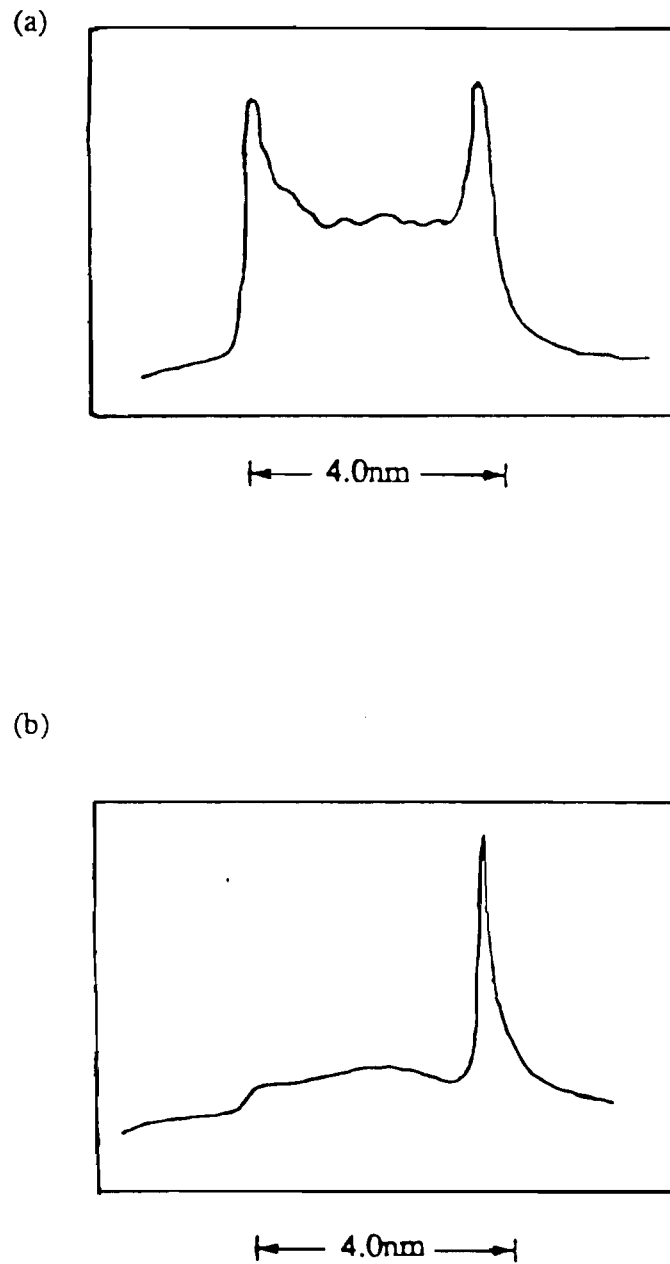


Figure 2 - 7. Frequency spectra where (a) just SPM is present and (b) Raman generation takes place

Also because we were using such a long fibre, the Raman pulse separated from the SPM pulse, and so a double pulse train was detected at the output of the fibre. The pulsewidth at the output of the fibre was measured using an autocorrelator. The autocorrelation of the stretched pulse is shown in Fig. 2-8. The correlation is triangular in shape, which corresponds to a rectangular pulse shape, with a pulsewidth of 300 ps.

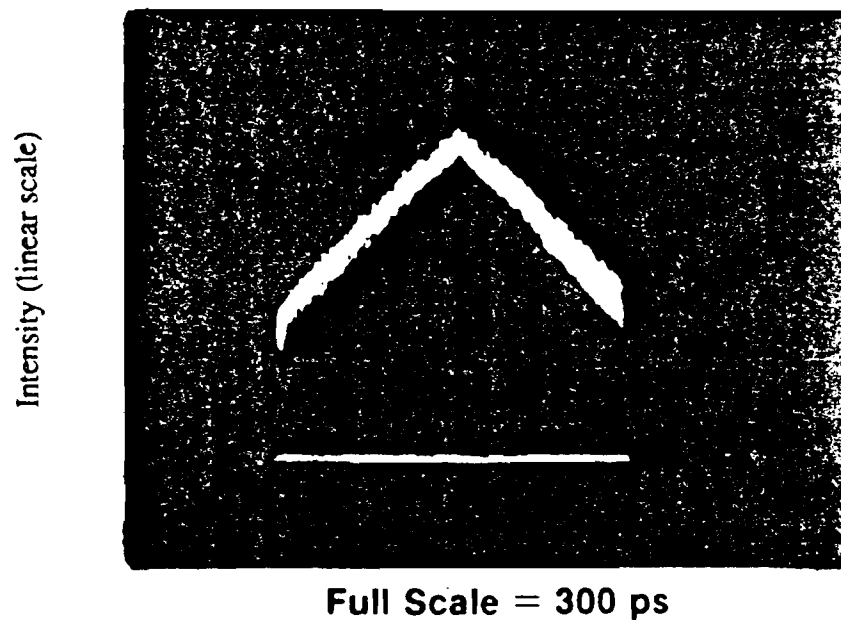


Figure 2 - 8. Autocorrelation measurement of stretched pulse

II. D. 2. CW Compression

The grating compressor was optimized for the best compression of the CW mode-locked pulses. Although the light that is input to the fibre has circular polarization, at the output the polarization is predominantly linear, because of the

nonlinear birefringence effect in the fibre. The birefringence is intensity dependent, and therefore the intense portion of the pulse is polarized in one direction, which is different from the low intensity wings. The grating compressor passes only P-polarized light and therefore acts as a polarizer. The grating compressor will then pass the intense, P-polarized portion of the beam and deflect the low intensity wings, into the zero order.¹⁴ A half-wave plate was placed before the gratings to rotate the polarization of the light from the fibre to have maximum output power after the gratings.

The grating compressor was comprised of two gratings and a right angle prism. The first gratings that were used were gold coated, holographic reflection gratings (American Holographic), with a grating constant of 1800 1/mm. They were used in a near Littrow configuration (ie. the diffracted beam is directed back along the incident beam), for best efficiency, so the angle of incidence was approximately 75°. The energy efficiency of these gratings was just 80% because of the large angle of incidence. To improve the efficiency, new gratings, with a grating constant of 1700 1/mm were used. The energy efficiency of these gratings was better than 90%, when used in a near Littrow configuration, with an angle of incidence of approximately 65°. The groove spacing was kept as small as possible, in order to have a reasonable distance between the gratings. Although reflection from two parallel gratings will compress a pulse temporally, the beam will be elongated in one direction, by the dispersion. To compensate for large compression factors, the dispersion will stretch the beam several times the beam diameter, making the beam profile almost linear in shape. The beam can regain its circular beam shape, by retroreflecting the beam back along the two gratings.¹⁵ A right angle prism was used to step the beam down, in a perpendicular direction to the dispersion direction, and then reflect the beam back through the gratings. In order to compensate for the same frequency chirp,

the separation of the gratings is halved. For optimum compression, the separation of the gratings, when used in a double pass configuration, was calculated to be 25 cm. The gratings were separated by approximately this distance then adjusted to give the minimum measured pulsewidth. An autocorrelator was used to measure the compressed pulsewidths. As can be seen from the autocorrelation, shown in Fig. 2-9, the CW compressed correlation width was 2.3 ps, which corresponds to a pulsewidth of 1.5 ps, assuming a gaussian profile.

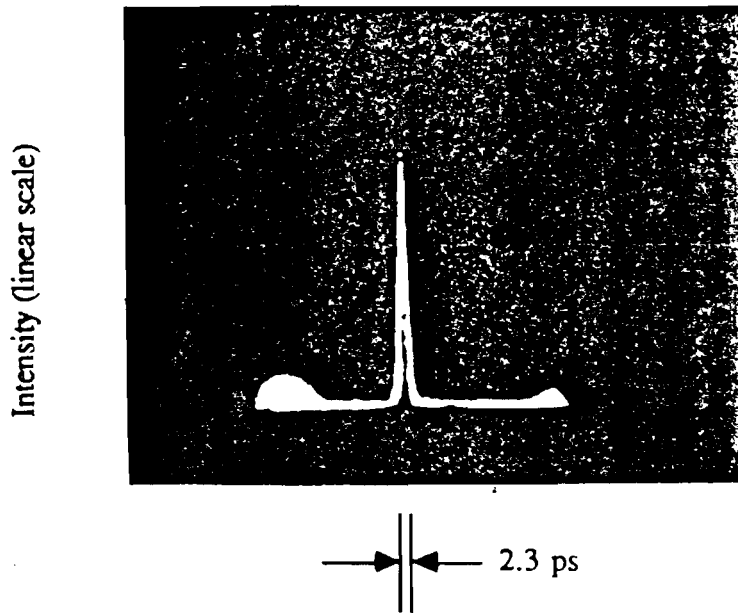


Figure 2 - 9. Autocorrelation measurement of compressed pulse

In previous compression experiments of $1.06 \mu\text{m}$ pulses, shorter fibre lengths were used because maximum power output was desired.¹² With the CPA technique, the stretched pulses are amplified and therefore the restrictions on the power in the fibre, because of Raman generation, are immaterial. The long fibre length required to linearize the chirp can then be used and the pulses can be compressed with

following set of equations to determine the optimum fibre length as a function of the input parameters: pulsewidth, peak power, fibre area and wavelength:¹⁶

$$z_0 = \frac{\tau_0^2}{C} \quad (2 - 17a)$$

$$C = \frac{D(\lambda) \lambda}{0.322\pi^2 c^2} = 0.031 \text{ m}^{-1} \text{ ps}^2 \quad (\lambda = 1.06 \text{ } \mu\text{m}) \quad (2 - 17b)$$

$$A = \sqrt{\frac{P}{P_1}} \quad (2 - 17c)$$

$$P_1 = \frac{nc\lambda A_{\text{eff}}}{16\pi z_0 n_2} = 7.92 \left[\frac{\lambda \text{ (cm)} A_{\text{eff}} \text{ (cm}^2\text{)}}{z_0 \text{ (cm)}} \right] \times 10^{14} \text{ (Watts)} \quad (2 - 17d)$$

$$Z_{\text{opt}} = \frac{1.6z_0}{A} \quad (2 - 17e)$$

where τ_0 is the input pulsewidth, P is the input peak power, λ is the wavelength, $D(\lambda)$ is the fibre dispersion, A_{eff} is the effective core area, n and n_2 are the linear and nonlinear refractive indices, respectively, c is the speed of light, and Z_{opt} is the optimum fibre length. It should be noted that 1.4 km is not the optimum length, but, rather the length of fibre we could obtain at the time. Although, as shown in the autocorrelation, the temporal profile is virtually wing-free to two orders of magnitude. For our parameters, the optimum fibre length is 2.2 km.

II. D. 3. Choice of Amplifying Media

A Quantel (SF 410-07) laser head was used for the amplifier. The laser head was fitted with a Nd:glass rod, 7 mm in diameter and 115 mm long. The glass (Kigre Q-246), was a lithium aluminum silicate glass, with a doping concentration of 2%. The gain material of the amplifier cannot be a Nd:YAG crystal, as in the oscillator, because the gain bandwidth of Nd:YAG is not large enough to accept the spectral bandwidth of the pulse, which has been broadened by SPM to 4.0 nm. The Q-246 glass has a fluorescent linewidth of 28 nm, whereas Nd:YAG has a linewidth of just 0.4 nm. Silicate glass was chosen as the host material, because the gain bandwidth peaks at 1.062 μm , which is near the lasing transition of a Nd:YAG laser, which is 1.064 μm .

II. D. 4. Regenerative Amplifier

The stretched pulses were amplified in a regenerative amplifier. A regenerative amplifier is basically a Q-switched laser, except that instead of starting from a noise spike, a laser pulse is switched into the cavity to act as the seed pulse. By using a regenerative amplifier, the laser pulse can be amplified many orders of magnitude with just one amplifier. Also, since the amplifier is run as a Q-switched laser, the pulse is amplified to the saturation level, so the amplification process is very efficient and can be quite stable.

The regenerative amplifier cavity, that was used, was made up of a 90% reflecting flat mirror and a 100% reflecting concave mirror, with a 5 m radius of curvature. The cavity length was approximately 1.5 m. A Pockels cell was placed directly in front of the curved mirror, where the beam diameter is largest in order to

avoid damage. KD*P is used for the electro-optic material because of its large damage threshold of 400 MW/cm^2 .⁹ A quarter-wave plate and Brewster plate polarizers were placed in the cavity to frustrate lasing in order to build up the population inversion. The gain medium was placed in the centre of the cavity and an adjustable pinhole was used in the cavity to force the beam to be in a TEM₀₀ mode.

The stretched pulses from the fibre pass through a half-wave plate, which is aligned to give S-polarization. The beam is then reflected from one mirror and then from an AR coated surface of a wedge. An AR coated surface was used to isolate the fibre from the output pulses of the regenerative amplifier, which are directed back along the input beam line. The energy of the seed pulse must be larger than any noise spike in order that the seed pulse be preferentially amplified. Pulse energies of just tens of picojoules are required for injection. The S-polarized beam is reflected into the cavity, by the polarizer and then passes through the $\lambda/4$ plate and Pockels cell. The Pockels cell is in its off state, that is, with zero voltage applied. The pulse is then reflected from the end mirror and makes a second pass through the Pockels cell and waveplate. The polarization of the pulse is rotated through 90° by a double pass of the $\lambda/4$ plate and so passes through the polarizer. The pulse is then amplified in the gain medium and reflected by the flat mirror. The pulse is amplified a second time and passes through the polarizer and again makes a double pass of the waveplate and Pockels cell. The polarization is again rotated by 90° , to S-polarization, and is reflected by the polarizer. Therefore, while the Pockels cell remains in the off-state, all the pulses make one complete round-trip.

The trigger signal to the voltage supply for the Pockels cell is timed, to apply the quarter-wave voltage, which is 4 kV for KD*P, at the peak of the fluorescence, and therefore Q-switch the laser at the peak of the gain. A hard tube Pockels cell driver was used, in order to have minimum jitter and maintenance, and a fast risetime.¹⁷ The

quarter-wave voltage turns on in less than 10 ns, which corresponds to one round trip of the cavity. The timing of the voltage signal is synchronized with the 41 MHz mode-locking signal of the oscillator, so that it can be fine tuned, to turn on after the pulse has made its first double pass of the wave plate and Pockels cell. With the voltage applied to the Pockels cell, it cancels the retardation of the quarter-wave plate. The pulse then remains in P-polarization and is trapped in the cavity.

As in a Q-switched laser, the energy of the pulse will increase to a saturation level and then decrease. The lamps were operated at an energy of 55 J, to give a saturation energy of 2 mJ. The energy is limited to 2 mJ because of the damage threshold of the KD*P Pockels cell. It takes approximately 1 μ s or 100 round trips, for the pulse to reach saturation. The Pockels cell voltage supply is triggered to deliver the half-wave voltage, at the time of the peak of the Q-switched envelope. Again the turn-on time was less than 10 ns. The total retardation of a double pass of the wave plate and the Pockels cell in this state is one half wave, so that the polarization is again rotated to S-polarization, and the pulse is reflected from the polarizer.

II. D. 5. Amplified Pulse Compression

The switched-out pulse is transmitted through the AR coated window and a half-wave plate before passing along the grating compressor. The half-wave plate is used to change the polarization to P-polarization for optimum energy efficiency of the gratings. The efficiency of the gratings, for S-polarization, is only a few percent. The energy efficiency of the compressor was approximately 60 %.

The pulsewidth of the amplified and compressed pulses was measured using a streak camera. In order to be detected by the photocathode, the pulses had to be frequency doubled. Figure 2-10 shows a streak camera trace of a pulse and a

reflection from an etalon. The spacing between the two pulses is 125 ps. The pulse width (FWHM) is 2 ps which is limited by the streak camera response. Regardless of any pulse distortion due to spectral and gain saturation of the amplifier, the pulse was compressed after amplification, indicating that the pulse chirp remains constant. This amplifier and compression system produced 2 ps pulses with energies of 1 mJ.

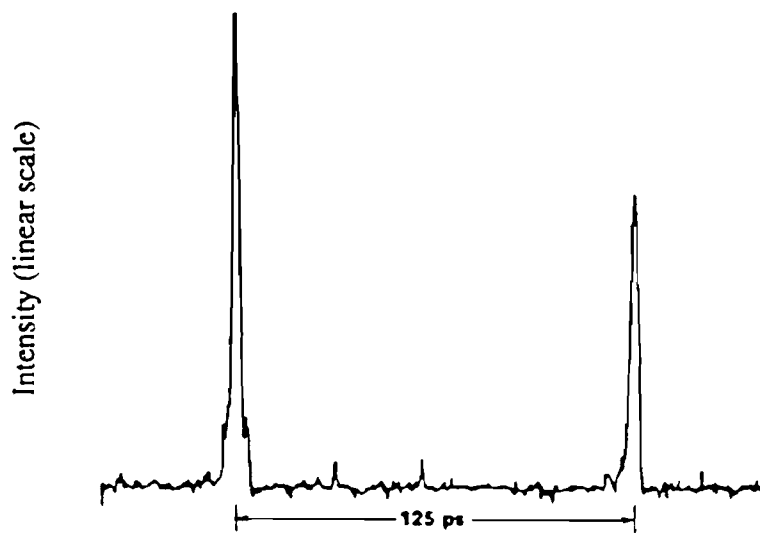


Figure 2 - 10. Streak camera trace of amplified and compressed pulse

II. D. 6. Improvements

The energy stability of the regenerative amplifier was very poor, with energy jitter of $\pm 50\%$. In order to determine if the laser instability corresponded to the flashlamp instability, Q-switched laser energy was measured and plotted as a function of flashlamp energy. The plot is shown in Fig. 2-11, and depicts a linear relation between the laser energy and the flashlamp energy.

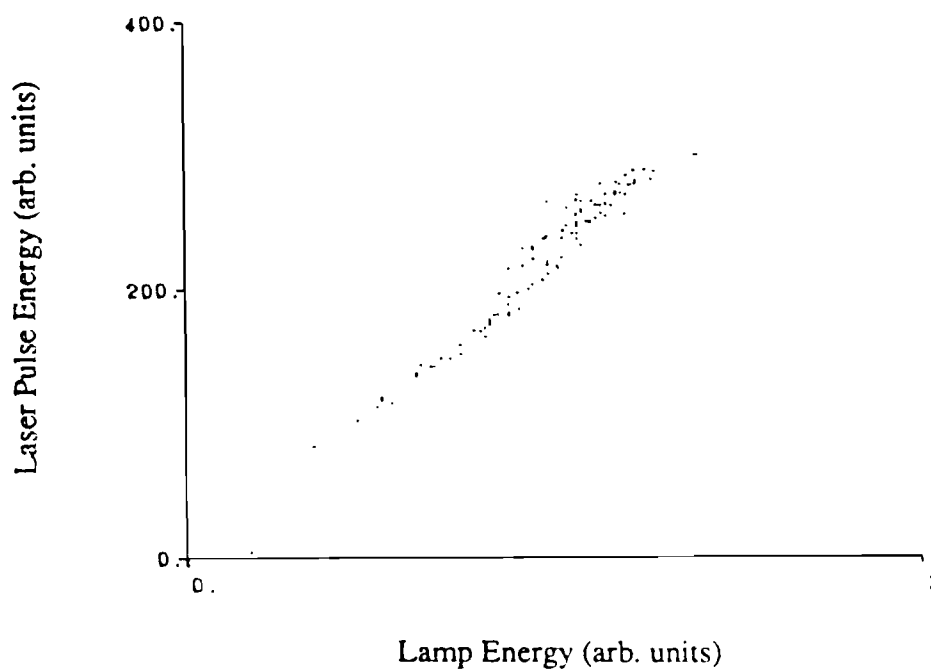


Figure 2 - 11. Laser pulse energy as a function of lamp energy

The flashlamp stability was $\pm 5\%$, which would be difficult to improve, with our amplifier. It was therefore necessary to compensate for the flashlamp jitter. A diode was set up to detect the flashlamp radiation. The electrical signal, from the diode, was electronically integrated, with a time constant of $350 \mu\text{s}$, which corresponds to the fluorescent lifetime of the gain medium. This electrical signal is then approximately the same as the fluorescent signal. The Pockels cell was triggered to the quarter-wave voltage, at a given time after the integrated flashlamp signal reached a threshold level of approximately half the peak signal. To determine the timing of the half-wave voltage of the Pockels cell, a second diode monitors the leakage from an end mirror of the regenerative amplifier cavity. A fast discriminator is used to trigger the cavity dumper, with respect to a particular mode-locked pulse, at the peak of the Q-switch pulse. By monitoring the flashlamps and the Q-switched train

an energy histogram of 2000 shots measured both (a) before and (b) after the grating compressor. Comparison of the two histograms indicates that the compression process does not introduce energy instability.

A second problem encountered was that the amplifier would produce multiple pulses, which were separated by 6 ps. A comparison was made of the SPM spectrum of the pulses, that were injected into the amplifier, and the amplified pulse spectrum. The two spectra are shown in Fig. 2-13. The amplified pulse spectrum shows that the red end, which is also the front end of the pulse is preferentially amplified, but, also that there is a 0.3 nm modulation. The modulation as well as the 6 ps pulse separation indicates the presence of a 1 mm thick etalon inside the cavity. The etalon could only be the quarter-wave plate. The multiple pulsing was eliminated by removing the quarter-wave plate and aligning the Pockels cell, such that its off state birefringence yielded a quarter-wave retardation.

II. E Table Top Terawatt Laser System

Once the concept of the CPA technique was shown to work, amplification stages were added to increase the energy to the Joule level. A second stage was added that brought the energy level to 40 mJ.¹⁸ A schematic of this amplification system is shown in Fig. 2-14.

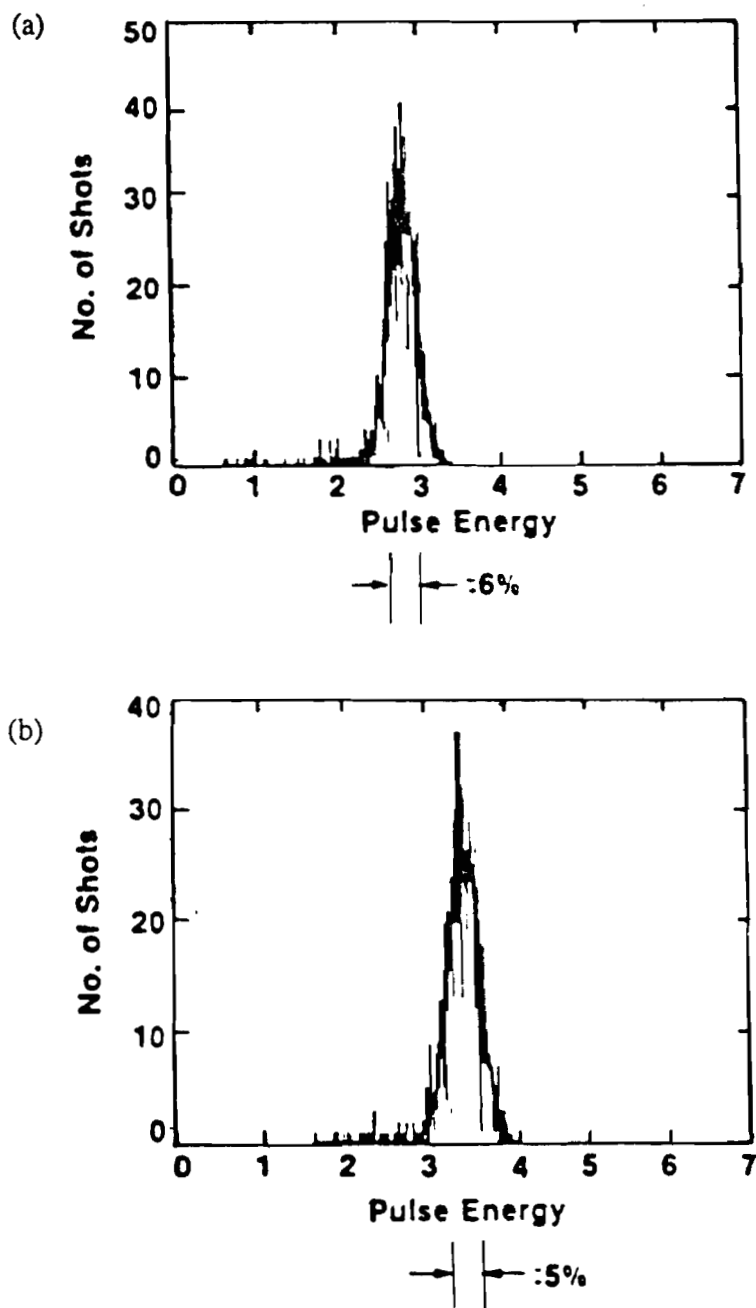


Figure 2 - 12. Pulse energy histogram of 2000 shots (a) before, (b) after grating compressor

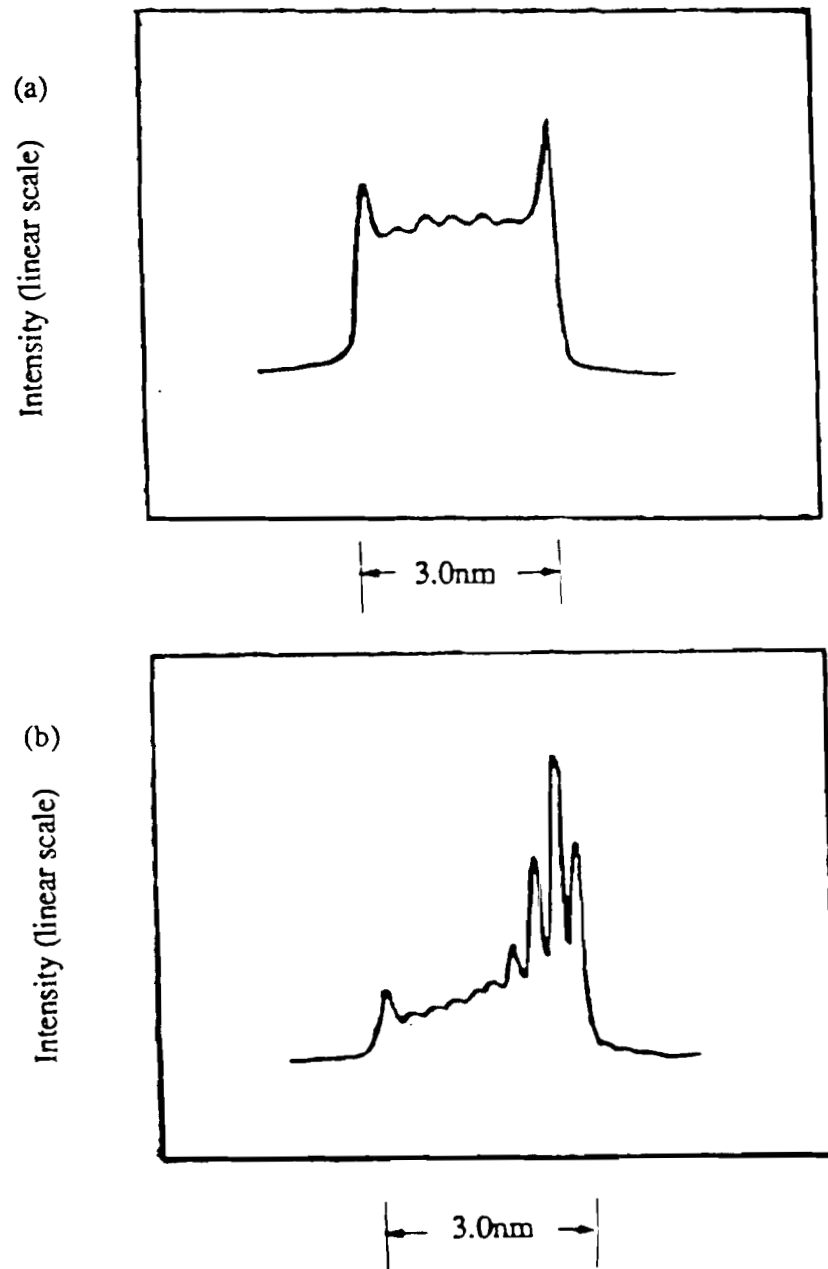


Figure 2 - 13. Frequency spectrum (a) before and (b) after amplification

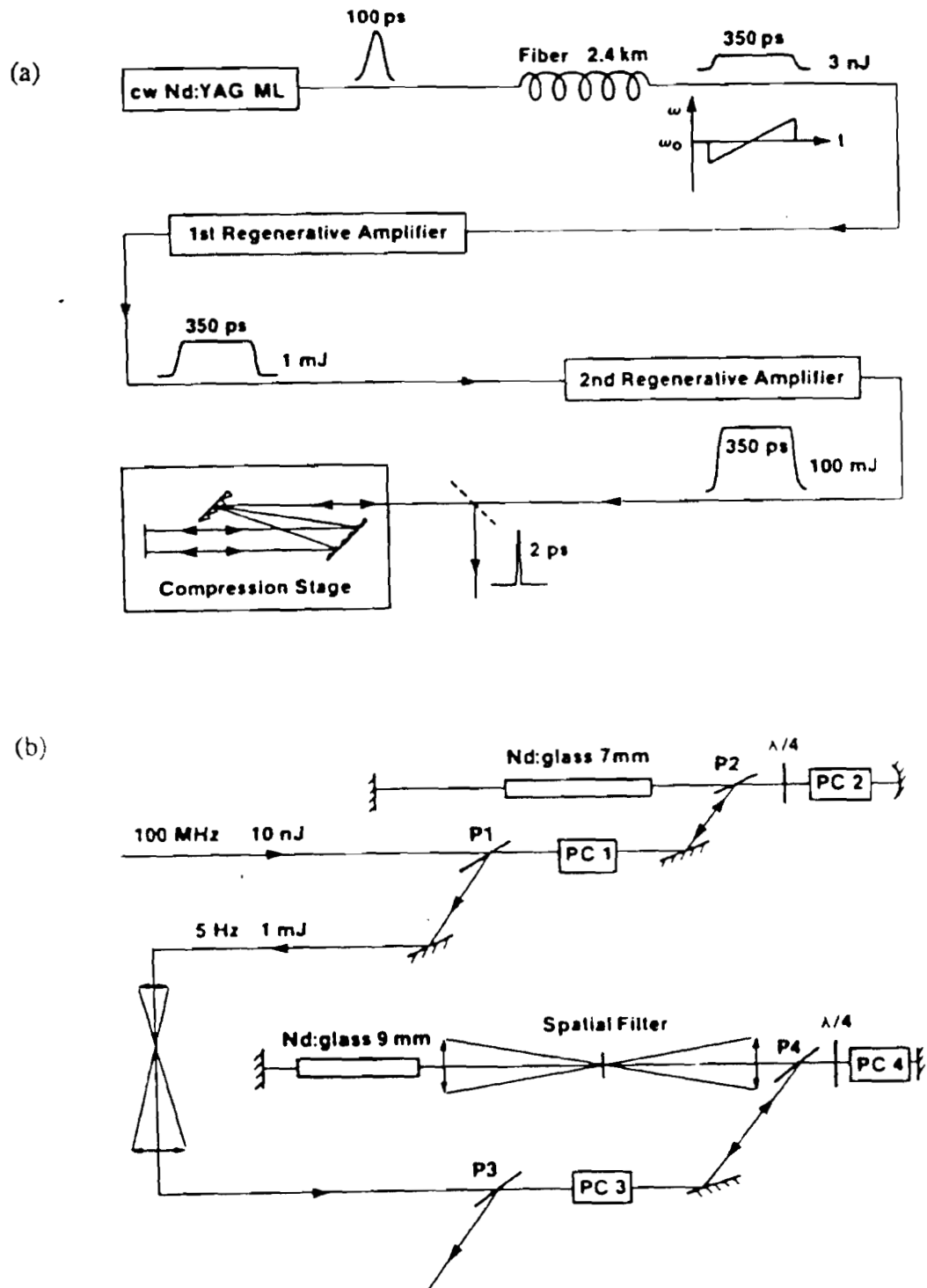


Figure 2 - 14. (a) Block diagram of 40 mJ CPA system, (b) amplifier configuration

II. E. 1. Fibre Expansion

The oscillator was changed to a CW mode-locked Nd:YAG, [Quantronix model 416], that produced 100 ps pulses at a 100 MHz repetition rate. The pulse was stretched to 200 ps by the GVD of the 1.4 km fibre, as can be seen in Fig. 2-15. Again, the power in the fibre was set at the threshold power for Raman generation, in order to have the optimum stability of the compressed pulses. At higher input powers, we measured the two pulses generated by SPM and Raman generation, with a fast diode and a sampling scope. The result is given in Fig. 2-16. It shows that the pulsewidth of the SPM pulse is about 200 ps and that the separation between the Raman and SPM pulses is 2 ns, for the 1.4 km length of fibre.

The fibre length was increased to 2.4 km to further improve the linearity of the chirp and reduce the compressed pulsewidth. The pulse was stretched to 350 ps, in this fibre, as is shown in Fig. 2-17, but, the compressed pulsewidth remained at 1.5 ps. The limitation of the pulsewidth is caused by the third order term of the group delay of the grating compressor, which will be discussed in a later section.¹⁹ Figure 2-17 also shows that the pulse shape is no longer rectangular when stretched to 350 ps. The front end of the pulse is reduced by the onset of Raman generation.

Instead of using an AR coated window to isolate the fibre, from the regenerative amplifier output, a Pockels cell, PC2, switch-out was used. PC2 was placed between two parallel polarizers. A half-wave plate was placed between the fibre output and the first polarizer in order to rotate the polarization, for maximum output through the polarizers. When PC2 was in the off state, the pulses would be transmitted through the second polarizer. Two 100% reflecting mirrors were used to deflect the pulse into the cavity, so that the total pulse energy was seeded into the cavity. When the amplified pulse was cavity dumped by the Pockels cell, PC1, inside the regenerative

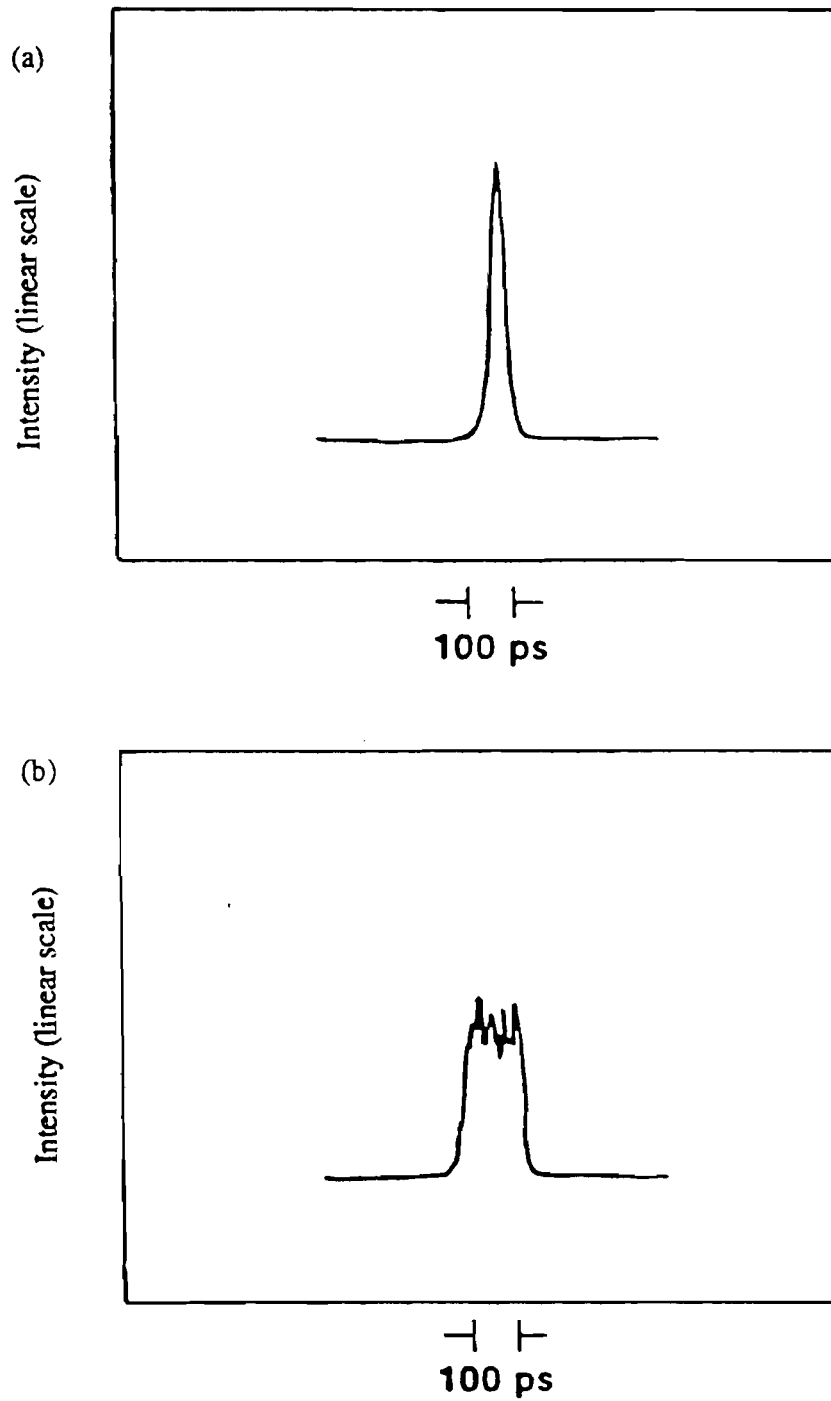


Figure 2 - 15. Streak camera traces of frequency doubled pulses at the (a) input and (b) output of the fibre

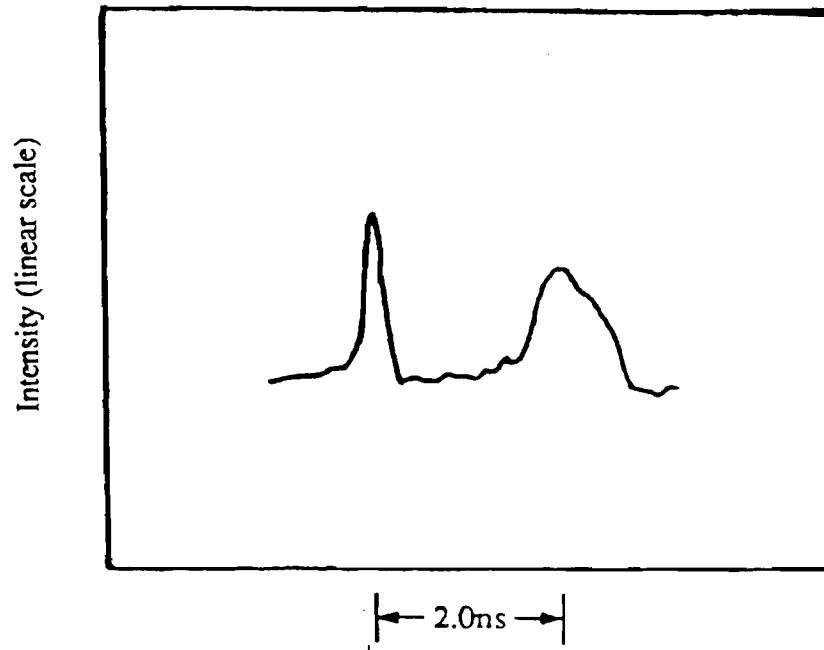


Figure 2 - 16. SPM and Raman generated pulses at output of fibre

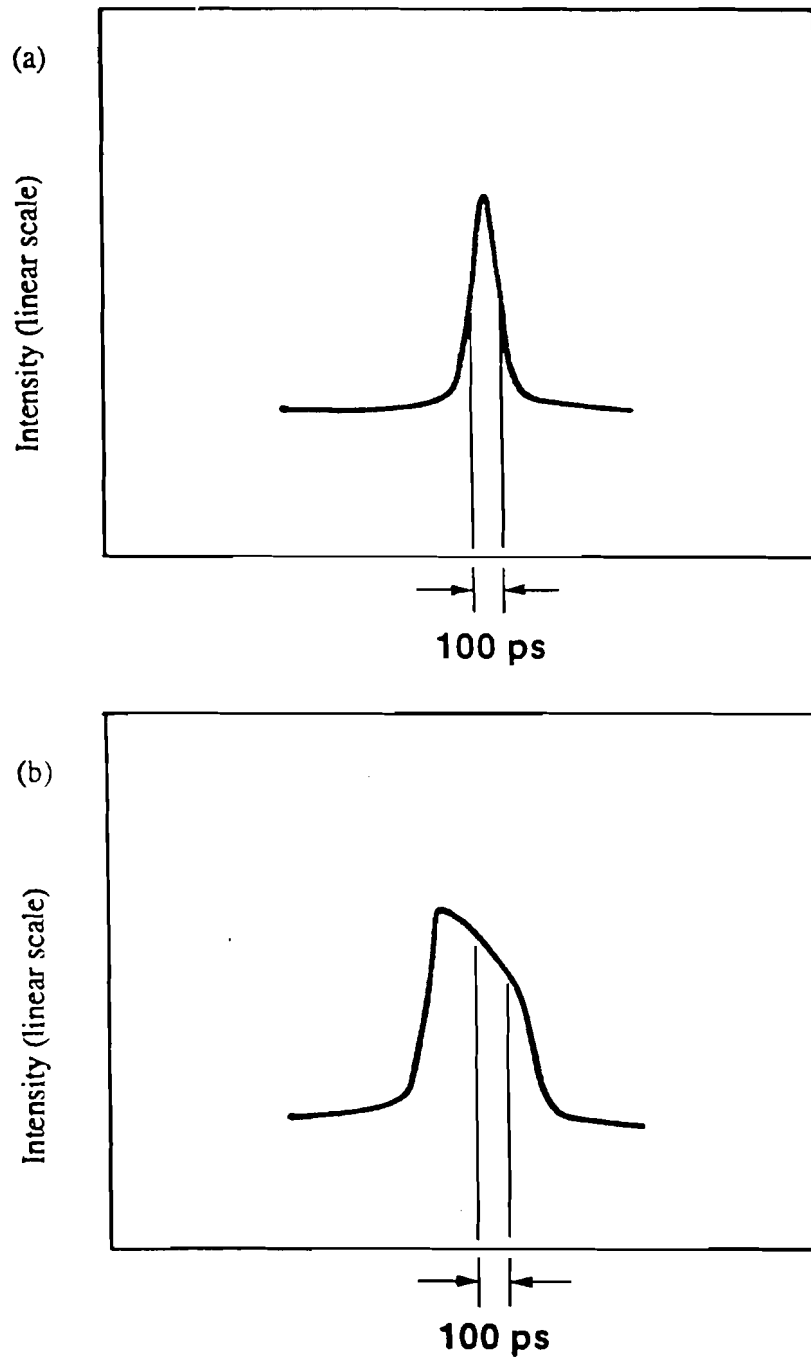


Figure 2 - 17. Streak camera traces of IR pulses at the (a) input and (b) output of the 2.4 km fibre

amplifier, it was reflected back through the second polarizer to PC2. The same trigger signal that was used to cavity dump the amplifier, was used to switch PC2. The timing of the trigger signal to PC2 was delayed such that it coincided with the arrival of the amplified pulse. PC2 was then turned on, that is a half-wave voltage was applied. The polarization was rotated by 90° and so the pulse was reflected by the first polarizer.

The Pockels cell, PC2, could also turn on and off, in 10 ns, so that only one pulse would be switched out. This improved the contrast ratio, of pulse to prepulse energy, to better than 1000 : 1. The Pockels cell driver could not deliver the 8 kV, required for half-wave rotation, in 10 ns. The polarization was therefore not rotated the entire 90° , so that only 80% of the pulse energy was reflected by the polarizer. The remaining 20% was transmitted through the polarizer, back to the fibre. This was enough energy to damage the fibre end. To stop the energy from reaching the fibre, a 99%, 45° , reflecting mirror was placed after the fibre output. The pulse train that was reflected by the mirror was sent to a second grating compressor, so that the CW pulse compression could be continually monitored. The remaining 1% of the pulse energy was transmitted through the mirror, Pockels cell and polarizers, and was seeded into the regenerative amplifier. The mirror reflected the retroreflected amplified beam away from the fibre.

II. E. 2. 100 mJ Amplification

In order to increase the pulse energy a larger gain medium was required. The amplifier (Quantel SF410-09), uses four xenon flashlamps to pump the laser rod. The Nd:YAG rod was again replaced with a Kigre Q-246, silicate glass rod, 3/8" in diameter and 11.5 cm long. A multipass configuration was used for the second

amplifier, in order to extract the maximum energy. The capacitance of the Quantel power supply was increased by a factor of 3, to 90 μF , for each set of two lamps, so the gain was sufficient to reach an energy of 40 mJ, with only a few passes. The lamps were run at a voltage of 1.9 kV. A gain of 2, per pass, was achieved for this lamp energy.

The output of the regenerative amplifier was up-collimated by a factor of 3 in order to fill the 9 mm rod. A third Pockels cell, PC3, is used to isolate the first amplifier stage from the second, in the same way that PC2 isolates the fibre from the first amplifier.

The second cavity was comprised of two flat 100% reflecting mirrors, with a 1:1 collimating spatial filter in the centre. The gain medium was placed between one end mirror and the spatial filter, and the quarter-wave plate, polarizers and a fourth Pockels cell, PC4, were placed at the other end of the cavity. The cavity length was approximately 2 m. The pulses were trapped in the second cavity in the same manner as in the first cavity. The timing of Pockels cells, PC3 and PC4, were all triggered by the cavity dumping trigger, and delayed to coincide with the arrival of the pulses. Krytron drivers were used to apply the high voltage, to the Pockels cells, PC3 and PC4, because of the availability of Krytron drivers, and the fact that the repetition rate of the amplifier, was just 0.02 Hz. The pulse was switched out after 10 roundtrips, with an energy of 40 mJ, which is less than the saturation energy, to avoid laser damage.

The gratings used have dimensions 59x59 mm and a damage threshold of about 50 mJ/cm^2 as will be discussed later. Because of this energy limitation, the 40 mJ pulse was attenuated before compression to avoid damage. The compressed pulsewidth was again measured using a streak camera and the result is shown in Fig. 2-18. Again the compressed pulsewidth was limited to 2 ps.

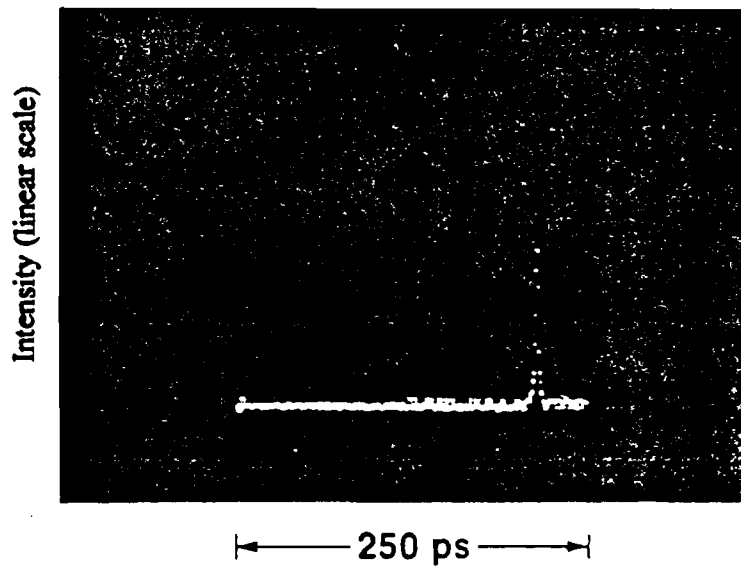


Figure 2 - 18. Streak camera trace of compressed 40 mJ pulse

This multipass amplifier configuration proved to have poor stability. Silicate glass suffers from strong thermal focusing and birefringence. Although we used a large pinhole (0.5 mm which was 10 times the Airy disc), the beam continually walked off.

The second stage was then changed to a short, 4 pass system. This configuration is shown in Fig. 2-19. The pulse first passes through a polarizer and Pockels cell in the off state, then a second polarizer. The polarization is then converted to circular, by a quarter-wave plate. The pulse then makes one pass through the amplifying medium and is reflected by a 100%, flat mirror that is placed directly after the amplifier. After the second pass through the amplifier, the polarization is rotated to S-polarization by the second pass of the $\lambda/4$ plate. The pulse is reflected off the

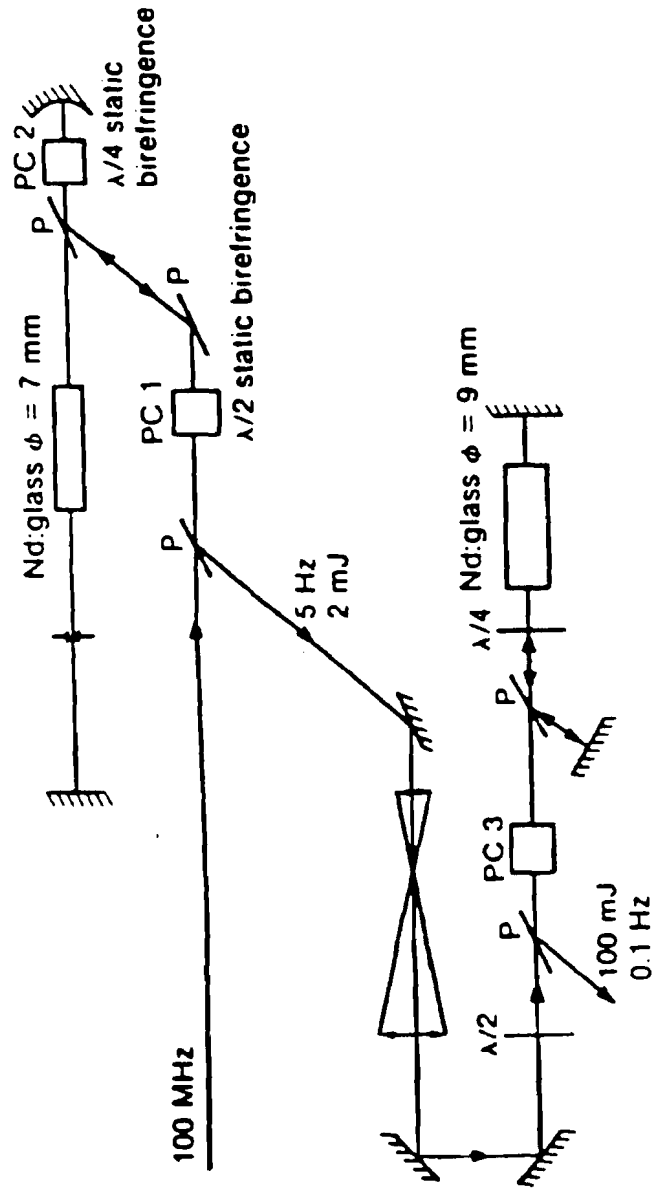


Figure 2-19. Regenerative amplifier and four pass system configuration

second polarizer to a 100%, flat mirror. The pulse is retroreflected and makes another double pass of the amplifier. The polarization is rotated to P-polarization by the double pass of the $\lambda/4$ plate, and the pulse passes through the second polarizer and Pockels cell. The half-wave voltage is applied to the Pockels cell in time to coincide with the reflected pulse. The polarization is again rotated by the Pockels cell, to S-polarization and the pulse reflects off the first polarizer. This amplifier produced 100 mJ pulses for a lamp energy of 725 J at a repetition rate, of 2 pulses per minute.

II. E. 3. 1 Joule Amplification

A double pass through a third amplifier was made, to bring the energy to the Joule level. The amplifier used was a Quantel SF320, which uses four xenon flashlamps to pump the rod. The gain medium was again a silicate glass rod, 16 mm in diameter and 26 cm long. The flashlamps were pumped at a voltage of 2 kV, to deliver a lamp energy of 96 kJ. The double pass gain, for this lamp energy was 13. Due to thermal loading of the rod, at this energy, the amplifier could only be fired once a minute. At the output of the third stage, the pulse energy was 1.3 J.

Again the amplified pulses were attenuated before compression and measured with a streak camera. The result, shown in Fig. 20, was once again a streak camera limited pulsewidth of 2 ps. Although, the pulse energy was not one Joule at the output of the compressor, this result showed that a chirped pulse could be amplified over 9 orders of magnitude from the nJ to the J level and be compressed to a two picosecond pulsewidth.²⁰

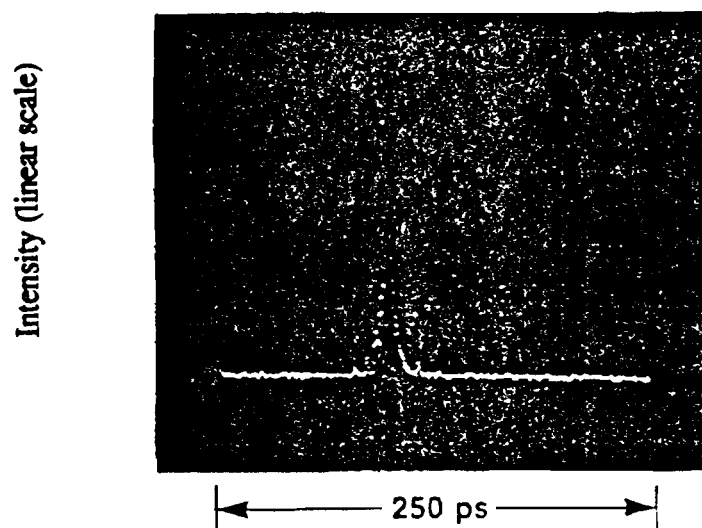


Figure 2 - 20. Streak camera trace of a 1.3 J, 2 ps pulse

II. E. 4. Nd:YLF / phosphate glass

Most large glass laser systems use phosphate glass rather than silicate glass because of its superior thermal properties. However, phosphate glass amplifiers cannot be used in conjunction with Nd:YAG oscillators because of the wavelength mismatch of 10 nm, and CW mode-locked glass lasers do not produce sufficient power, to be compressed by fibre compression techniques. The lasing wavelength of Nd:YLF matches that of phosphate glass amplifiers exactly and can therefore be used as the oscillator for a phosphate glass system. At the Laboratory for Laser Energetics, a CW mode-locked Nd:YLF laser was developed which produces 50 ps pulses at 100

MHz with 1 W of average power.²¹ Nd:YLF oscillators can produce shorter mode-locked pulsewidths than Nd:YAG lasers because of the larger linewidth of 1.35 nm rather than 0.45 nm and so can produce shorter compressed pulses.

The oscillator of our CPA system was therefore switched to a Nd:YLF laser and the silicate glass rods in the amplifiers were replaced with phosphate glass (Kigre Q-98) rods, with a doping concentration of 6%. The schematic of this CPA system is shown in Fig. 2-21. To achieve even shorter pulsewidths than 50 ps, the mode-locker was run at the double harmonic frequency of 100 MHz.²² Pulsewidths as short as 30 ps were achieved, but the pulsewidth stability was poor. To have optimum stability the mode-locker was aligned such that the pulsewidth remained at 50 ps. To further improve the stability of the compressed pulsewidths, a mode-locker stabilizer was implemented. It varies the RF power to the modulator, to maintain a constant temperature and thereby keep the quartz crystal in resonance with the modulating frequency.

A 1.3 km length of fibre was used to stretch the pulsewidth to 300 ps and the bandwidth to 4.0 nm. The backward Rayleigh scattered light from the fibre, coupled back into this oscillator and disturbed the mode-locking. In order to isolate the oscillator from the back scattered light, a Faraday isolator was placed between the fibre and oscillator. The CW pulses were then compressed by a double pass of a double grating compressor. Again the grating constant was 1700 l/mm and the gratings were used in a near Littrow configuration. To compensate for the frequency chirp of 4.0 nm over a 300 ps pulsewidth, the gratings were placed ~ 50 cm apart. The compressed pulsewidth was 1.0 ps.

A kinematic mount with a 45° mirror, was placed before the compressor, to reflect the light into a second short fibre, which transports the stretched pulses to the room with the amplifiers. The amplification system was basically the same. A Faraday isolator was used to isolate the fibre from the amplified pulse that leaked through the Pockels cell switch-out, rather than the 45° mirror. The phosphate glass exhibited higher gain so the 7 mm and 9 mm amplifiers were run at lower energies : 30 J and 200 J respectively. The pulse energy from the regenerative amplifier was kept at 2 mJ to avoid laser damage of the KD*P Pockels cell. Also, an energy level of 1 J could be achieved in a single pass of the 16 mm amplifier. Thermal focusing was greatly reduced so that we could run at higher repetition rates. The 100 mJ amplifier could run at 0.1 Hz and the 1 Joule system could operate 2 shots per minute.

The gratings were 80 by 110 mm² in dimension. The separation of the gratings was ~ 2 m. The grating compressor was used in a single pass configuration so that the beam diameter could be increased to fill the entire grating and allow an energy of 0.6 J. The single pass efficiency was 85% to yield a 0.5 J pulse. A single shot autocorrelator was used to measure the amplified and compressed pulse.²³ The result is depicted in Fig. 2-22. The temporal profile most closely matches a Lorentzian profile with correlation width of 1.4 ps, which corresponds to 0.7 ps pulse duration.

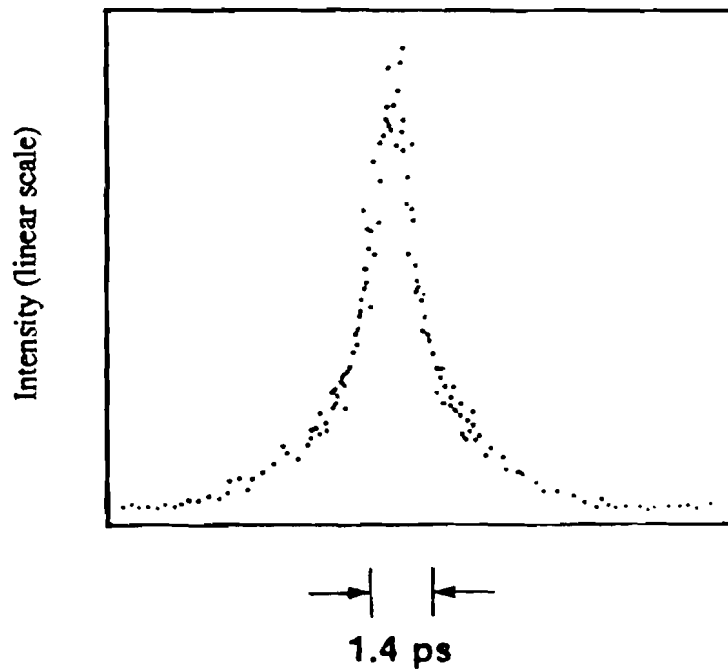


Figure 2 - 22. Autocorrelation of 0.5 J compressed pulse - Correlation width = 1.4 ps

II. E. 5. Grating Expansion

The dispersion of a grating pair has been considered in the previous sections to be linear and so capable of perfectly compressing a linearly chirped pulse. The dispersion of a grating pair is only linear to a first order approximation. For either large bandwidths or large compression ratios the third order term in the phase delay of the grating pair becomes significant and the compressed pulse is left with a residual quadratic phase distortion. The group time delay for a pair of parallel gratings can be expanded in a Taylor series, which to second order is given by:

$$\tau(\lambda_0 + \Delta\lambda) = \tau_0 + \frac{2\lambda_0 L m^2}{c d^2 \cos^3 \theta} \Delta\lambda + \frac{3L m^2}{c d^2 \cos^3 \theta} \left[1 + \frac{\lambda_0 m \sin \theta}{d \cos^2 \theta} \right] (\Delta\lambda)^2 \quad (2 - 18a)$$

$$= \tau_0 + \tau_1 + \tau_2, \quad (2 - 18b)$$

where $\lambda = \lambda_0 + \Delta\lambda$, is the wavelength, λ_0 is the central wavelength, c is the speed of light, L is the distance between the gratings, m is the diffraction order, d is the groove spacing, and θ is the diffracted angle. The grating spacing of the compressor is adjusted such that the frequency chirp is compensated by τ_1 , leaving the pulse with a group time delay of τ_2 . The ratio of the second order term to the first order term is then:

$$\frac{\tau_2}{\tau_1} = \frac{3}{2} \frac{\Delta\lambda}{\lambda_0} \left[1 + \frac{\lambda_0 m \sin \theta}{d \cos^2 \theta} \right]. \quad (2 - 19)$$

The quadratic term grows linearly with the compression factor given by τ_1 . Also the second order group delay increases with bandwidth. When the gratings of the CPA system are set to compress a 300 ps pulse, with a 3.0 nm bandwidth, the pulse is left with a quadratic time delay of approximately 10 ps. This value is already large and certainly the pulse cannot be stretched further in a fibre to allow the amplification of 1 ns pulses. The quadratic term therefore limits the compression factor and the ultimate pulsewidth by limiting the bandwidth.

It has been shown that for short pulse dye laser systems, prisms can be used to compensate for the second order group delay of the gratings and add zero first order.¹¹ This form of solution is not practical for the 50 ps pulses from the Nd:YLF laser because it would require exceedingly large distances between the prisms.

Martinez has shown theoretically that gratings in an antiparallel configuration, can give positive group dispersion and that all orders of group time delay can be compensated by a pair of parallel gratings.²⁴ Pessot and co-workers showed this experimentally, by expanding a 100 fs dye laser pulse 1000 times to a duration of 100 ps and then recompressing it back to 100 fs, with a grating expander and a grating compressor.²⁵

By using grating expanders rather than fibre expanders, the pulse can be stretched over several orders of magnitude and be recompressed to their original pulsewidth. Fibres are required, however, to generate larger bandwidths by SPM, in order to produce shorter compressed pulsewidths than the original width. Also, the fibre must be long enough to generate the required GVD, necessary to have a linear chirp across the pulse duration. For larger expansion ratios a grating expander should be used. Maine showed that the pulse could be stretched to 1 ns, then amplified to the 2 mJ level and recompressed to 0.8 ps.²⁶ In order to have a 1 ns pulse duration for efficient amplification, both an 800 m length of fibre and a grating expander, comprised of two antiparallel gratings and a 1:1 collimating telescope were used. The combined action of the SPM and GVD of the fibre produced a 3.0 nm bandwidth over a 150 ps pulsewidth. The gratings again had a grating constant of 1700 l/mm and were placed within the focal planes of the lenses of the telescope. The separation of the gratings was ~ 3 m. Four passes were made to stretch the 150 ps pulse to 1 ns. The configuration is shown in Fig. 2-23. The grating expander was placed after the short fibre that brought the 150 ps pulses from the other room. The 1 ns pulses were injected into the regenerative amplifier as they were before. A double pass of the grating compressor was made to compress the pulses to the 0.8 ps duration.

Since the 0.5 J pulse could only be compressed with the available gratings in a single pass configuration, they were not wide enough to handle the dispersion required to compress a 1 ns pulse to 1 ps duration. The expander was changed to a double pass

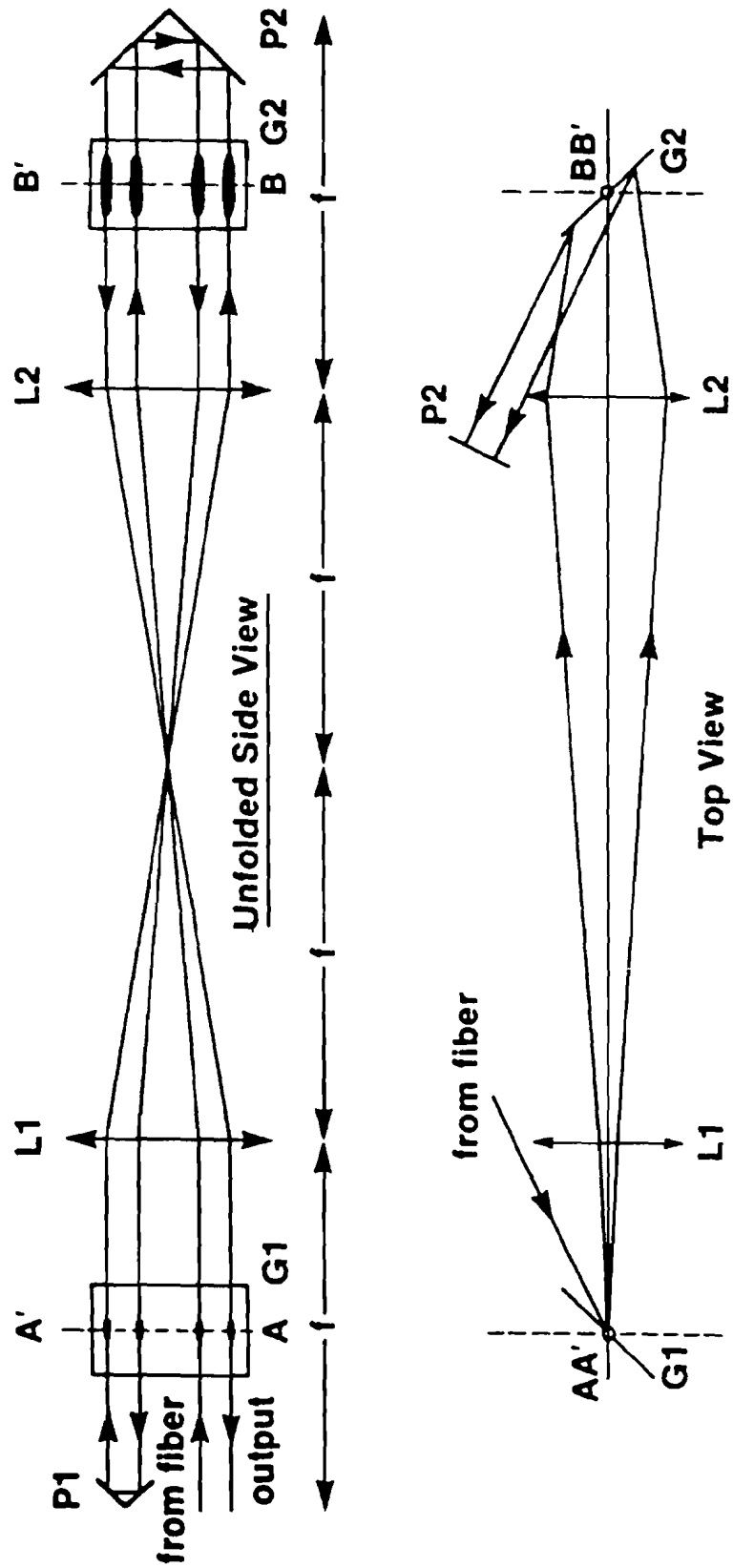


Figure 2 - 23. Four pass grating expansion configuration

configuration, which stretched the pulse to 500 ps. The separation of the compression gratings was set to ~ 2.5 m to achieve a compressed pulsewidth of 1 ps.

II. E. 6. Grating Damage Threshold

The gratings used in the present compression system are gold coated holographic gratings. The damage threshold of these gratings is the limitation on the energy that is achievable, with this type of amplifier system. Two different damage tests were performed on these at the Laboratory of Laser Energetics. The first test used a well characterized 0.8 ns, 1 J Nd:glass laser system. The beam profile is measured with a 256 x 256 pixel CID camera. The grating was moved after each laser shot. The damage sight was photographed, with a field of view of 600 x 800 μm , before and after the shot. This test showed that for a laser flux of more than 100 mJ/cm^2 , the gold coating would damage if there was a micron sized scratch present at the spot previous to the laser shot.

The second test used the CPA laser system to generate 1 ps, 100 mJ pulses, to determine if the damage threshold was pulsewidth dependent. Again the threshold flux was 50 -100 mJ/cm^2 . The spot size could only be determined to a within a factor of two, which lead to the error in the flux measurement.

Dichromated gelatin holographic gratings were also damage tested in the same manner. The damage threshold flux was found to be 1 J/cm^2 , which is better than the gold coating by an order of magnitude. To date, dichromated gelatin gratings have not been made to have the high dispersion and energy efficiency at a wavelength of 1.05 μm , that is required for a CPA laser system.

References

1. Donna Strickland and Gerard Mourou, *Opt. Commun.* 56, 219 (1985)
2. C. E. Cook, *Proc. IRE* 48, 310 (1960)
3. F. Gires and P. Tournois, *Compte. Rend. Acad. Sci. (Paris)*, 258, 6112 (1964)
4. J. A. Giordmaine, M. A. Duguay, and J. W. Hansen, *IEEE J. Quantum Electron.* QE-4, 252 (1968)
5. E. B. Treacy, *Phys. Letters*, 28A, 34 (1968)
6. Robert A. Fisher, P. L. Kelley and T. Gustafson, *Appl. Phys. Lett.* 14, 140 (1969)
7. R. H. Lehberg and J. M. McMahon, *Appl. Phys. Lett.* 28, 204 (1976)
8. W. Knox, and G. Mourou, *Opt. Commun.* 37, 203 (1981)
9. W. Koechner, Solid-State Laser Engineering, (Springer-Verlag, New York,

Heidelberg, Berlin, 1976), p.511

10. H. Nakatsuka, D. Grischkowsky, and A. C. Balant, *Phys. Rev. Lett.* 47, 910 (1981)
11. R.L. Fork, C.H. Brito Cruz, P.C. Becker, and C. V. Shank, *Opt. Lett.* 12, 483 (1987)
12. J. D. Kafka, B. H. Kolner, T. Baer, and D. M. Bloom, *Opt. Lett.* 9, 505 (1984)
13. P. M. W. French, A. S. L. Gomes, A. S. Gouveia-Neto, and J. R. Taylor, *IEEE J. Quantum Electron.*, QE-22, 2230 (1986)
14. N. J. Halas and D. Grischkowsky, *Appl. Phys. Lett.* 48, 823 (1986)
15. J. Desbois, F. Gires and P. Tournois, *IEEE J. Quantum Electron.*, QE-9, 213 (1973)
16. R. H. Stolen and C. V. Shank, *Ultrafast Phenomena IV*, Ed. D. H. Auston and K. B. Eisenthal (Springer - Verlag, Berlin, 1984) p. 46
17. P. Bado and M. Bouvier, *Rev. Sci. Instrum.* 56, 1744 (1985)

18. D. Strickland, P. Maine, M. Bouvier, S. Williamson, and G. Mourou, *Ultrafast Phenomena V*, Ed. G. R. Fleming and A. E. Siegman (Springer - Verlag, Berlin, 1986) p. 38
19. D. McMullen, *Appl. Opt.* 18, 737 (1979)
20. P. Maine, D. Strickland, M. Bouvier, G. Mourou, paper FR2, CLEO (1987)
21. P. Bado, M. Bouvier and J. Scott Coe, *Opt. Lett.* 12, 319 (1987)
22. M. F. Becker, D. J. Kuizenga, and A. E. Siegman, *IEEE J. Quantum Electron.* QE-8, 687 (1972)
23. J. Janszky, G. Corradi, and R. N. Gyuzalian, *Opt. Commun.* 23, 293 (1977)
24. O. E. Martinez, J. P. Gordon and R. L. Fork, *J. Opt. Soc. Am. A* 1, 1003 (1984)
25. M. Pessot, P. Maine, and G. Mourou, *Opt. Commun.* 62, 419 (1987)
26. P. Maine and G. Mourou, paper FF2 CLEO (1988)

CHAPTER III

MULTI-PHOTON IONIZATION EXPERIMENTS

Multi-photon ionization has been studied extensively in the past twenty years. Some of the experiments were mentioned in Chapter I. In particular, the Saclay group¹ has thoroughly studied multi-photon ionization at a wavelength of 1.064 μm , over an intensity range of 10^{11} to 10^{15} W/cm^2 . At an intensity of 1×10^{15} W/cm^2 , maximum charge states of He^{2+} , Ne^{2+} , Ar^{3+} , Kr^{4+} , and Xe^{4+} were observed. One of the early experiments studied the effect of laser coherence on the ionization rate.² It was observed that multi-mode lasers created a higher ionization rate than single mode lasers. This increase was attributed to the modes beating and creating peaks of higher intensities than the average measured intensity. The role of wavelength was studied by comparing the infrared results for xenon and neon with those obtained at the second harmonic.³ The charge states Xe^{4+} and Ne^{2+} were created at a green intensity approximately an order of magnitude less than in the IR experiments. The pulse width of a Nd:glass laser was varied between 5 and 200 ps to determine the effect of pulse duration.⁴ At 200 ps the second charge state was produced only by sequential ionization. As the pulse width decreased, direct ionization was observed at low intensities. At the lowest pulse duration of 5 ps, only direct ionization to the second charge state was observed.

The CPA laser system is an ideal source to extend the near infrared experiments to the intensity range of 10^{17} W/cm^2 . We have measured, the relative ion yield and recorded it as a function of laser intensity for five noble gases: helium, neon, argon,

krypton, and xenon.

The frequency of the laser radiation was doubled, with 25% efficiency, and the role of wavelength was investigated by comparing the ion yields for the two different wavelengths, for all five gases. The uncompressed pulses of the CPA laser are 200 ps long and have the same frequency bandwidth as the 1 ps pulses. These long pulses were used to ionize xenon atoms to determine the effect of pulse duration and bandwidth on the multi-photon ionization process.

III. A. Experimental Technique

A schematic of the experimental system is shown in Fig. 3-1. The amplified and compressed pulses are focused into a vacuum chamber by a 20 cm focal length lens. The beam diameter was 5 cm resulting in effective $f/4$ focusing. The lens was placed directly before the input window of the interaction chamber. The experimental configuration of the interaction chamber is shown in Fig. 3-2. A six inch liquid nitrogen trapped diffusion pump was used to pump the interaction chamber to a background pressure of $\sim 1 \times 10^{-8}$ Torr. The air intake line was connected to a N_2 gas line, so that the chamber was never vented to room air. The gas bottles were connected to the chamber by a two foot length of $5/8$ inch stainless steel pipe, isolated from the chamber by means of a leak valve. To minimize the contaminants in the pipe, it was baked out overnight. In order to have a continuous leak of gas into the chamber, the pipe was initially filled with the gas with the leak valve closed. The gas bottle valve was then closed and the leak valve opened. In order to flush out contaminants from the chamber, the gas was introduced to the chamber to an excessive pressure of greater than 10^{-4} Torr. The gas was then pumped down to a pressure of

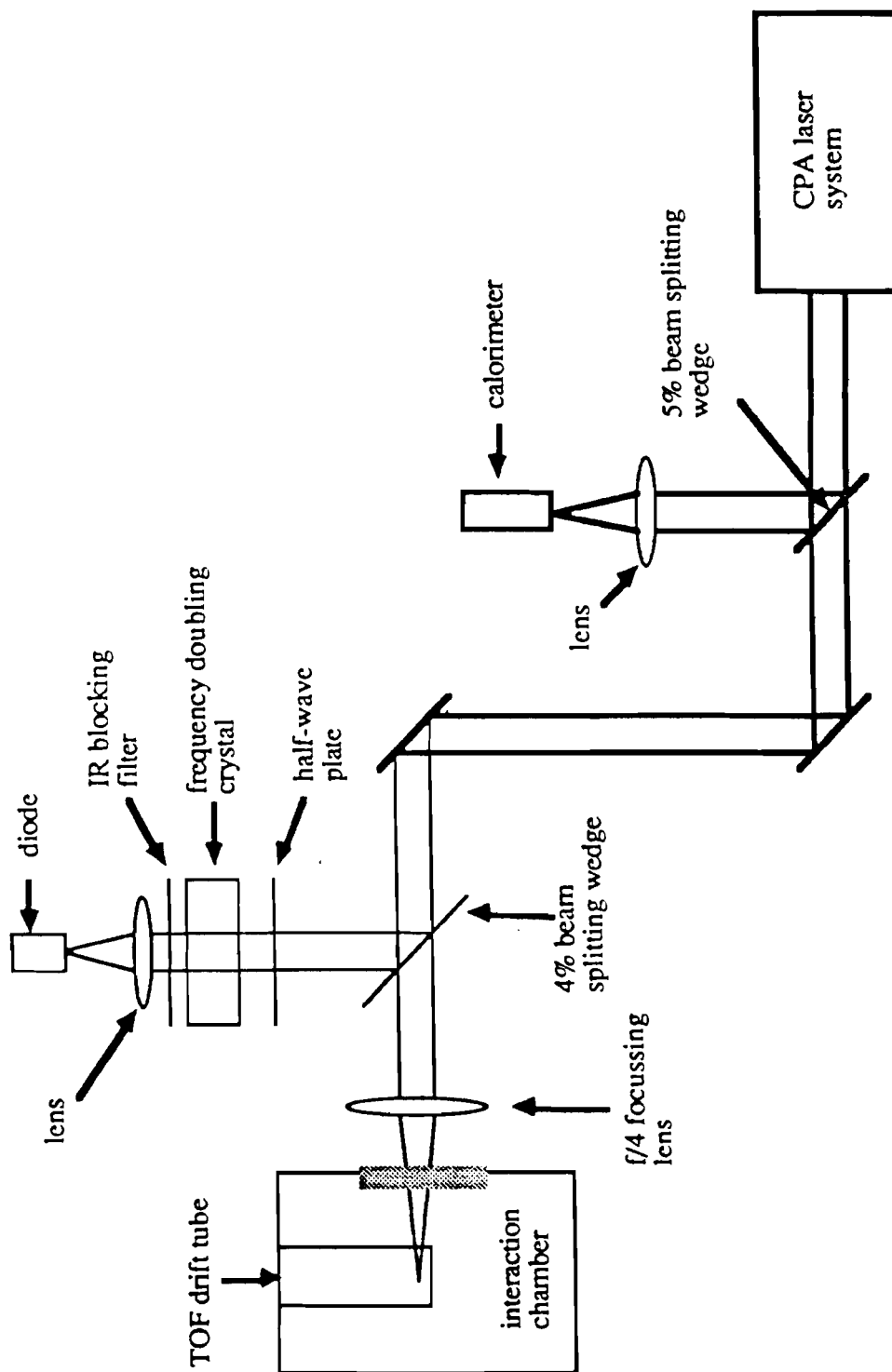


Figure 3 - 1. Schematic of experimental system

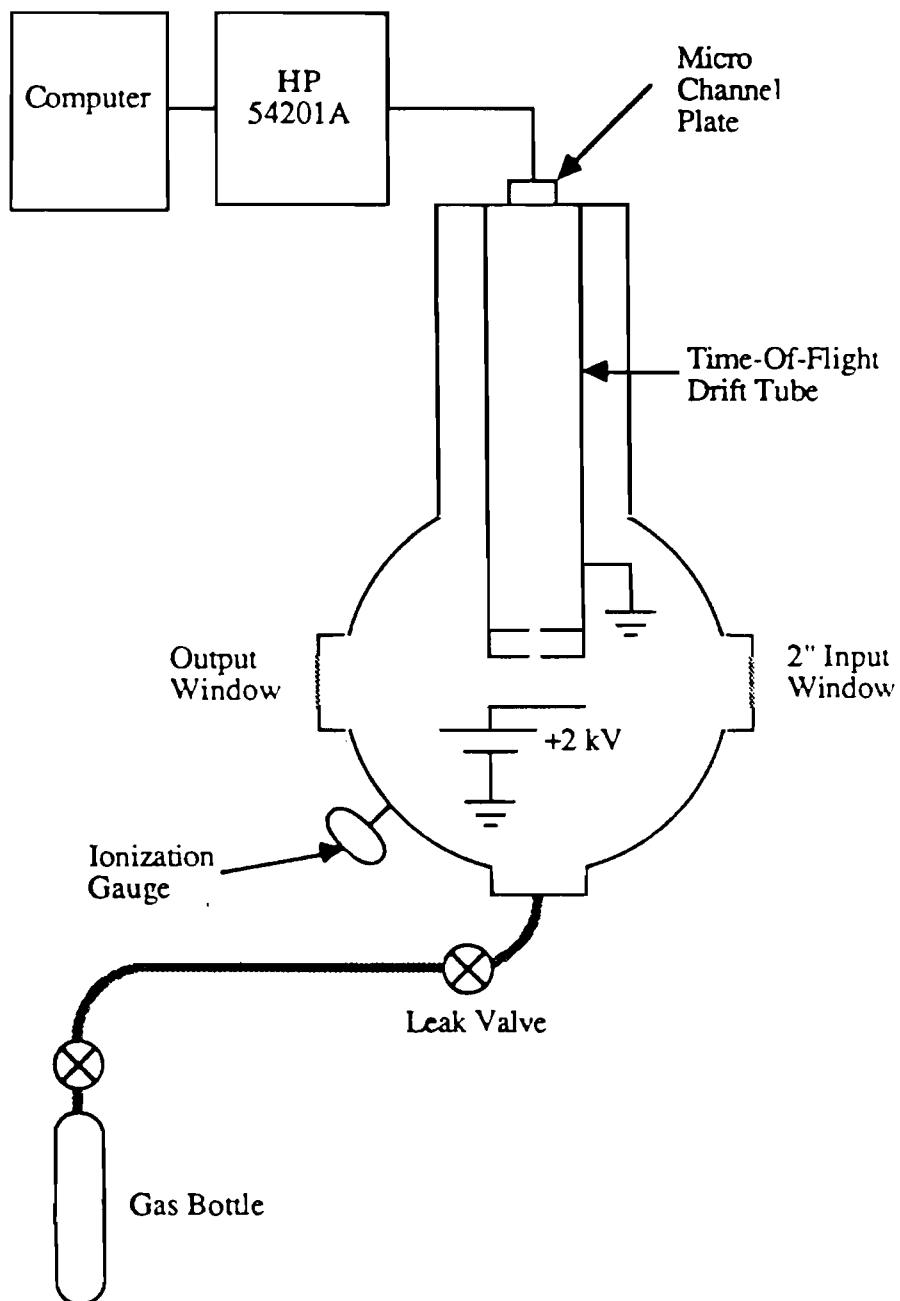


Figure 3 - 2. Interaction chamber configuration

either 1×10^{-5} or 1×10^{-6} Torr for the experiment. The pressure was measured by an ionization gauge, corrected for each gas species using the calibration curve given for the gauge. The laser beam enters the chamber through a 2" AR coated window and exits the chamber through a second uncoated window. An exit window is used so that the intense beam does not interact with a surface and create background ions.

A Time-of-Flight (TOF) ion spectrometer was used to measure the different ion species produced by the interaction of the radiation with the atoms. Two copper discs, two inches in diameter were placed on either side of the interaction volume, 5 cm apart. In the centre of one disc there was a 5 mm hole, with 100 μm copper mesh across it. The disc with the mesh was grounded while a voltage of 2000 V was applied to the other disc, in order to accelerate the ions out of the interaction region (focal volume), towards the drift tube. A third grounded disc with a similar 5 mm hole with wire mesh across it was placed 2 cm down the drift tube from the first grid. This second grid acted as a stop for any ions that might be generated in any region other than the interaction region. After passing through the first grid, the ions travelled freely down a 25 cm long grounded copper tube. At the end of the drift tube the ions were detected by an 18 mm, Comstock Microchannel Plate (MCP). A second MCP plate is used in chevron configuration. The MCP is operated at the maximum voltage of 2 kV, which gives a signal gain of $\sim 10^6$ e⁻/ion. The signal from the MCP is digitized and displayed by a HP54201A digitizing oscilloscope, which has a temporal resolution of 20 ns. This resolution is sufficient to distinguish the different charge states up to Xe¹³⁺, but not resolve the individual isotopes of the higher charge states. The digitized signal is stored in a computer, which integrates the different peaks to give the relative ion signals.

The laser intensity was varied by changing the pulse energy and keeping the

spot size and pulse width constant. The energy was varied by rotating a half-wave plate placed before the first polarizer of the second amplifier stage. The energy changed by over two orders of magnitude without reducing the contrast of pulse to prepulse. The pulse energy was reduced by rotating a wave plate rather than varying the lamp energy of the amplifiers, so that the thermal loading of the gain medium remains constant. Thermal loading causes temperature gradients, which create index variations across the rod. The index variations cause birefringence and lens effects in the laser rod and so a change in the thermal loading causes a change in the polarization and collimation of the beam. The difference in collimation leads to a change in the focal spot size and a birefringence variation will alter the contrast of the main pulse to prepulses. By varying the energy without changing the thermal loading on the amplifiers, the spot size and contrast remains constant

The pulse energy is measured for every laser shot. A wedge was placed in the beam after the grating compressor to reflect 4% of the light. The reflected beam was focused onto a calorimeter, (Laser Precision Rj-7200), such that the entire beam area was incident on the detector surface. The maximum energy that can be deposited on the calorimeter is 2 mJ, so that calibrated neutral density filters were placed before the detector, for the high energy shots. The monitor was calibrated by comparing the average of ten shots as measured by the monitor and that measured directly before the input window. The energy fluctuated by $\pm 6\%$ leading to a calibration error of 2.5 %. The laser energy was then corrected for the losses of the window, which was measured by a spectrophotometer to be 25% for the first window used in the experiments. This window was replaced with one that had 10% losses. The transmission of the windows were also measured with the CPA laser to ensure the losses were the same at high power.

The relative intensities had to be measured for each laser shot because the pulse width fluctuated 20%. A second wedge was used to reflect 4% of the energy which was then frequency doubled. The frequency doubled light was monitored for every laser shot and compared to the 1.05 μm energy to determine the relative intensities of every shot.⁵ The power of the green pulses is proportional to the square of the IR power. The detector measures the integrated green signal, which is proportional to the product of the energy and the power of the IR signal. The relative power of the IR pulse is given by the integrated green signal divided by the IR energy. The green energy was plotted as a function of the IR energy to verify that the green energy was proportional to the square of the IR energy, which indicates that the doubling crystal was not run at a saturation level. An example is shown in Fig. 3-3. The slope indicates that the green energy was a function of the IR energy to the power of $2.05 \pm .05$. The plot also shows the pulse width stability. The relative pulse durations were not measured for the green experiments. The green pulse width was approximated as the average pulse width for the IR experiments.

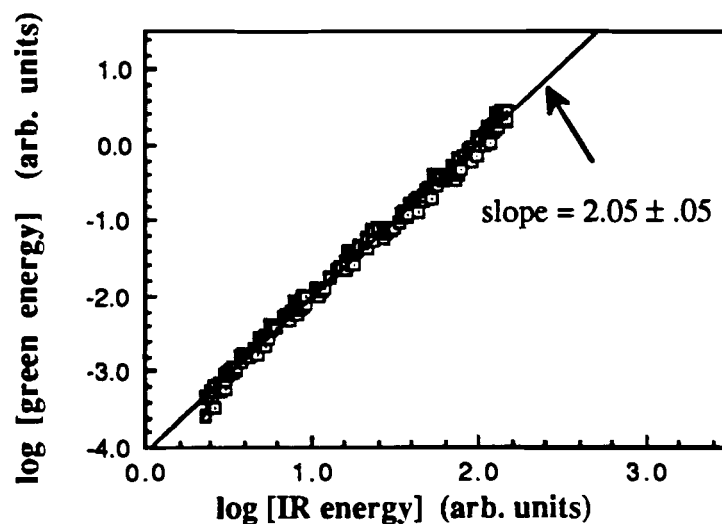


Figure 3 - 3. Plot of green energy as a function of IR energy

III. B Intensity Determination

A critical and difficult aspect of these experiments is the determination of the intensity profile. The autocorrelation of the CPA laser pulse, shown below, is best characterized by a Lorentzian profile and the spatial beam profile is best described by a Gaussian profile. The CPA technique keeps the peak power in the amplifiers low so that nonlinear effects do not occur and after the compressor, the intense beam does not pass through enough glass to cause self-focusing. The focusing of the beam should therefore be constant throughout the duration of the pulse and so the spatial and temporal components are assumed to be separable. The intensity distribution of the laser pulse at the focus can then be represented as:

$$I(r,z,t) = I_0 F(r,z) T(t), \quad (3-1a)$$

where

$$F(r,z) = \left[\frac{1}{1 + (\lambda z / \pi \omega_0^2)^2} \right] \exp \left[\frac{-2r^2}{\omega_0^2 \left[1 + (\lambda z / \pi \omega_0^2)^2 \right]} \right], \quad (3-1b)$$

is the Gaussian spatial distribution, where λ is the central wavelength, z is the distance along the optical axis from focus, ω_0 is the beam radius at the $1/e^2$ intensity points and r is the radial distance and

$$T(t) = \frac{1}{1 + (\pi t / T_p)^2}, \quad (3-1c)$$

is the Lorentzian temporal profile. The peak intensity is given by;

$$I_o = \frac{E_{\text{pulse}}}{A T_p}, \quad (3-1d)$$

where

$$T_p = \int_{-\infty}^{\infty} T(t) dt, \quad (3-1e)$$

is the average pulse width and

$$A = \int_0^{2\pi} \int_0^{\infty} F(r,0) r dr d\phi = \frac{\pi \omega_0^2}{2}, \quad (3-1f)$$

is the focal spot area measured at the $1/e^2$ intensity points.

The pulse width is measured using a single shot autocorrelator. The correlation is shown in Fig. 3-4. The pulse shape is fit with a Lorentzian profile, with a correlation width, (FWHM), of 1.4 ± 0.3 ps, which corresponds to a pulse width of 0.7 ± 0.2 ps.

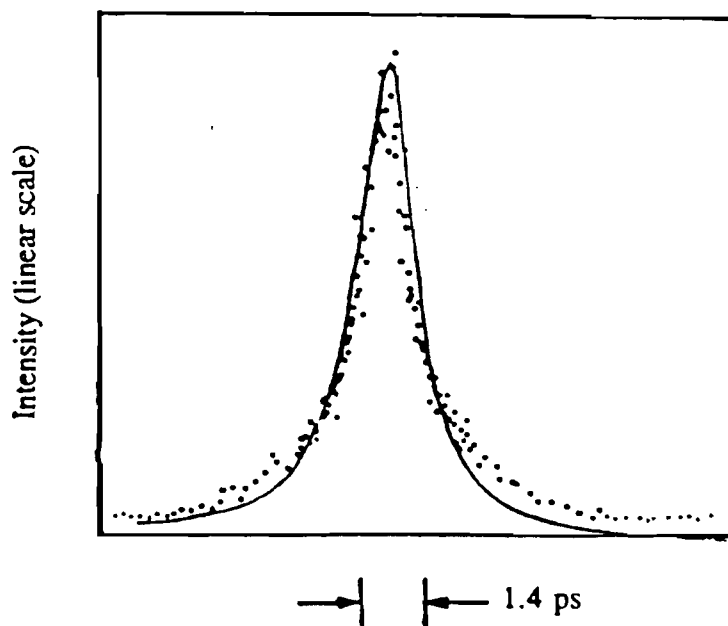


Figure 3 - 4. Autocorrelation of pulse profile. The solid line is a best fit Lorentzian profile.

Since ionization has been observed at intensity levels of 10^{11} W/cm², the temporal profile must be measured over several orders of magnitude, for pulses with peak intensities in the 10^{17} W/cm² range. The temporal profile of the laser pulse used in these experiments was measured over 5 orders of magnitude, using a third order correlation technique.⁶ The correlation is shown in Fig. 3-5. It shows a 1 ps pulse superimposed on a 200 ps background pulse which is three orders of magnitude less intense. Therefore when the pulse is focused to give intensities in the 10^{17} W/cm² range, a pulse of 10^{14} W/cm² intensity precedes it by 100 ps. The energy in the background pedestal was measured to be 10% of the measured energy.

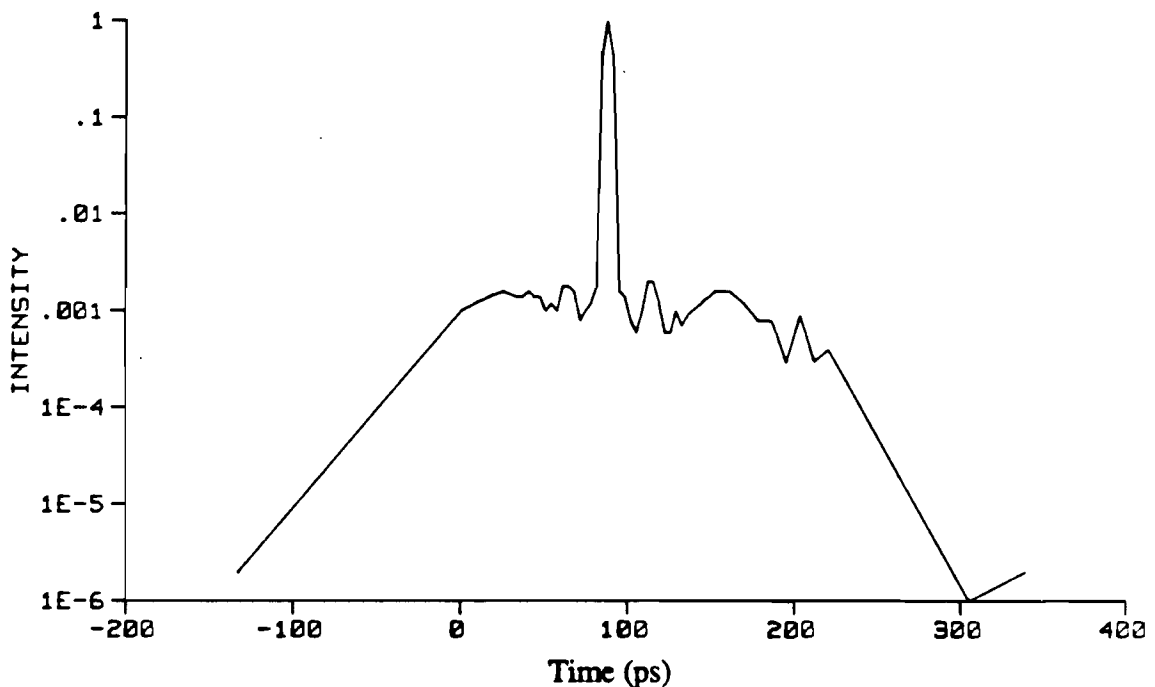


Figure 3 -5. Third order correlation of temporal profile.

There was also a secondary pulse from the regenerative amplifier occurring ~ 700 ps after the main pulse that had an energy equal to $\sim 65\%$ of the main pulse. A streak camera trace of the two pulses is shown in Fig. 3-6. The secondary pulse exists

because the entire mode-locked pulse train from the oscillator is injected into the regenerative amplifier and the cavity lengths are mismatched by ~ 700 ps. The Pockels cell is not fast enough to isolate the primary pulse. This secondary pulse could be eliminated, by using a Pockels cell switch out to isolate one pulse from the mode-locked train for injection into the regenerative amplifier.

As is later discussed in Chapter IV, the ion yield is equivalent for long and short pulses with the same intensity and the production of a charge state is dependent only on the peak intensity. Although the second pulse arrives at the interaction region before the ion has escaped, it should not cause ionization to a higher charge state, because the second pulse has a lower intensity than the first pulse. If the energy is corrected to account for the second pulse and background pedestal, the energy in the main pulse is 60 % of the measured energy.

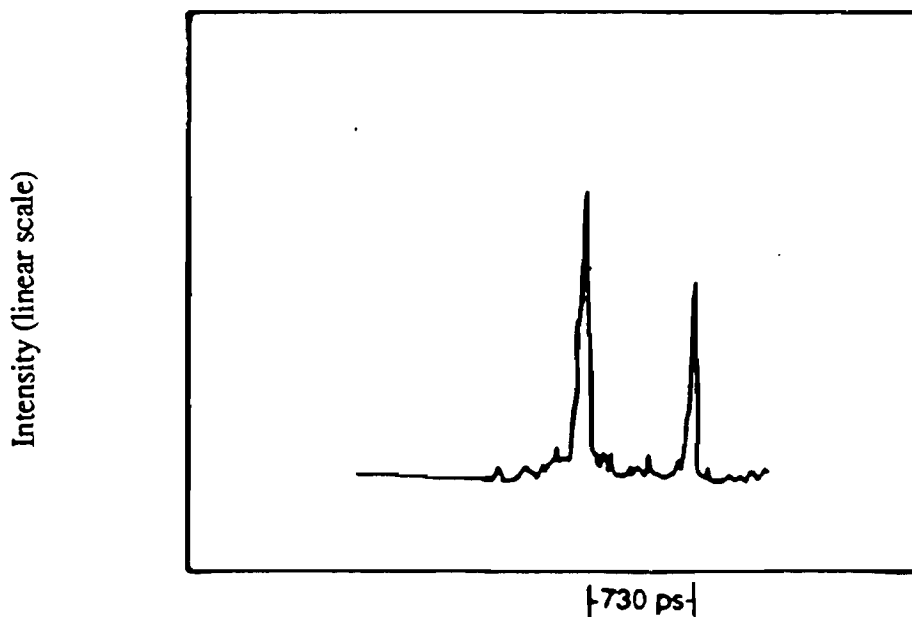


Figure 3-6. Streak camera trace of two pulses at the output of the compressor

In order to measure the focal spot, the chamber was removed and the input window was placed in the beam at the same position, so that the beam was transmitted through the same optics. The focal spot was imaged by a 40x microscope objective onto film. The density of the image on the film was digitized to measure the beam profile. The spot size was measured for both low and high energy pulses in the amplifiers to ensure that there was no effect from self-focusing in the gain medium. The energy was reduced with ND filters after the amplifiers, to avoid air breakdown and protect the imaging optics. The presence of self-focusing of the high power pulses in the final optics was then not measured. After the gratings, the pulses pass through ~ 4 cm of glass (ie. two wedges, the lens and the vacuum window). At the intensity of the compressed, unfocused beam ($\sim 10^{10}$ W/cm²) and a 4 cm length of glass the value of the B integral is ~ 2 , which should lead to insignificant self-focusing. It should also be mentioned that the dispersion in 4 cm of glass would lead to a temporal spread of only 0.01 ps for the 2 nm bandwidth. The spot size was measured for the uncompressed as well as the compressed pulses and the green spot size was measured.

The densitometer traces of the IR spot size measurements are shown in Fig. 3-7. The beam profile of the uncompressed pulses shows the focal spot size to be 7.8 ± 0.6 μm in diameter, at the $1/e^2$ intensity points, which is 1.5 times the diffraction limit. The compressed pulses on the other hand had an elliptical focused beam shape. This ellipticity is a result of using the gratings in a single pass configuration. When the compressor is used in this configuration, imperfect collimation and an incidence angle different from the Littrow condition causes astigmatism of the beam.⁷⁶ The spot size of the compressed pulses was 13.7 ± 0.5 μm for the minor axis and 35 ± 2 μm along the major axis at the $1/e^2$

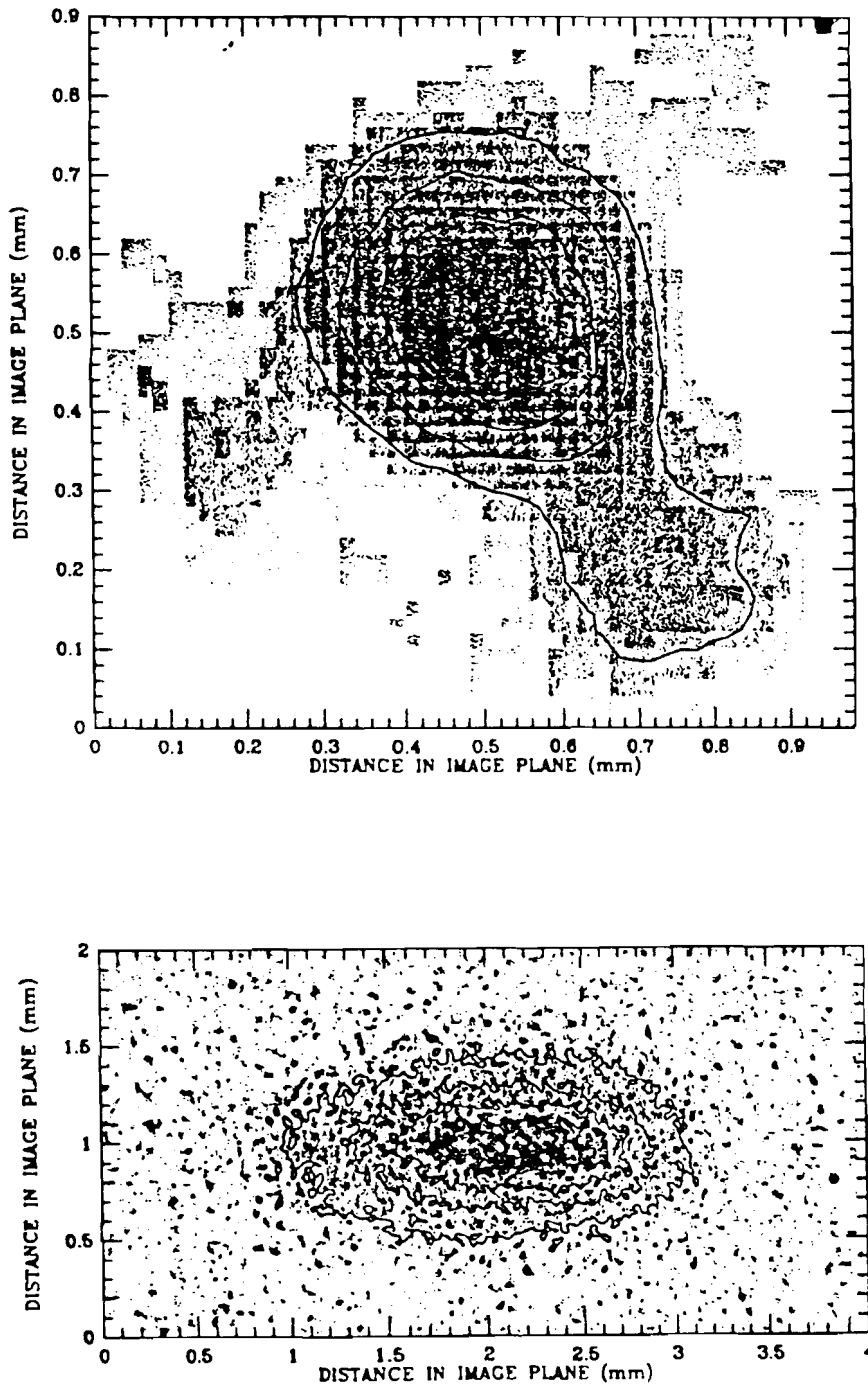


Figure 3 - 7. Densitometer trace of (a) uncompressed and (b) compressed pulses.

Lines show contours of constant intensity

intensity points. The spot size of the green beam was $10 \pm 1 \mu\text{m}$ for the minor axis and $18 \pm 2 \mu\text{m}$ along the major axis at the $1/e^2$ intensity points. The error in the spot size was determined by taking three cuts across the profile in each direction and comparing the diameters.

The largest source of absolute error in the intensity measurement occurs because the spot size was only measured once, after all the ionization yields were measured. As was discussed above, the ellipticity of the beam at focus depends on the alignment of the gratings. The gratings were realigned on a daily basis and so the spot size could have varied. An estimate of the error can be determined by comparing the ionization yields measured for xenon at low and high pressure. The difference in the pressure was an order of magnitude and so the ion yield of the low pressure xenon must be increased by a factor of ten to make the comparison. The ion curves for the different charge states overlap when the estimated intensity of the low pressure experiment is reduced by three. This indicates that the intensity measurement is only accurate to a factor of three. Similar comparisons of ion yields, measured at different times, showed that the measured intensities were typically within a factor of two. The dependence on the alignment of the gratings could be eliminated in the future by using a double pass of the gratings. The astigmatism due to poor alignment is cancelled in the second pass of the gratings. In future experiments, the relative spot size could also be monitored by measuring the focal spot size of a reflected fraction of the beam using a second lens.

The other source of error in the ion yield curves is that of the detector noise. This noise was measured by integrating the signal over a time interval where no ion peak existed, with a duration comparable to the width of an ion peak. The noise was measured to be approximately 25 units of the ion yield curves. Much of the detector

noise was subtracted out by measuring the noise adjacent to the peak and subtracting the noise from the signal.

III. C Time of Flight Spectra

Typical TOF spectra are shown in Fig. 3-8, for the highest intensity levels at 1.053 μm , for each of the five noble gases. The time of arrival, t , for the various ions is given by the following expression (neglecting the very short flight times in the accelerating regions, before the grid and MCP) :

$$t = L \sqrt{\frac{m}{2 V q}}, \quad (3 - 2)$$

where V is the extraction voltage at the interaction region, L is the length of the drift tube, m is the ion mass, and q is the ion charge.

Since, the exact voltage at the interaction region and distance to the detector is not known, the time of arrival of the peaks are measured relative to the flight time of a known ion species, typically H^+ , which comes from ionization of impurities in the vacuum system.⁸ The relative time of arrival identifies the various peaks by the relative charge to mass ratio. This identification can lead to some ambiguity because different ions, such as H_2^+ and He^{2+} , have common charge to mass ratios and although the background pressure was reduced to 1.2×10^{-8} Torr, several impurities still existed in the chamber. The most common impurities were nitrogen, hydrocarbons, oxygen and water. The identification of He^{2+} was done by measuring the pressure dependence of the peak height. The TOF spectra for He at high and low pressure are shown in Fig. 3-8a and 3-8b, respectively. The peak increased with

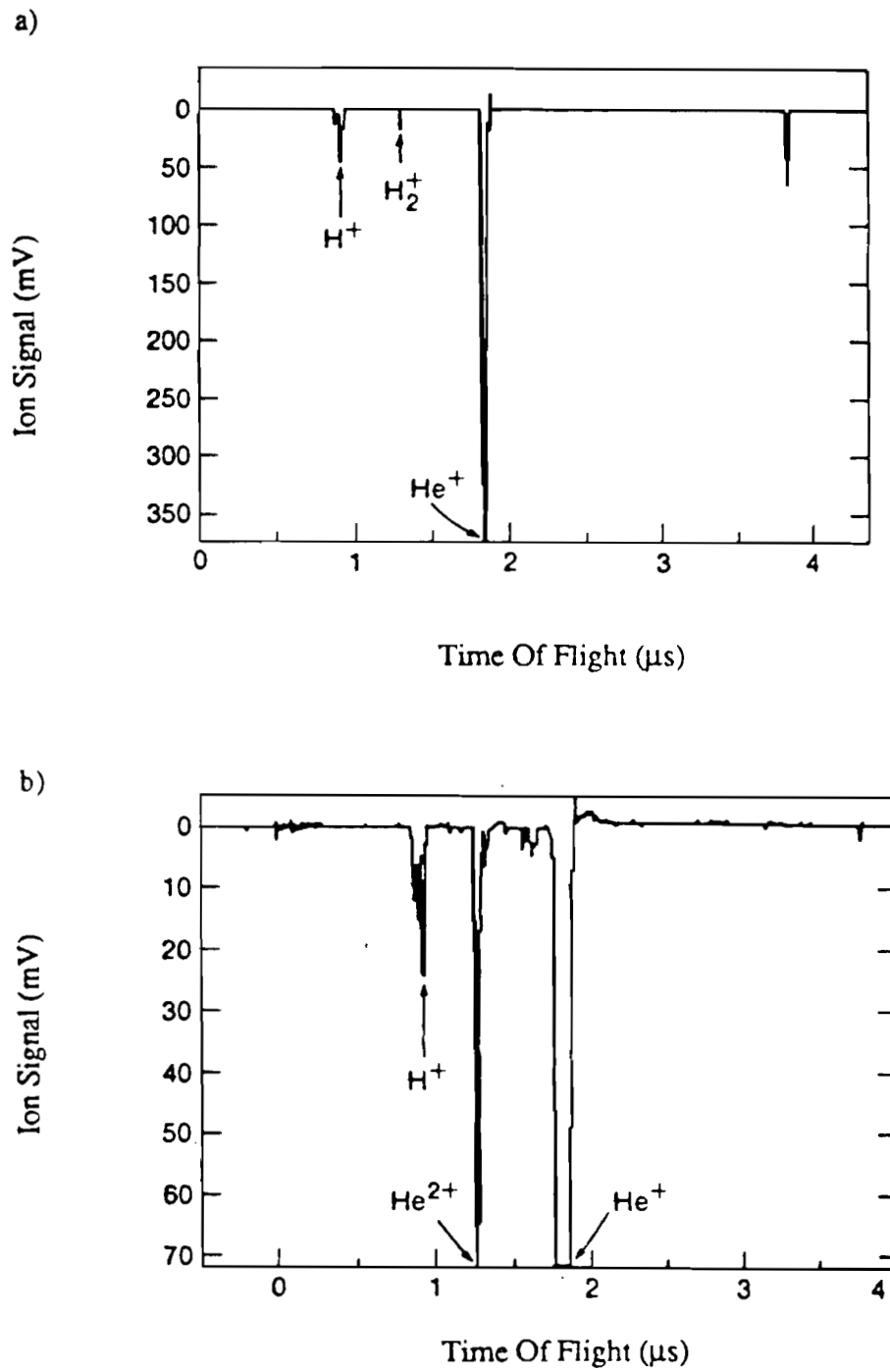


Figure 3 - 8. TOF spectra of Helium at (a) low pressure and (b) high pressure

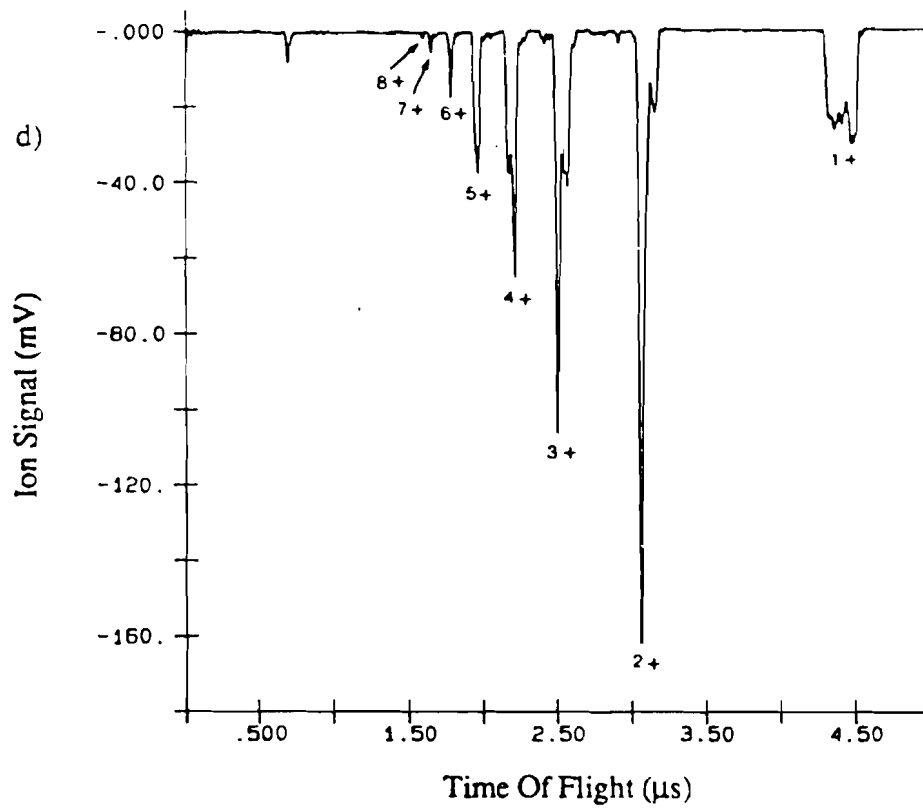
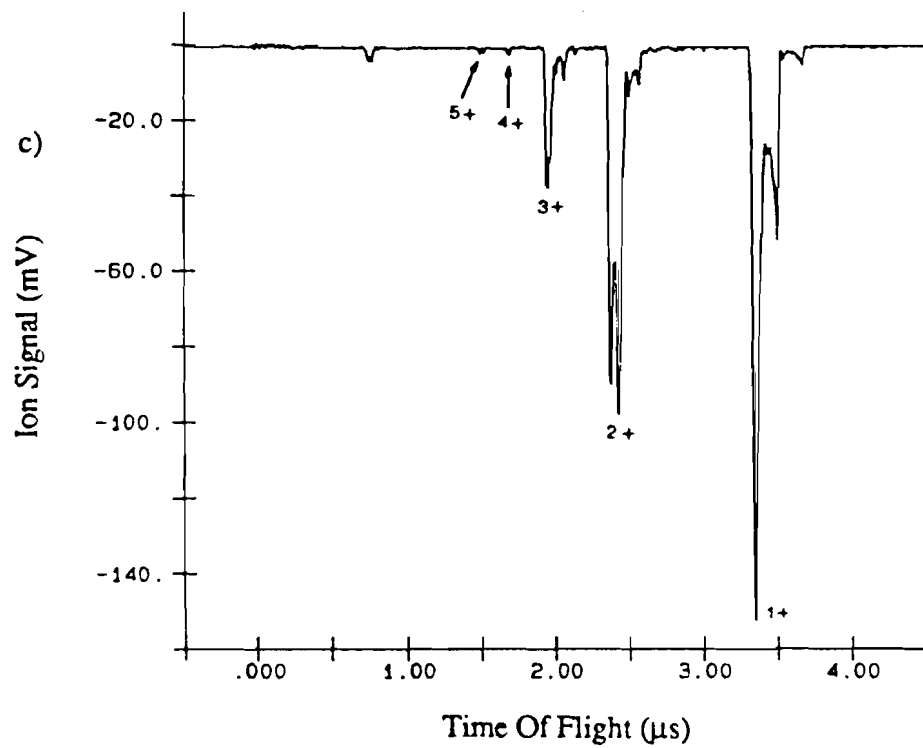


Figure 3 - 8. TOF spectra of (c) Neon and (d) Argon

helium pressure, indicating that it was indeed a helium ion.

The position of the peaks of the TOF spectra were also altered by space charge effects, making identification even more difficult. The space charge effect can be estimated by considering all the atoms in the interaction volume to be ionized to the first charge state. At a pressure of 10^{-5} T, the electric field generated by the ions could account for an approximate 3% shift in the arrival time. The peaks were identified as the ions which had the corresponding closest expected time of arrival. An example of this identification is given in Table 3-1, for the TOF spectrum of xenon gas, shown in Fig. 3-9. The table lists the different peak times and gives the identified ions with the % error of the measured to the calculated time of flight.

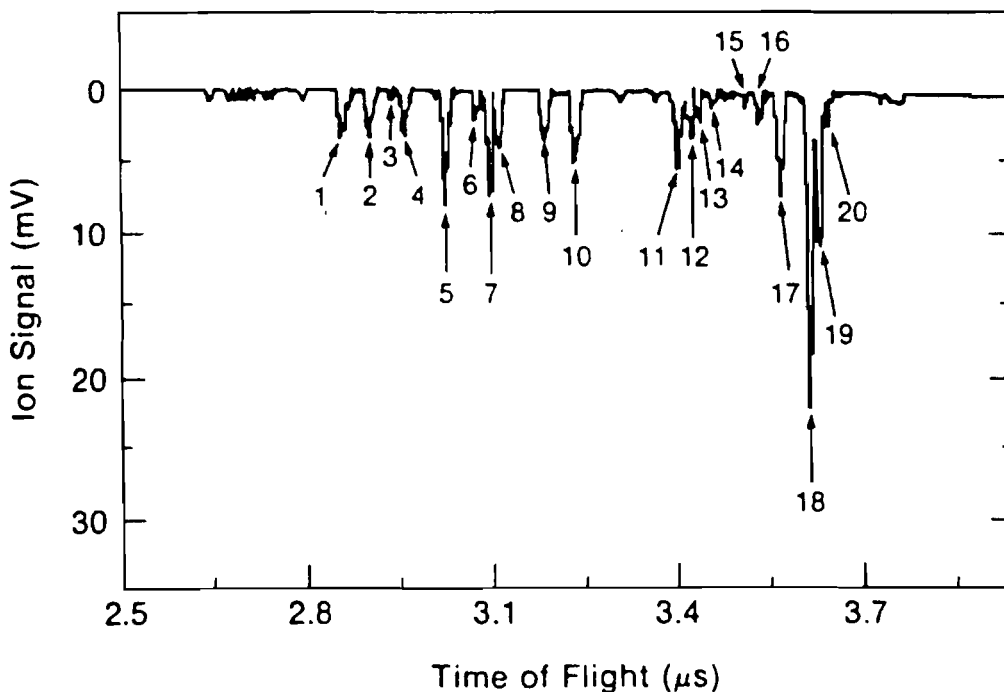


Figure 3-9. TOF spectrum of xenon showing the maximum charge state, Xe^{12+}

Peak	Position (μs)	Ion	Expected Position Using H^+ as the Reference (μs)	Largest % Error with Respect to Expected Position	
1	2.885	Xe^{12+}	2.84 - 2.89	1.4	
2	2.93	} Xe^{11+}	2.96	3.1	
3	2.965			1.8	
4	2.985			-3.02	1.2
5	3.05	C^+	3.00	1.7	
6	3.10	} Xe^{10+}	3.11	2.2	
7	3.125			-3.17	1.4
8	3.135			1.1	
9	3.21	N^+	3.24	0.9	
10	3.26	Xe^{9+}	3.27 - 3.34	2.4	
11	3.435	} O^+	3.46	0.7	
12	3.455			0.01	
13	3.47			0.03	
14	3.49	} Xe^{8+}	3.49 - 3.54	5.0	
15	3.55			1.7	
16	3.57	} OH^+	3.57	2.3 (Xe^{8+})/0.0 (OH^+)	
17	3.61			1.1	
18	3.665	H_2O^+	3.67	0.14	
19	3.68	} Xe^{7+}	3.71 - 3.78	2.6	
20	3.695			2.2	

Table 3 - 1. Identification of peaks of TOF spectrum of Fig. 3-9

The TOF spectra shown in Fig. 3-9 shows the xenon charge states of 7+ and higher. A charge state of Xe^{12+} can be identified in this spectrum. Charge states above Xe^{9+} occurred only for a few shots. The higher charge states may be a result of hot spots occurring in the beam yielding higher intensities than measured.

III. D Intensity Dependence

The ion yields for the various charge states of the noble gases are plotted as a function of intensity on a logarithmic scale. A moving point average was used because only 200 shots are made for each run. The experimental points were arranged in order of increasing intensity and each point was averaged with the three succeeding points. These averaged results were then plotted.

III. D. 1 IR Wavelength Interaction

The ion yield was measured for the interaction of $1.053 \mu\text{m}$ radiation with the five noble gases over an intensity range of 1×10^{14} - $6 \times 10^{16} \text{ W/cm}^2$. The ion yields as a function of intensity are shown in Fig. 3-10. The ionization of xenon was measured for two different gas pressures of 1×10^{-5} and 1×10^{-6} Torr in order to determine the effects of detector saturation. The two ion yields are overlaid, in Fig. 3-10a, by increasing the ion yield of the low pressure results by an order of magnitude to account for the pressure difference. As was discussed previously, the estimated intensity of the low pressure run had to be reduced by three to have the curves overlap. The ion yields for the other four gases shown in Fig. 3-10 are for high pressure without correcting for the detector saturation.

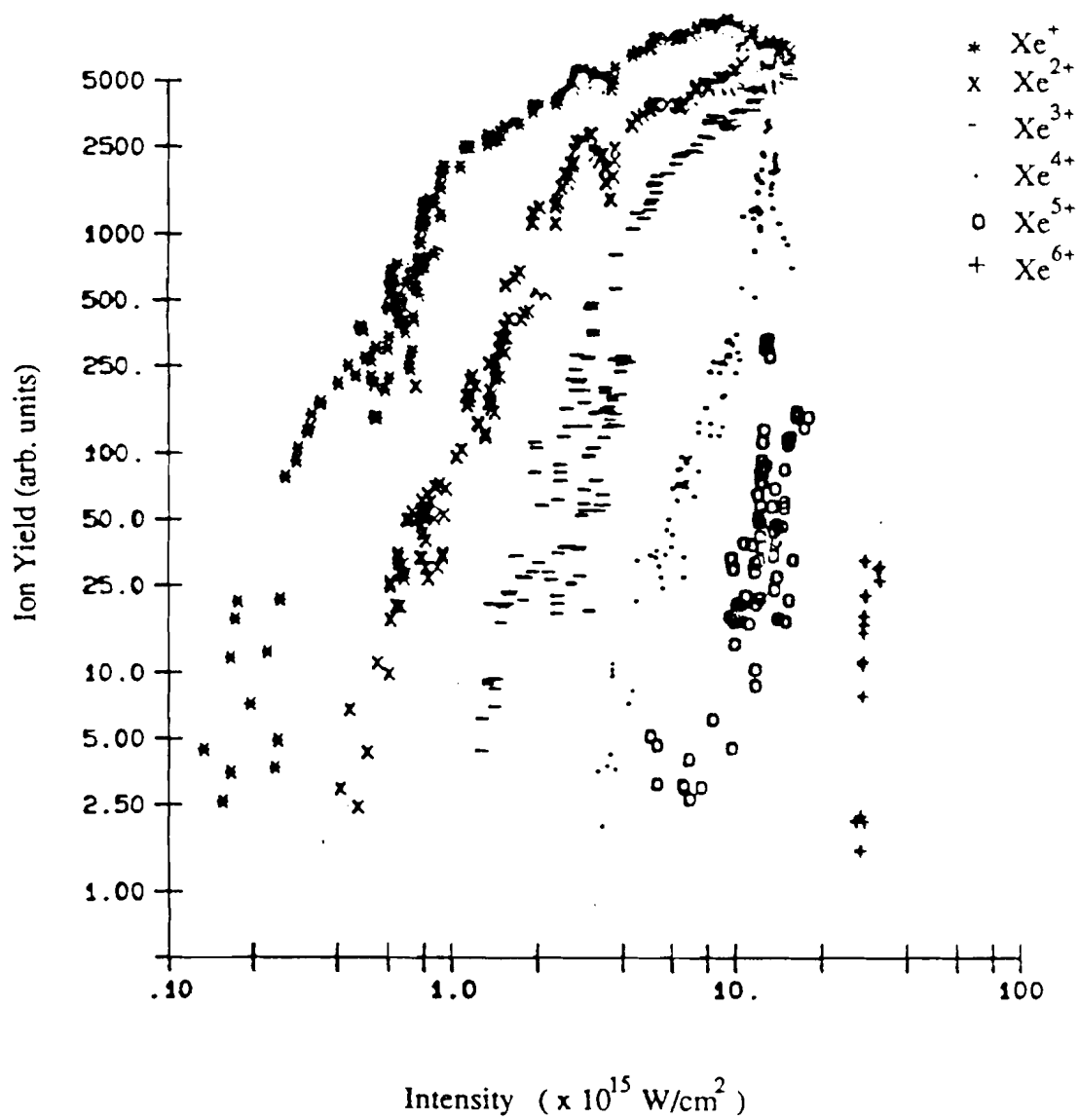


Figure 3 -10a. Ion yield as a function of IR intensity for xenon. Low and high pressure data overlaid

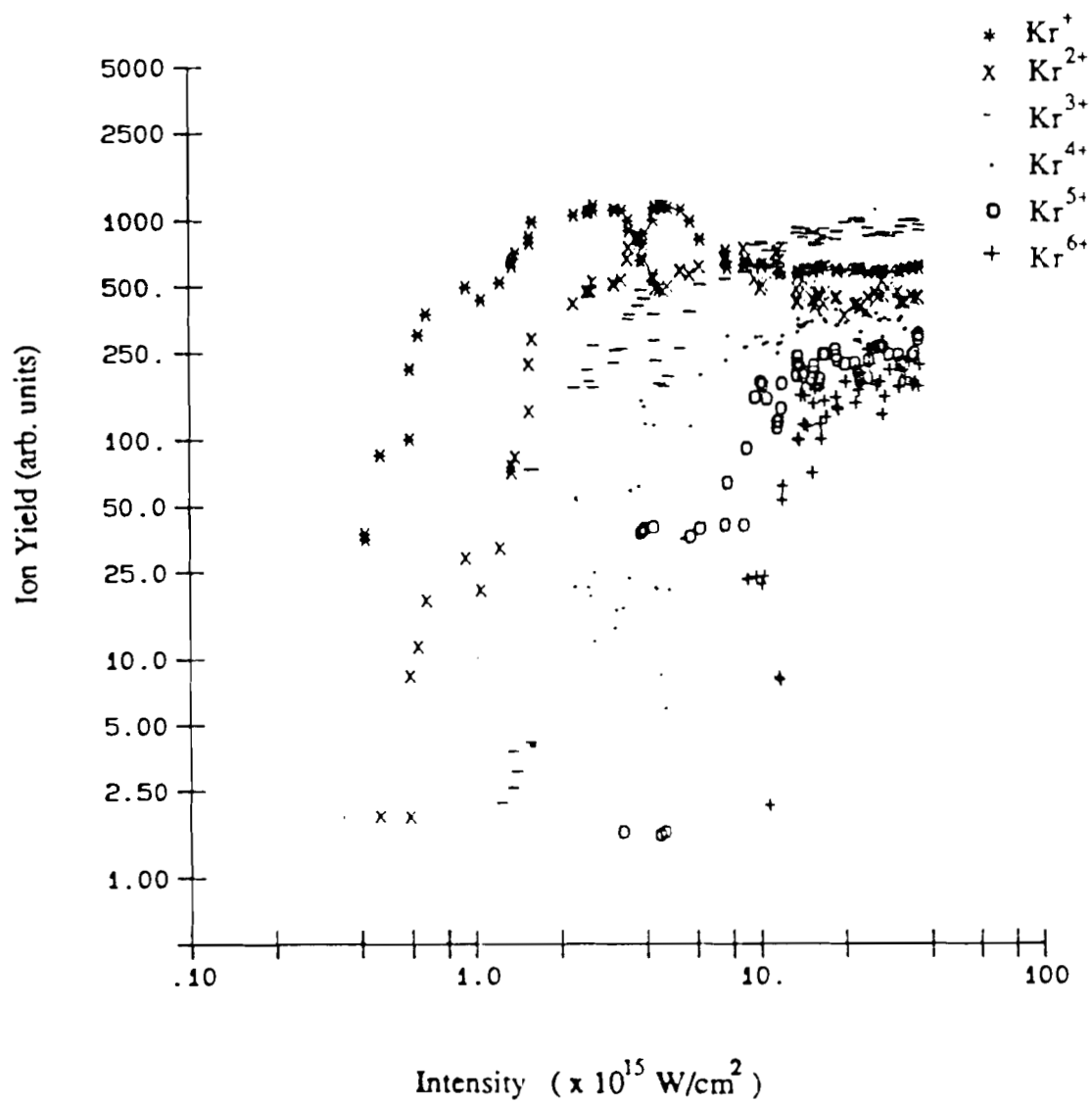


Figure 3 -10b. Ion yield as a function of IR intensity for krypton

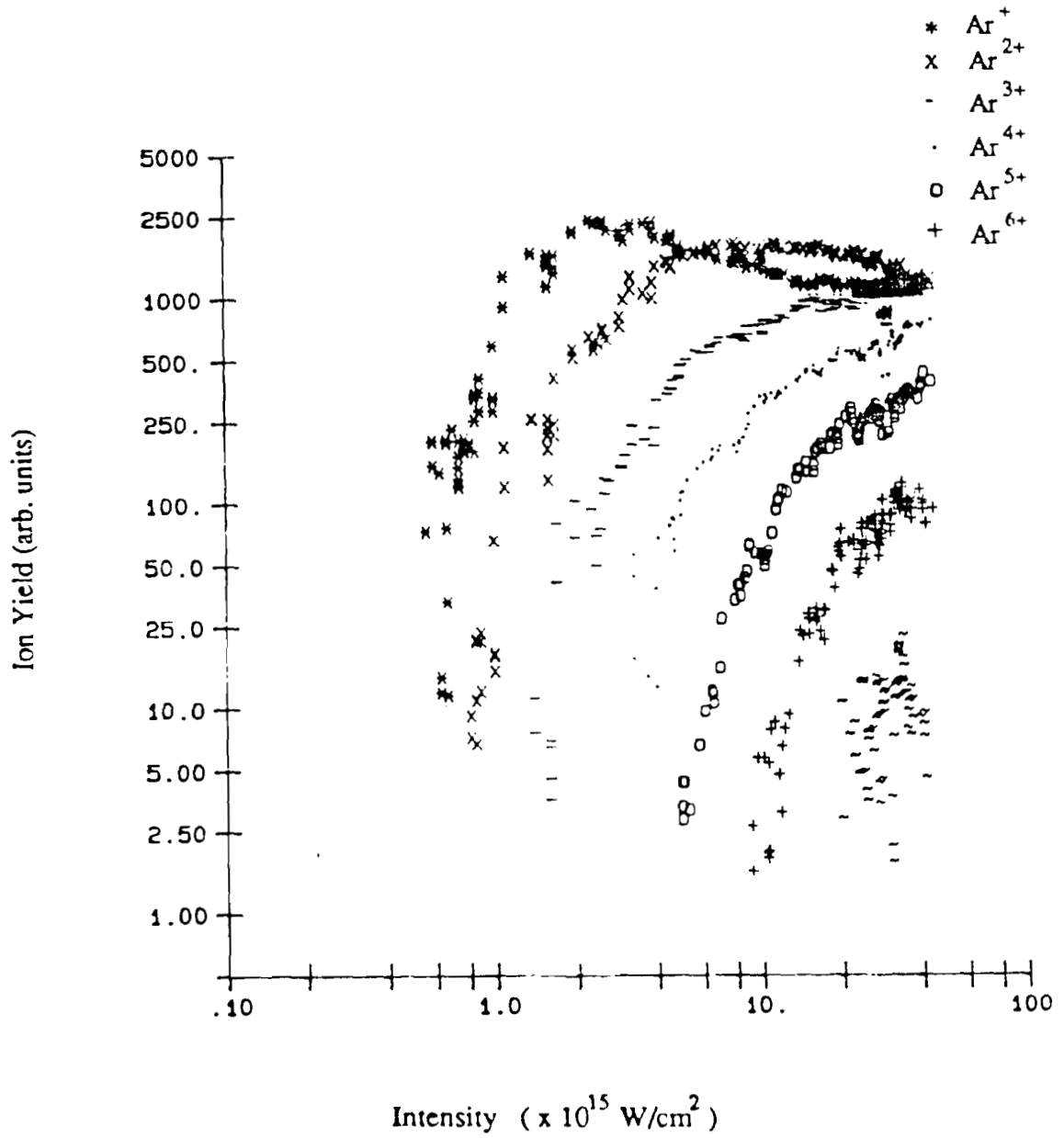


Figure 3-10c. Ion yield as a function of IR intensity for argon

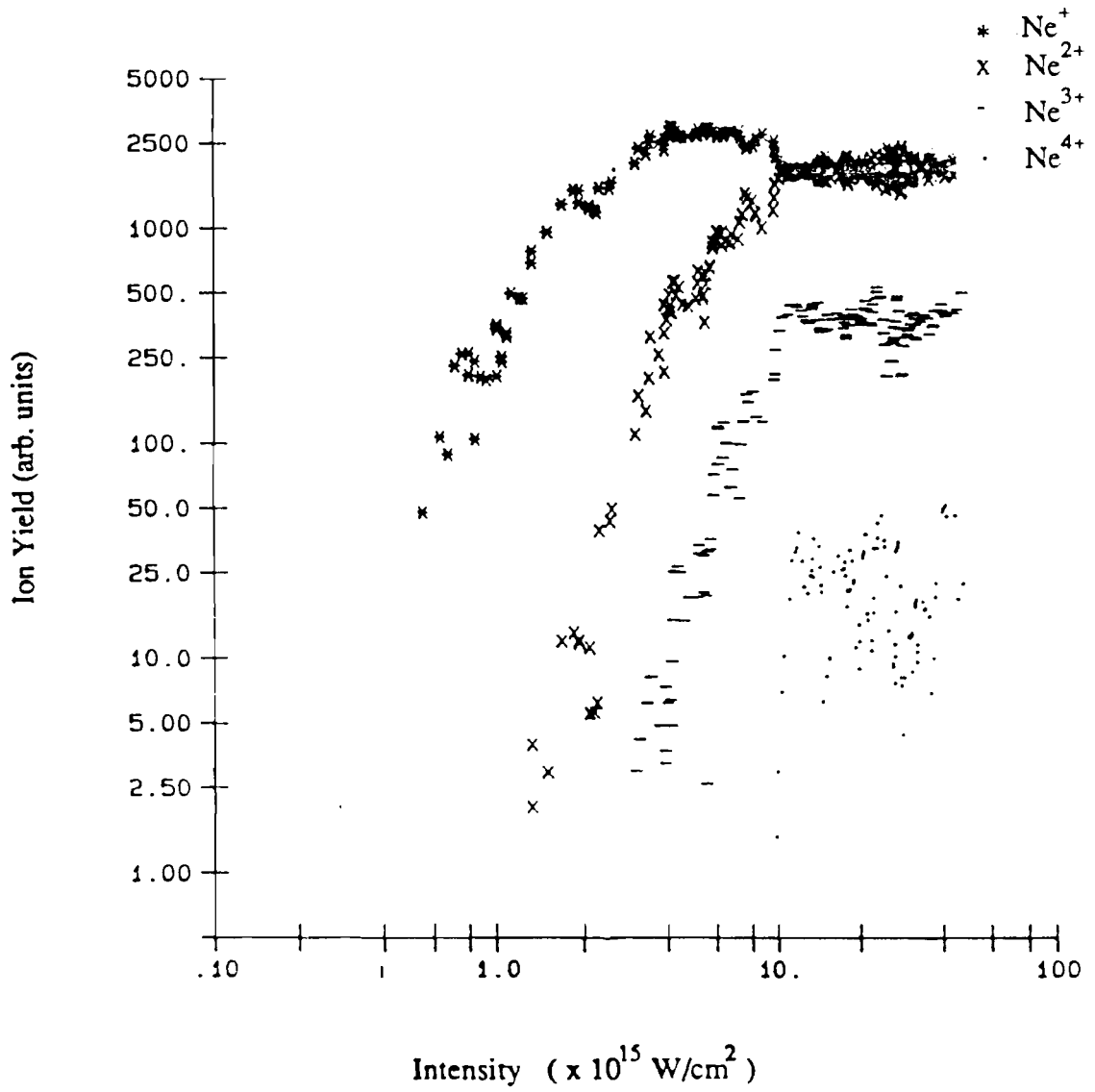


Figure 3 -10d. Ion yield as a function of IR intensity for neon

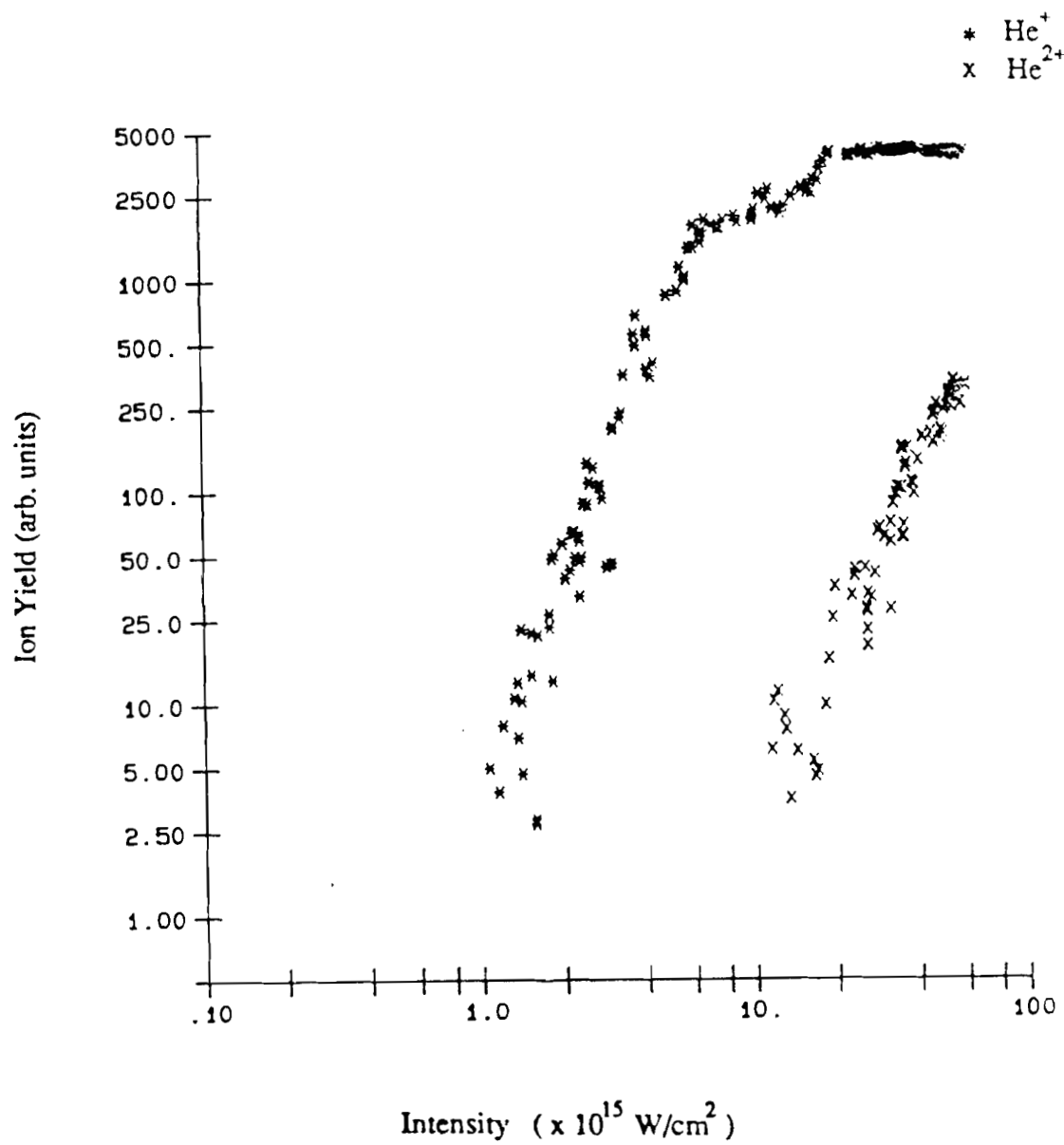


Figure 3 -10e. Ion yield as a function of IR intensity for helium

III. D. 2 Green Wavelength Interaction

In order to measure the wavelength dependence of creating high charge states, the ion yield as a function of intensity at 0.53 μm was measured for the five noble gases. The doubling efficiency was 25%, resulting in a maximum green intensity of $3 \times 10^{16} \text{ W/cm}^2$. The ion yields as a function of intensity for the green wavelength are shown in Fig. 3-11. Figure 3-11a shows a combined plot of two runs for xenon. The other plots are for single runs.

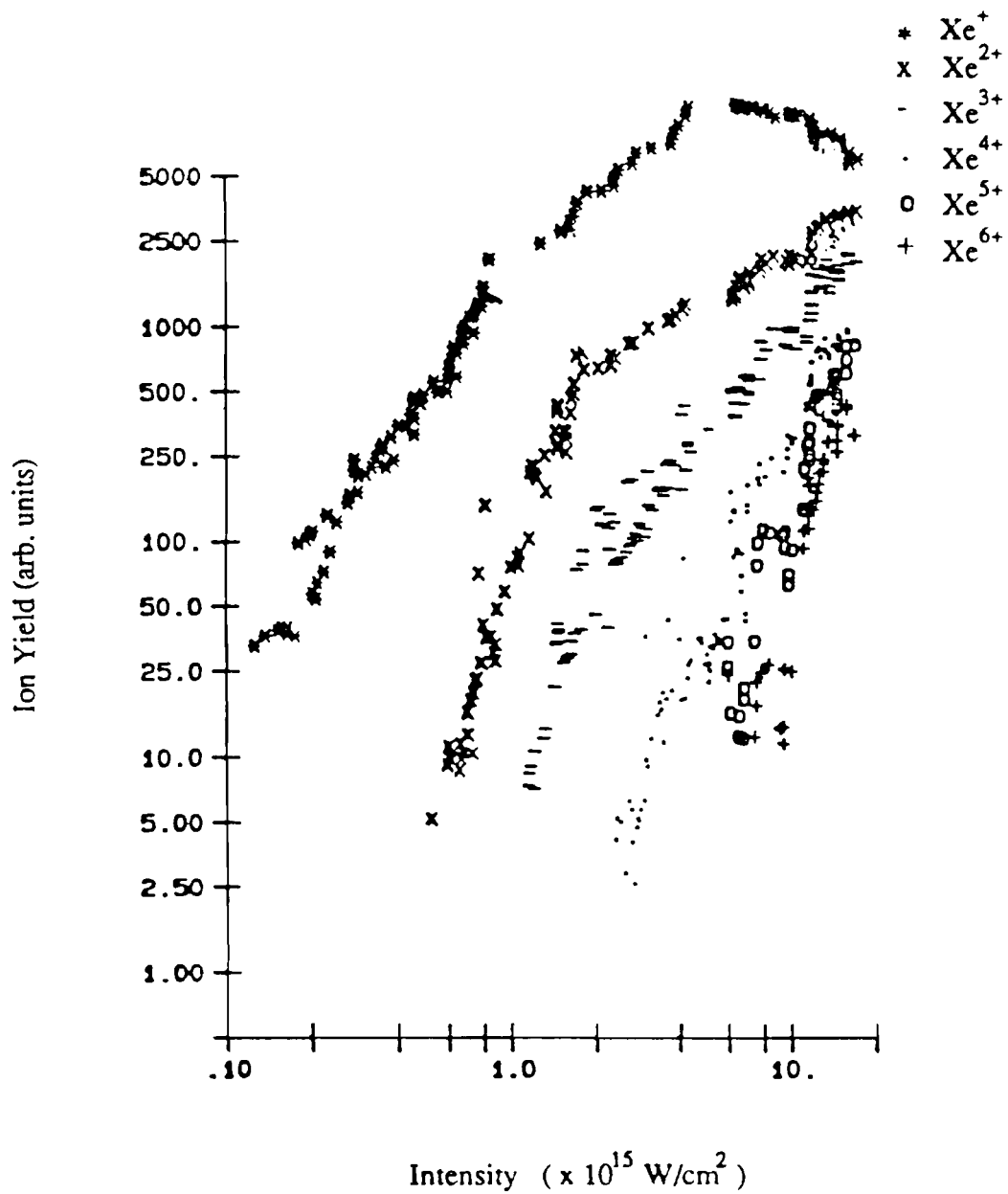


Figure 3 -11a. Ion yield as a function of green intensity for xenon

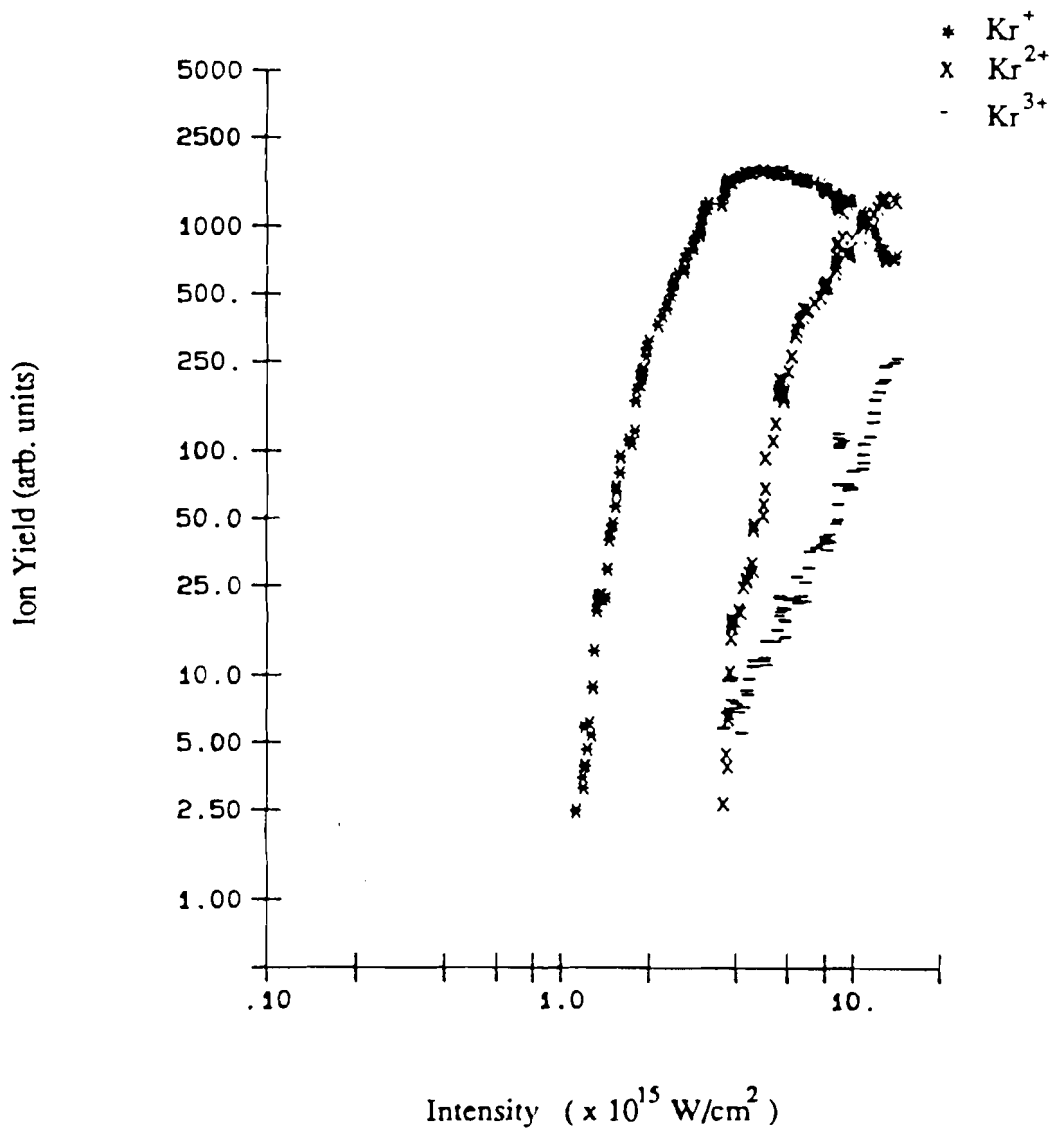


Figure 3 -11b. Ion yield as a function of green intensity for krypton

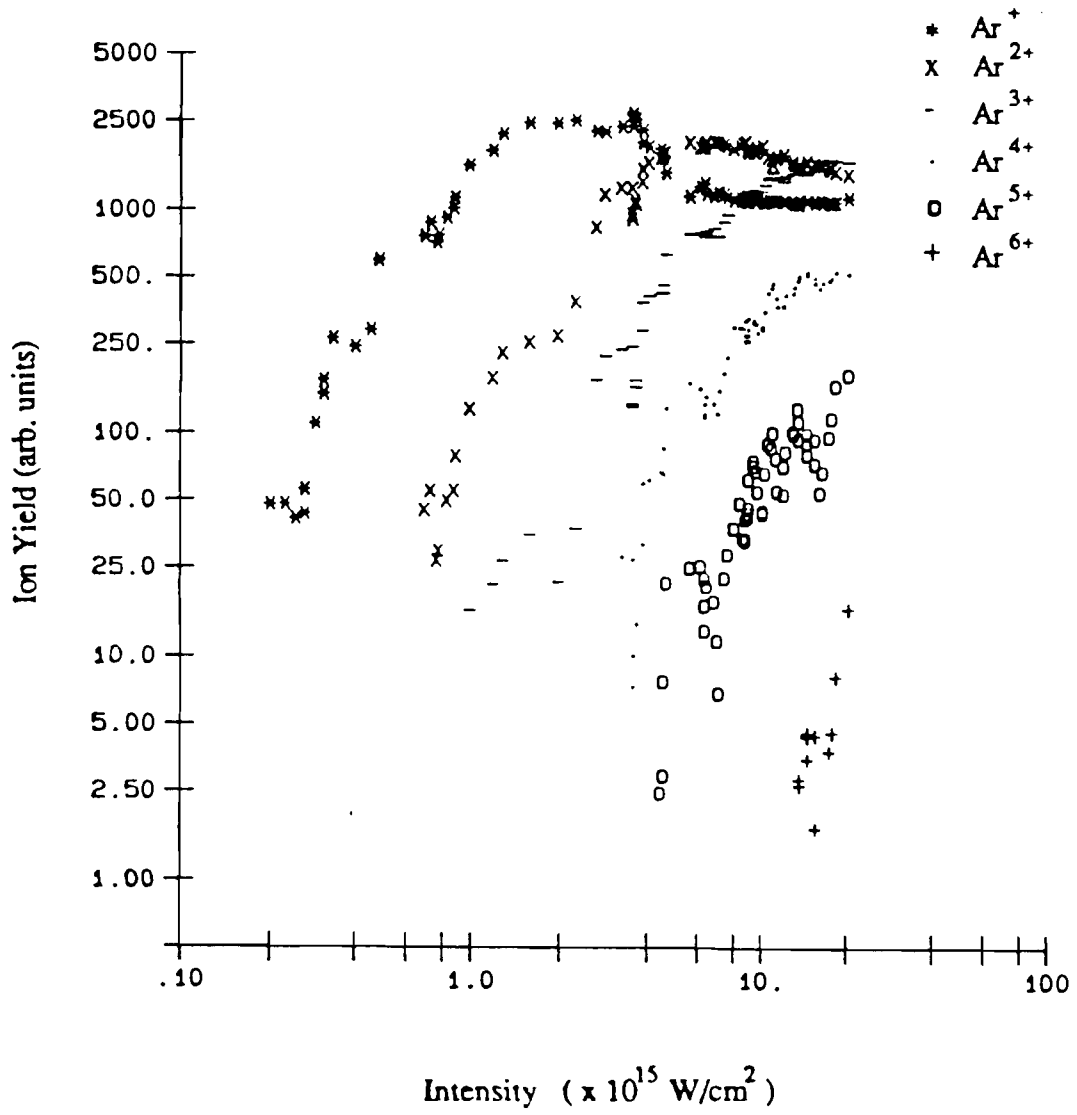


Figure 3-11c. Ion yield as a function of green intensity for argon

III. D. 3 Long Pulse Interactions

The CPA laser offers the unique possibility of measuring the effect of bandwidth and pulse duration, independently. The pulse width can be altered simply by changing the spacing of the gratings. The bandwidth can be varied in one of two ways. The first would be to use interference filters with different bandwidths. The second method would be to aperture the beam after a single pass of the gratings where the spectral frequencies are mapped onto space. At present, the effect of pulse duration has been measured at only the two extremes of the pulse width. The ionization yield produced by the compressed pulse is compared to the ion yield produced by the interaction of the uncompressed pulse. The duration of the uncompressed pulse was measured using a streak camera. The streak camera trace is shown in Fig. 3-12.

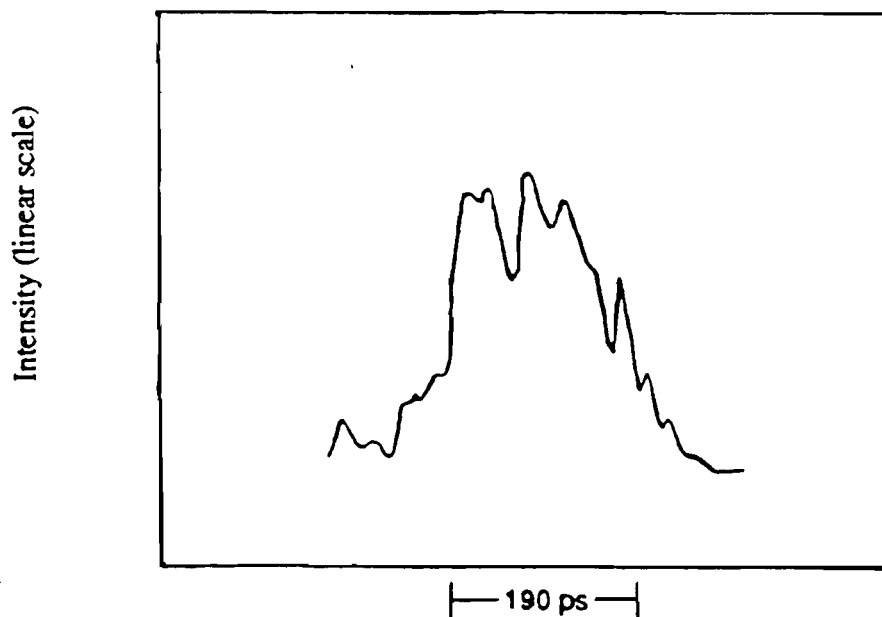


Figure 3-12. Streak camera trace of uncompressed pulse.

The pulse is nearly rectangular in shape and has a duration of approximately 200 ps. The spectral bandwidth is reduced to approximately half the initial bandwidth of 4 nm by gain narrowing in the Nd:glass amplifiers. The frequency spectrum is mapped onto the temporal profile so that as the bandwidth is reduced, the pulse duration also decreases. The fluctuations in the measured profile are mainly due to streak camera noise, but the temporal profile will be modulated as the frequency spectrum from SPM.

The long pulses have a large bandwidth of ~ 2.0 nm and are therefore far from transform limited pulses. The uncompressed pulses yielded different results from the Saclay 20 ps transform limited pulse experiments. However, the uncompressed pulses are comparable to the background pedestal of the compressed pulse and so the effect of the pedestal on the ionization process can be determined by measuring the ionization created by the 200 ps uncompressed pulse. The multi-photon ionization rate was measured for the interaction of these long pulses with xenon gas at a pressure of 1×10^{-5} Torr. This ion yield as a function of the intensity is shown in Fig. 3-13.

At the maximum compressed pulse intensity, of 6×10^{16} W/cm², the intensity of the background pedestal was 6×10^{13} W/cm². Figure 3-12 shows that at this intensity, the neutral atoms are not ionized with the 200 ps pulses, which indicates that the pedestal had no effect on the ionization process.

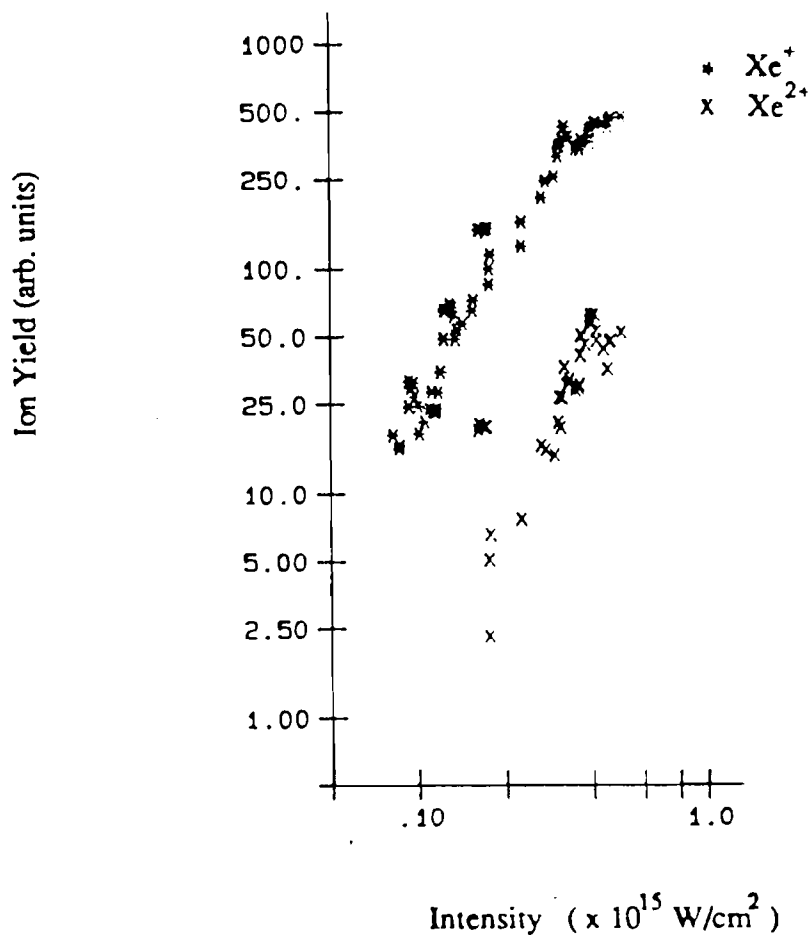


Figure 3-13. Ion yield as a function of 200 ps pulse intensity.

References

1. A L'Huillier, L A Lompré, G Mainfray and C Manus, *J. Phys. B: At. Mol. Phys.* 16, 1363 (1983)
2. C. Lecompte, G. Mainfray, C. Manus, and F. Sanchez, *Phys. Rev. A* 11, 1009 (1975)
3. A. L'Huillier, L. A. Lompré, G Mainfray and C Manus, *Phys. Rev. A* 27, 2503 (1983)
4. A. L'Huillier, L. A. Lompré, G Mainfray and C Manus, *J. Physique* 44, 1247 (1983)
5. M. D. Perry, O. D. Landen, A. Szoke, and E. M. Campbell, *Phys. Rev. A* 37, 747 (1987)
6. G. Albrecht, A. Antonetti and G. Mourou, *Opt. Commun.* 40, 59 (1981)
7. O. E. Martinez, *J. Opt. Soc. Am. B* 3, 929 (1986)
8. S. L. Chin, *Can. J. Phys.* 48, 1314 (1970)

CHAPTER IV

DISCUSSION OF MPI RESULTS

In this chapter, the features of the ion curves presented in Chapter III are discussed. The multi-photon ionization results measured with the CPA laser are compared to results obtained at the same wavelengths by the Saclay group.^{1,2,3,4} Finally the experimental results are compared to a Keldysh theory that has been modified by Szöke, to account for the Coulomb potential.⁵ The following discussion points out the large discrepancies that exist between the different experiments and between the experiments and the present theory. The discrepancies cannot be explained at present. More extensive experimentation and a better theoretical model are still needed to fully understand the multi-photon ionization process.

IV. A Ion Yield Curves

The experimental curves have much smaller slopes in the saturation region than the predicted value of $3/2$ and in many cases the curves roll over. In order to distinguish between the saturation due to the depletion of the charge state in the interaction volume and the saturation of the detector the ionization of xenon was measured at both low and high pressure. Only the detector saturation is pressure dependent. The low pressure xenon curve does not roll over, indicating that the roll over is due to the detector saturation. The detector saturates such that the total number of measured ions is a constant. The higher charge states arrive at the detector first and

saturate it at high intensities and so the detector cannot detect all the ions in the lower charge states. Even at the lower pressure only the saturation of the third charge state approaches the $I^{3/2}$ limit, predicted in the theory. The lower slopes of the first two charge states are most likely still due to detector saturation. The saturation will deviate slightly from the $I^{3/2}$ limit because the beam deviated from a Gaussian profile due to the astigmatism of the beam.

The ion yield curves show consistently higher saturation intensities than the Saclay results at the same wavelengths.^{1,2,3,4} The saturation intensity is defined here as the point where the slope of the curve at low intensity intersects the slope of the curve at high intensity. Saturation intensities for the first charge state of He, Ne, Ar, Kr and Xe, for the IR plots shown in Fig. 3-10 are 3, 2, 1, 0.8, and 0.8×10^{15} W/cm² and 3, 4, 1, 2, and 1×10^{15} W/cm² for the green curves shown in Fig. 3-11, respectively. The roll over in the green experimental curves are most likely due to detector saturation and so the saturation intensities may be higher than measured.

As was discussed in Chapter I, the appearance of the second charge state before the saturation of the first charge state is an indication that the second charge state was produced as a result of direct ionization from the ground state. Direct ionization was observed in the four heavier gases with IR and in Xe, Ar, and Ne with green radiation. He²⁺ was produced only by sequential ionization for both wavelengths as was Kr²⁺ ionized with green radiation. The second charge state of xenon resulted from direct ionization with the long 200 ps pulses as it had with the 1 ps pulses. Direct ionization from the first charge state to the third charge state was also observed in the four heavier noble gases, for both IR and green radiation. There was no evidence of direct ionization from the ground state to the third charge state in any of the noble gases. That is, the third charge state always appeared at a higher intensity than the saturation intensity of the first charge state.

In the curves of the second charge states, inflection points occur at the saturation intensity of the first charge state, in the four heavier species with IR, and in xenon, argon and neon with green radiation. The inflection point is considered the intensity that the ionization process switches from direct to sequential. The appearance of the second steep slope in Ar and Ne in the IR is reduced by detector saturation. With IR radiation, He^{2+} was produced only by sequential ionization whereas Ne^{2+} and Ar^{2+} occurred mostly by direct ionization and the two heaviest species ionized to the second charge state by both processes equally. With green radiation, He^{2+} and Kr^{2+} were produced by sequential ionization, Ne^{2+} was generated totally by direct ionization and Xe and Ar were ionized to the second charge state by a combination of direct and sequential ionization.

The inflection points can be seen more clearly if the data points are replaced with best fit lines. The experimental ion yield curves for Kr with IR radiation are again shown in Fig. 4-1, where best fit lines are given to represent the data. The inflection point of the second charge state is at the saturation intensity of the first charge state. The number of data points is insufficient to resolve any inflection points that may occur on ion yields of the higher charge states.

Perry et al.⁶ give two other explanations for the inflection points on the curves of the ionization rates. One reason given is that there are hot spots in the beam, which have higher intensities than the average intensity. The ionization rate would saturate in the region of the hot spot at the saturation intensity and lead to the inflection point. The curve would continue to rise as the ionization is not saturated over the entire beam. Unlike inflection points due to the ionization process switching from direct to sequential, inflection points due to hot spots would be random, with no correlation to the saturation of the first charge state.

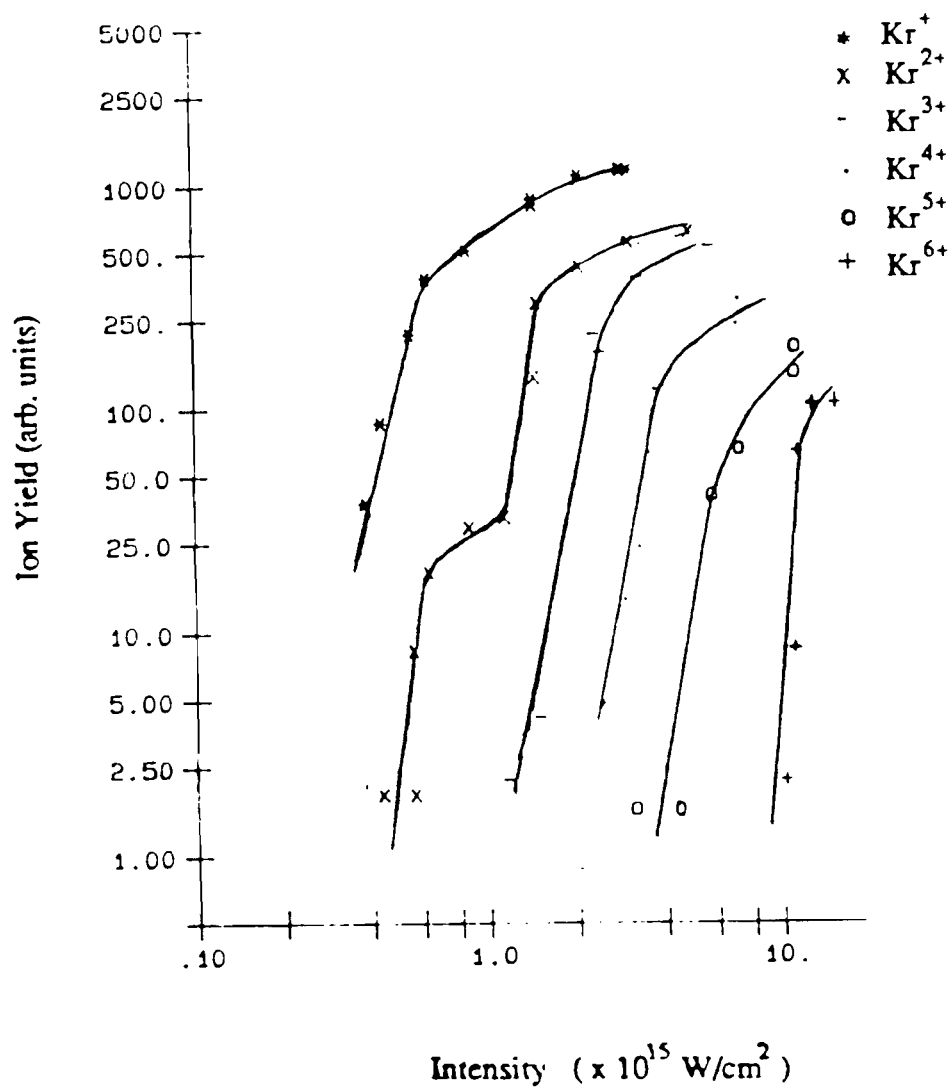


Figure 4 - 1. Ion yield curves of Kr with IR radiation. The data points are represented by best fit lines.

The second explanation is that of channel closing. Channel closing is a result of the intensity increasing to the point that the ponderomotive potential is increased by one photon of energy. The number of photons required for ionization would then increase by one causing the ionization rate to decrease. The ionization rate would increase again at the intensity where the $N + 1$ photon rate equaled the N photon rate. Fig. 4-2 shows the ionization rate of a xenon atom to the first charge state, determined by the Keldysh formula.^{7,8} The theoretical curve shows the inflection points due to channel closing, which are very small perturbations on the curve. The intensity width of the theoretical inflection points is smaller than the intensity fluctuations of the data so the effects of channel closing are too small to be detected in the data. The theory assumed a monochromatic field. For the case of broad bandwidths, the inflection points due to channel closing would be reduced because the channels would close at different intensities for the different wavelengths.

Inflection points occur in the first charge states in both the CPA experiments and the dye experiments of Perry and coworkers. The inflection points do not coincide in the two different experiments, indicating that they are most likely due to spatial inhomogeneities. Inflection points also occur in the CPA experiments because of detector noise, which was shown to be on the order of 2.5 units of the ion yield curves.

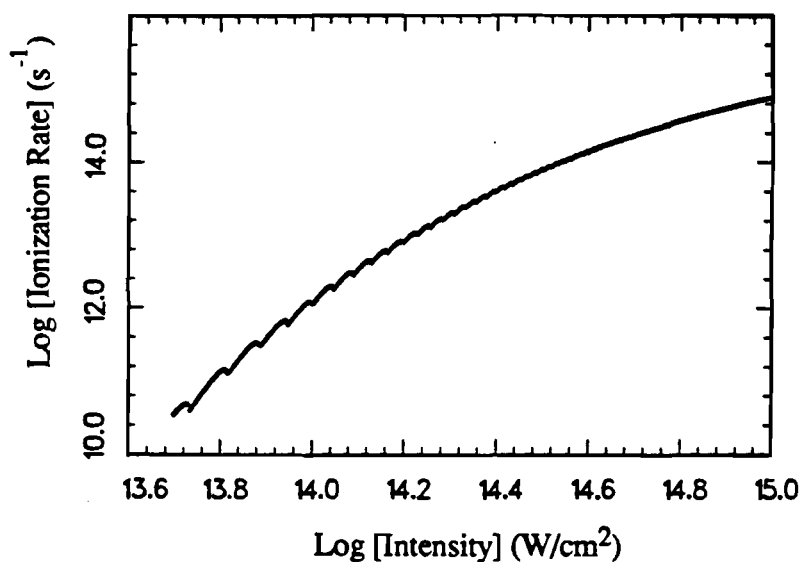


Figure 4 - 2. Ion yield of Xe^+ as a function of intensity determined by the Keldysh formula

The ion yields of xenon with the long 200 ps pulses given in Fig. 3-13 and the short 1 ps pulses given in Fig. 3-10a, show that the ionization process is independent of pulse duration if the bandwidth is the same. The first and second charge states occurred at the same intensities for the 1 and 200 ps pulses. The maximum intensity of the long pulses was less than the saturation intensity of the first charge state so that the saturation intensity could not be identified. The second charge state occurred due to direct ionization from the neutral atom just as it had with the short pulses at intensities less than the saturation intensity of the first charge state.

IV. B Z Dependence

One question that has long been debated in the field of multi-photon ionization, is the effect of the atomic structure and, in particular, the shell structure. Perry et al.⁶ showed that the threshold intensities of the charge states of Kr, Ar, and Xe appeared as a smooth function of the ionization potential up to the fourth ionization state. The CPA experiments showed that that the smooth dependence of the threshold intensities on the ionization potential is also valid up to the sixth charge state, for Ar and Kr, with 1.05 μm radiation. The appearance intensity of krypton and argon, as a function of ionization potential, assuming sequential ionization, is shown in Fig. 4-3. The charge states for both ions lie on the same curve indicating that the ionization process is more dependent on the ionization potential than the atomic weight or specific atomic structure. He, Ne and Xe cannot be compared with these ions because the ionization was measured under different conditions. The appearance intensity as defined here is the intensity at which a prescribed number of ions was created. The number was chosen to be above the noise level and well below saturation. The number is also below any inflection points due to the ionization process switching from direct to sequential. The intensities were measured from the ion yield curves shown in Fig. 3-10b and 3-10c.

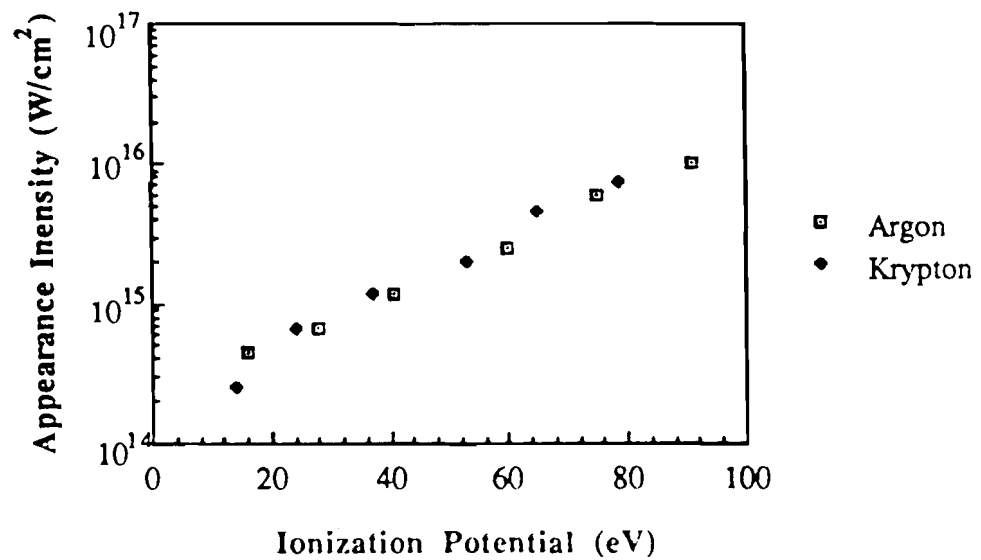


Figure 4 - 3. Appearance Intensity as a function of ionization potential of the charge state

Perry et al. considered that the smooth curve of appearance intensity as a function of ionization potential for the individual charge states was an indication that the ionization occurred as a sequential process. However, if the appearance intensity is plotted as function of the summation of the ionization potentials for the charge states of Kr and Ar, with 1.05 μm radiation, a smooth curve is also obtained. The plot of appearance intensities can therefore not rule out direct ionization in the IR. This plot for krypton and argon is shown in Fig. 4-4.

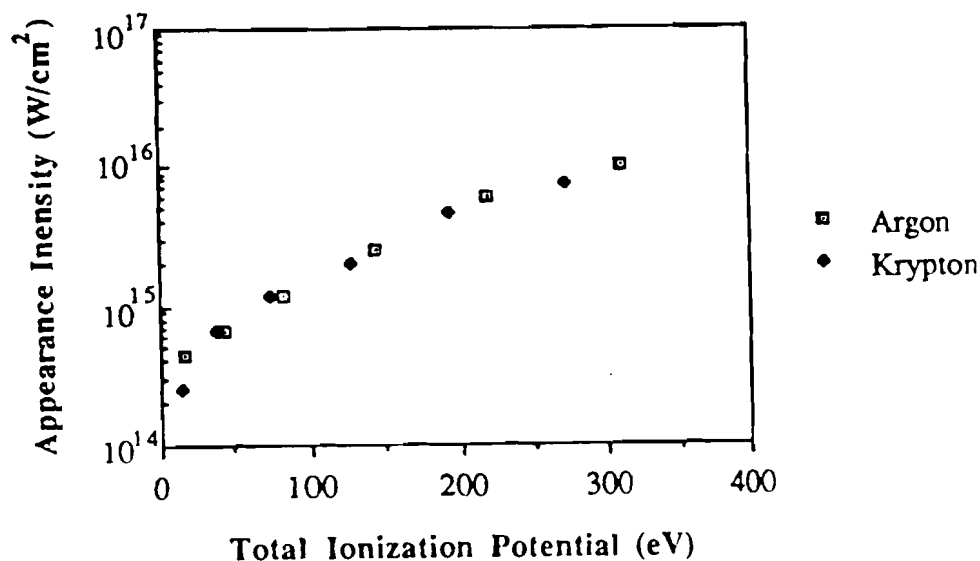


Figure 4 - 4. Plot of appearance intensities for Ar and Kr as a function of sum of ionization potentials

The effect of the shell structure can also be studied by comparing the maximum charge state that is created at the highest intensity. Charge states up to He^{2+} , Ne^{5+} , Ar^{8+} , Kr^{8+} , and Xe^{9+} were observed routinely for the highest intensity level of $\sim 3 \times 10^{16} \text{ W/cm}^2$, with the infra red radiation. These results are shown, as a function of total absorbed energy required to reach the charge state, in Fig. 4-5. These results can be compared to the maximum charge states for 193 nm radiation as measured by Luk et al.⁸ and the results at 248 nm as reported by Rhodes.⁹ The intensity levels and pulse durations are comparable for all three sets of experiments. At 193 nm He^{1+} , Ne^{2+} , Ar^{6+} , Kr^{6+} , and Xe^{8+} were observed whereas with 248 nm radiation, higher charge states of He^{2+} , Ne^{4+} , Ar^{8+} , Kr^{8+} , and Xe^{9+} were observed. The maximum charge state appears to be related to the ionization potential for the gases; Ar, Kr, and Xe. The minimum energy absorbed to overcome the ionization

202 eV, assuming sequential ionization, for xenon. A higher ionization potential would need to be reached to create the ninth charge state for argon or krypton. Shell structure does not seem to play a role in the ionization process. In the case of xenon, an inner 4d shell electron is removed where the final electron in the outer shell of neon is not. In all three experiments, the ionization rate of neon did not have the same dependence on the ionization potential as the three heavier atoms. Ionization to the sixth charge state requires the absorption of just 158 eV, which is less than the energy required to create Xe^{8+} , assuming sequential ionization.

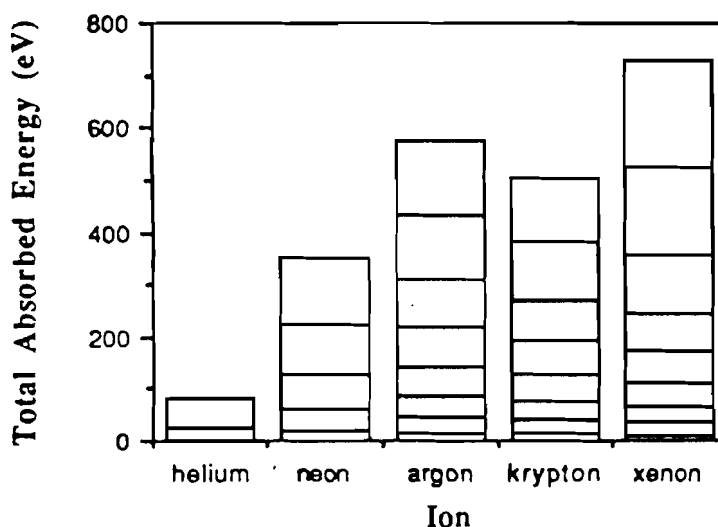


Figure 4 - 5. Maximum charge states observed at $6 \times 10^{16} \text{ W/cm}^2$ at $1.05 \mu\text{m}$ as a function of total absorbed energy

IV. C Wavelength Dependence

In the past, it was considered that atoms would be ionized easier with high energy photons, because fewer photons were required for ionization. Luk et al.⁹ compared the relative abundances of the Kr charge states at an intensity of

compared the relative abundances of the Kr charge states at an intensity of $\sim 10^{14}$ W/cm², that they measured at 193 nm with the 1.06 μ m results of the Saclay group.¹ The comparison showed that the abundance of the charge states fell more sharply for the infra red photons. The comparison does not take into account the fact that the measurements were taken under different experimental conditions. Not only the wavelength, but also the pulse duration was different. Since intensities cannot be determined to better than a factor of two and the ionization rates depend strongly on the intensity, a comparison of data taken under different conditions cannot be very accurate. A more accurate wavelength comparison can be made using green and infra red results taken with the CPA laser. A plot of appearance intensity for the first six charge states, as a function of ionization potential, for argon measured with the IR and green radiation is shown in Fig. 4-6, which shows that the lower charge state ionizes at a lower intensity for green, but the highest charge state ionizes at a lower threshold with the infra red radiation.

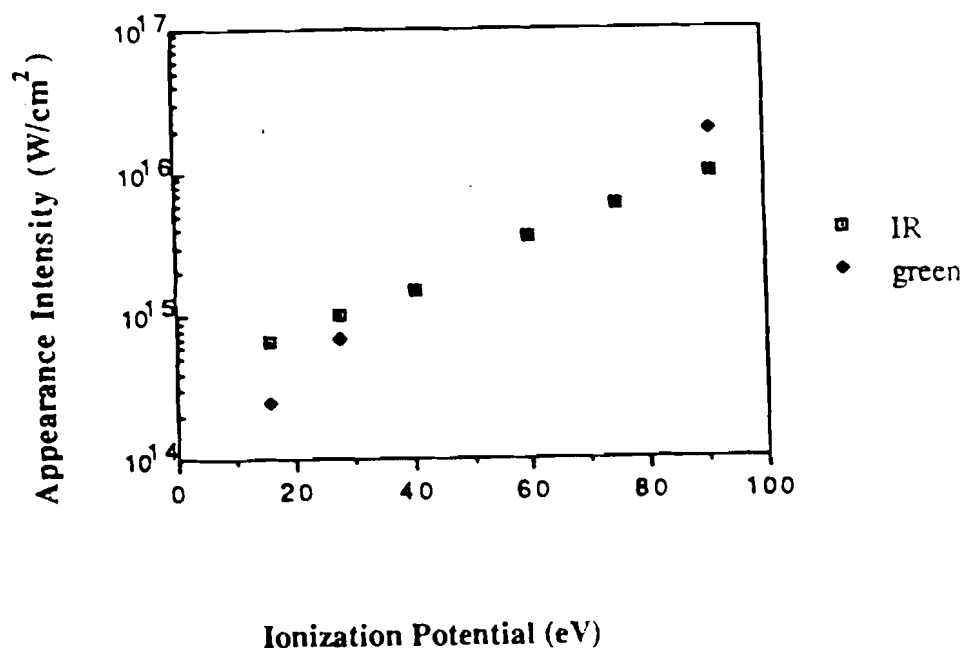


Figure 4 - 6. Plot of appearance intensity for Ar with green and IR radiation

At the lower intensities where the first charge states are generated, the ionization is most likely due to a multi-photon process. The ionization process will occur at a lower intensity for a lower nonlinear order and so green radiation will ionize the atom with less intensity than the IR. At the higher intensities the ponderomotive potential of the radiation field is much stronger than the binding energy of the atom and the ionization process is most likely due to a tunnelling effect. In the tunnelling regime, the time it takes the electron to tunnel out of the barrier is much shorter than the period of oscillation of the electric field. The ionization process is then independent of the frequency of the radiation in this regime. Figure 4-6 is an indication the the ionization process which creates the higher charge states is best described by a tunnelling theory

IV. D Comparison with Saclay Results

As was previously discussed in Chapters I and III, the Saclay group has extensively studied multi-photon multiple ionization of the noble gases, in the near IR at $1.06 \mu\text{m}$,¹ and at the second harmonic frequency^{2,3,4} with a Nd:glass laser system. There are two differences between the Saclay and CPA experiments. The Saclay experiments used 50 ps pulse durations at intensities between 10^{11} and 10^{15} W/cm^2 , whereas the CPA experiments were done with single picosecond pulses at intensities in the 10^{14} to 10^{17} W/cm^2 range. The main difference in the results is that the saturation intensities of the first charge states are much lower for the Saclay experiments. The Saclay saturation intensities are approximately three orders of magnitude lower for Xe and two orders of magnitude for He and Ne with the green radiation. With the IR radiation, the Saclay results show saturation intensities

approximately two orders of magnitude lower for the three heavier species. However, Ne and He exhibit saturation intensities just a factor of 5 lower than the CPA results. These results are given in Table 4-1.

Species	Saturation Intensities (W/cm ²)			
	1.053 μm		0.527 μm	
	CPA	Saclay	CPA	Saclay
Xenon	8×10^{14}	1.2×10^{13}	1×10^{15}	8×10^{11}
Krypton	8×10^{14}	2.5×10^{13}	2×10^{15}	
Argon	1×10^{15}	3×10^{13}	1×10^{15}	
Neon	2×10^{15}	4×10^{14}	4×10^{15}	1×10^{13}
Helium	3×10^{15}	6×10^{14}	3×10^{15}	2×10^{13}

Table 4 - 1. Comparison of the CPA and Saclay saturation intensities of the first charge states

As discussed in section IV. B, neon behaved differently than the three heavier noble gases. The highest charge state of neon, Ne^{5+} , had a much lower ionization potential than the highest created charge states of the heavier species, Ar^{8+} , Kr^{8+} and Xe^{8+} . The discrepancy in the CPA and Saclay results is again very different for the heavier and the lighter gases. The ionization rates are similar for the 50 ps transform limited pulses and the 1 ps pulses of the CPA laser only for the two lighter species, He and Ne. The large discrepancies in the saturation intensities of the heavier species

cannot be accounted for by experimental error and so the large bandwidth or short duration of the CPA pulses must have an effect on the ionization process for the heavier atoms.

In the Saclay experiments, direct ionization to the second charge state was observed in all five noble gases, but, there was no evidence of direct ionization to the third charge state from the first charge state in any of the gases. In the green experiments Xe^{2+} was generated by a combination of direct and sequential ionization, but, Ne^{2+} and He^{2+} were produced by sequential ionization. Ar and Kr were not studied with green radiation. There is agreement between the two experiments, on the ionization process to the second charge state only for He and Xe with green radiation. This is most likely due to the difference in pulse duration and bandwidth. The Saclay group showed that the appearance of the inflection point in Xe^{2+} with green radiation was a function of the pulse duration. The process continually changed from a direct to a sequential process as the duration increased from 5 to 200 ps. However, with the single picosecond pulses of the CPA laser, Xe^{2+} is a result of the combination of direct and sequential ionization. Also, the comparison with the 200 and 1 ps CPA pulses showed no difference in the ionization process with different pulse durations with the same bandwidth.

IV. E Comparison with Modified Keldysh Theory

Two approximate theories have been developed to treat high-order multi-photon ionization. Bebb and Gold¹¹ modified an ordinary perturbation theory in order to consider intermediate multi-photon resonances in a simple way. According to perturbation theory, the atom is ionized by the direct one-step absorption of N photons where $Nh\nu$ exceeds the ionization potential. Perturbation theory does not consider

separately the oscillatory motion of the electron due to the radiation field. At high field strengths and long wavelengths the energy due to the oscillatory motion can become comparable to the Coulomb field binding energy, and therefore may be useful to consider explicitly in treating the ionization process.

Keldysh proposed a theory which considered the final state of the electron to be a Volkov state, which is the state of a free electron in a radiation field.⁷ The ionization rate was determined by applying the Fermi golden rule, with the initial state the ground state of the atom and the final state a Volkov state. With these initial and final states, Fermi's golden rule gives the following ionization rate, W (s^{-1});

$$W = A \omega \left[\frac{V_{IP}(0)}{\hbar\omega} \right]^{3/2} \left[\frac{\gamma}{\sqrt{1+\gamma^2}} \right]^{5/2} S \left[\gamma, \frac{V_{IP}(\omega)}{\hbar\omega} \right] \\ \times \exp \left[-\frac{2 V_{IP}(\omega)}{\hbar\omega} \left[\sinh^{-1} \gamma - \gamma \frac{(1+\gamma^2)^{1/2}}{1+2\gamma^2} \right] \right], \quad (4-1)$$

where A is a numerical factor on the order of unity, which is assumed to account for the details of the atom, $V_{IP}(0)$ is the field-free ionization potential and

$$V_{IP}(\omega) = V_{IP}(0) + \frac{e^2 E^2}{4 m_e \omega^2}. \quad (4-2)$$

The second term in Eqn. 4-2 is the ponderomotive potential or the quiver energy due to the electric field, where ω is the frequency of the radiation, E is the applied electric field strength, and e and m_e are the charge and mass of the electron, respectively. The Keldysh tunnelling parameter, γ , is given by

$$\gamma = \omega \frac{\sqrt{2m_e V_{IP}(0)}}{eE}, \quad (4-3)$$

and S is given by the following:

$$S \left[\gamma, \frac{V_{IP}(\omega)}{\hbar\omega} \right] = \sum_{m=0}^{\infty} \left\{ \exp \left[\left[2 \left\langle \frac{V_{IP}(\omega)}{\hbar\omega} + 1 \right\rangle - \frac{V_{IP}(\omega)}{\hbar\omega} + m \right] \left[\sinh^{-1} \gamma - \frac{\gamma}{(1+\gamma^2)^{1/2}} \right] \right] \right\} \\ \times \Phi \left\{ \left[\frac{2\gamma}{(1+\gamma^2)^{1/2}} \left[\left\langle \frac{V_{IP}(\omega)}{\hbar\omega} + 1 \right\rangle - \frac{V_{IP}(\omega)}{\hbar\omega} + m \right] \right]^{1/2} \right\}, \quad (4-4)$$

where,

$$\Phi(x) = \int_0^x e^{t^2 - x^2} dt, \quad (4-5)$$

and $\langle x \rangle$ denotes the integer value and $\langle (V_{IP}(\omega) / \hbar\omega) + 1 \rangle$ is the minimum number of photons required to ionize the atom.

Keldysh showed that this formula for ionization probability would go to the perturbation result of multi-photon ionization in the limit of $\gamma \gg 1$ and in the opposite limit of $\gamma \ll 1$, the expression would give the result of tunnelling ionization. In the CPA experiments, the intensity ranged from 1×10^{14} to 6×10^{16} W/cm² and so the tunnelling parameter had a value that ranged from 1 to .03. At the high intensities the ionization process is in the tunnelling regime. In the tunnelling limit, the expression for S simplifies to;

$$S \left[\gamma, \frac{V_{IP}(\omega)}{h\omega} \right] = \frac{\sqrt{3\pi}}{4\gamma^2}, \quad (4-6)$$

and the ionization probability becomes;

$$W = \frac{\sqrt{6\pi}}{4} \frac{V_{IP}(0)}{\hbar} \left[\frac{eE\hbar}{m_e^{1/2} V_{IP}(0)^{3/2}} \right]^{1/2} \times \exp \left[\frac{4\sqrt{2m_e} V_{IP}(0)^{3/2}}{3eE\hbar} \left[1 - \frac{m_e \omega^2 V_{IP}(0)}{5e^2 E^2} \right] \right] \quad (4-7)$$

At present, modified Keldysh theories^{5,12} are the most widely accepted theories to describe MPI results. The Keldysh theory can be modified by adding a finite range potential, to account for the Coulomb field of the atom. The experimental results are compared to a theory, which has been modified by Szöke.⁵ Szöke modifies the Keldysh theory by approximating the Coulomb potential by the ionization potential. The potential is constant with respect to the electron position. The initial state is hydrogenic, with the appropriate ionization energy, but unmodified by the laser field. The model gives the following formula for the ionization rate,⁵

$$W = \sum_{n=n_0}^{\infty} \frac{32 \omega (n - n_b - n_{osc}) n_b^{5/2} n^2}{(n - n_{osc})^{1/2} (n + n_b - n_{osc})^4} \int_0^1 J_n^2 \left(n_f m, -\frac{n_{osc}}{2} \right) d\mu, \quad (4-8a)$$

where

$$n_b = \frac{V_{IP}(0)}{\hbar\omega}, \quad (4-8b)$$

$$n_{osc} = \frac{e^2 A^2}{4m_e c^2 \hbar\omega}, \quad (4-8c)$$

and

$$n_f = (8 (n - n_{osc}) n_{osc})^{1/2}, \quad (4 - 8d)$$

and

$$n_0 = n_b + n_{osc}. \quad (4 - 8e)$$

where A is the vector potential of the electric field and $J_n(a, b)$ is a modified Bessel function¹² and $d\mu$ is the differential solid angle, $d(\cos\theta)$. The individual terms give the expressions for the differential cross sections of absorption of N photons and emitting an electron in a given direction. Szöke's program integrates the rate equations over the solid angle to determine the different electron energies and then integrates over all the electron energies to give the total number of ions of each charge state. His model uses a Gaussian laser pulse shape.

The comparison of the experimental data and theory is shown in Fig. 4-7. The intensity of the experimental data had to be decreased by a factor of 10 to fit the saturation intensities with the theory for Xe^+ for both wavelengths and He^+ with green radiation and a factor of 40 to fit the theory for He^+ with the IR radiation. The discrepancy comes from the assumption that the potential is constant with respect to electron position, which is a good approximation in the ultra violet at moderate intensities, but breaks down for infra red and visible radiation at high field strengths.

The amplitude, r , of the oscillatory motion of an electron in an electro-magnetic field is given by;

$$r = \frac{e E}{m \omega^2}. \quad (4 - 9)$$

At an intensity of 10^{15} W/cm², the amplitude of the oscillations is ~ 4.8 and

~ 1.2 nm, at a wavelength of 1.05 and 0.53 μm , respectively. These amplitudes are much greater than the atomic radius. The electron will oscillate around the position that it left the atom, where the potential is given by the ionization potential. As the electron oscillates towards the ion, it will see a much stronger Coulomb potential than the ionization potential. Because of the approximation of a constant potential in Szöke's model, the theoretical ionization rate will be orders of magnitude higher than the actual ionization rate for 1.05 μm radiation. The increased ionization rate leads to a calculated threshold intensity many times smaller than the actual threshold.

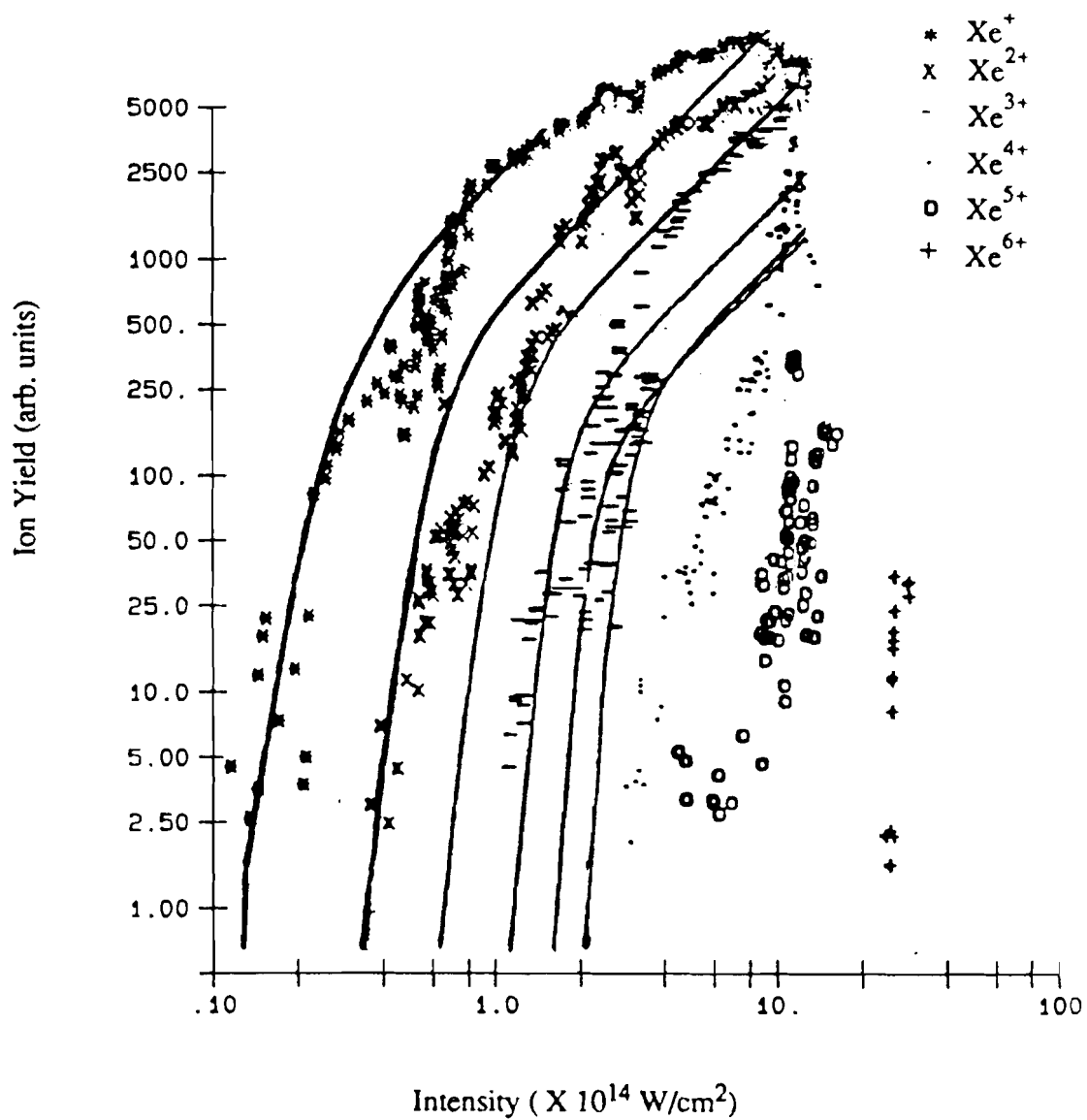


Figure 4 - 7a. Comparison of theoretical and experimental results for xenon with IR radiation. The experimental intensities have been reduced by a factor of 10 to fit the theory.

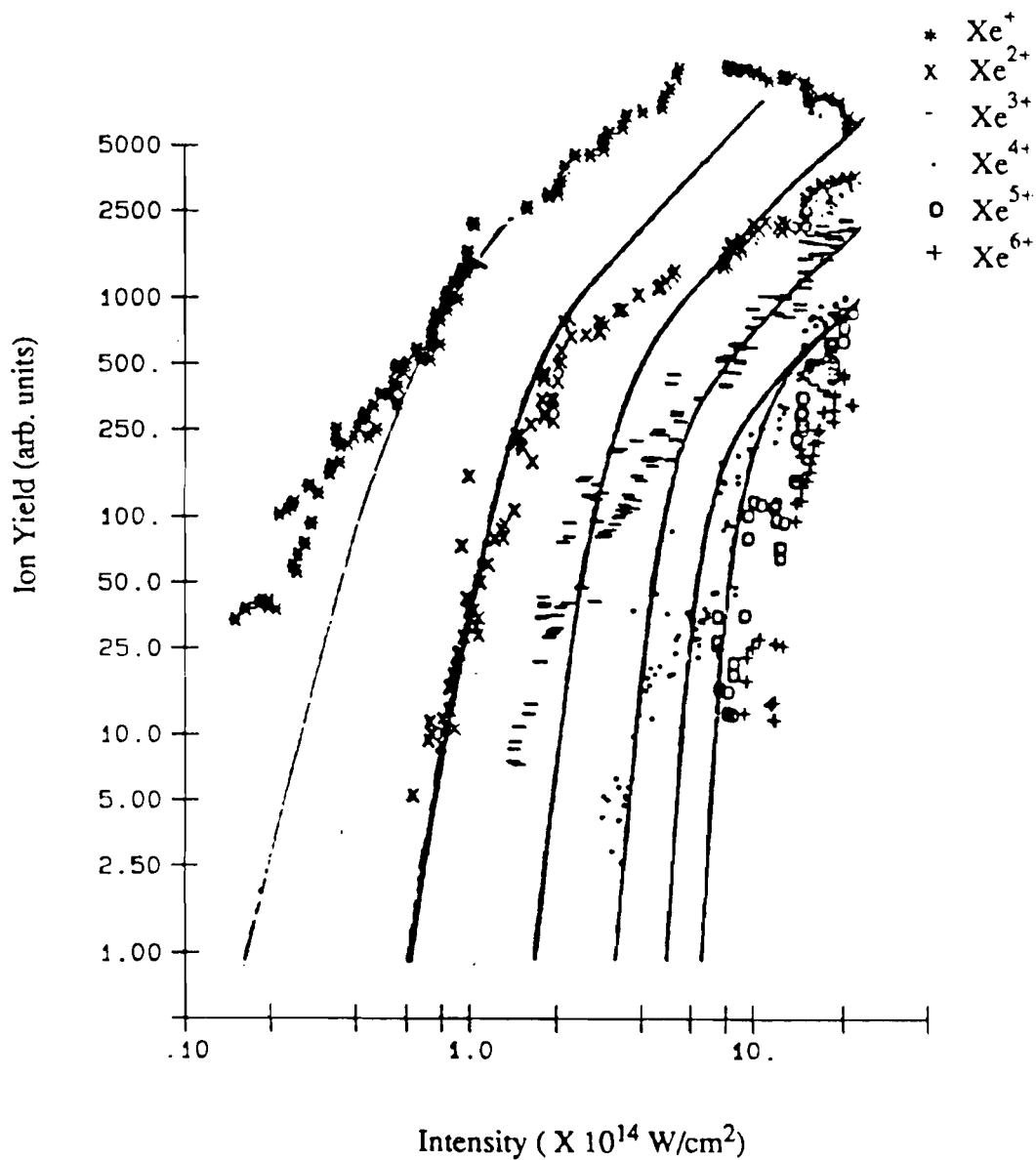


Figure 4 - 7b. Comparison of theoretical and experimental results for xenon with green radiation. The experimental intensities have been reduced by a factor of 10 to fit the theory.

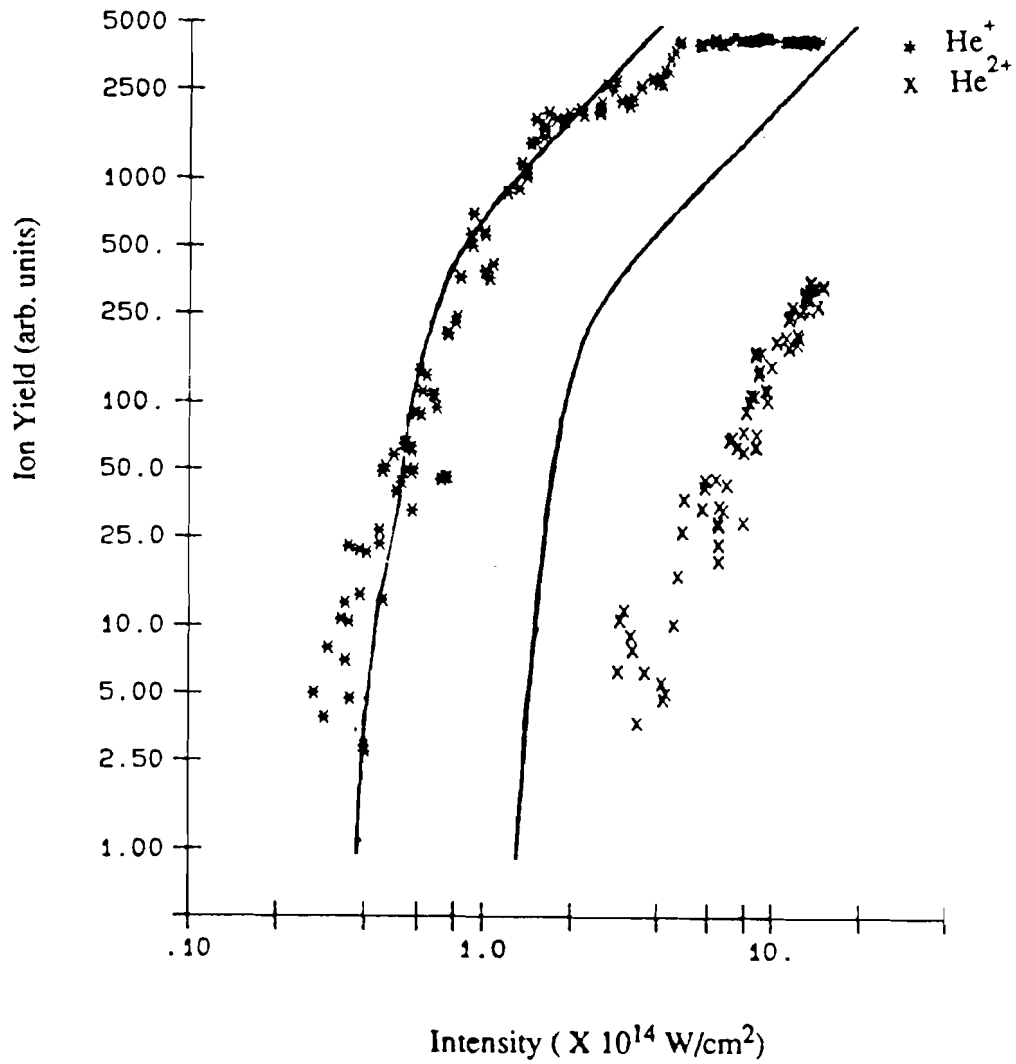


Figure 4 - 7c. Comparison of theoretical and experimental results for helium with IR radiation. The experimental intensities have been reduced by a factor of 10 to fit the theory.

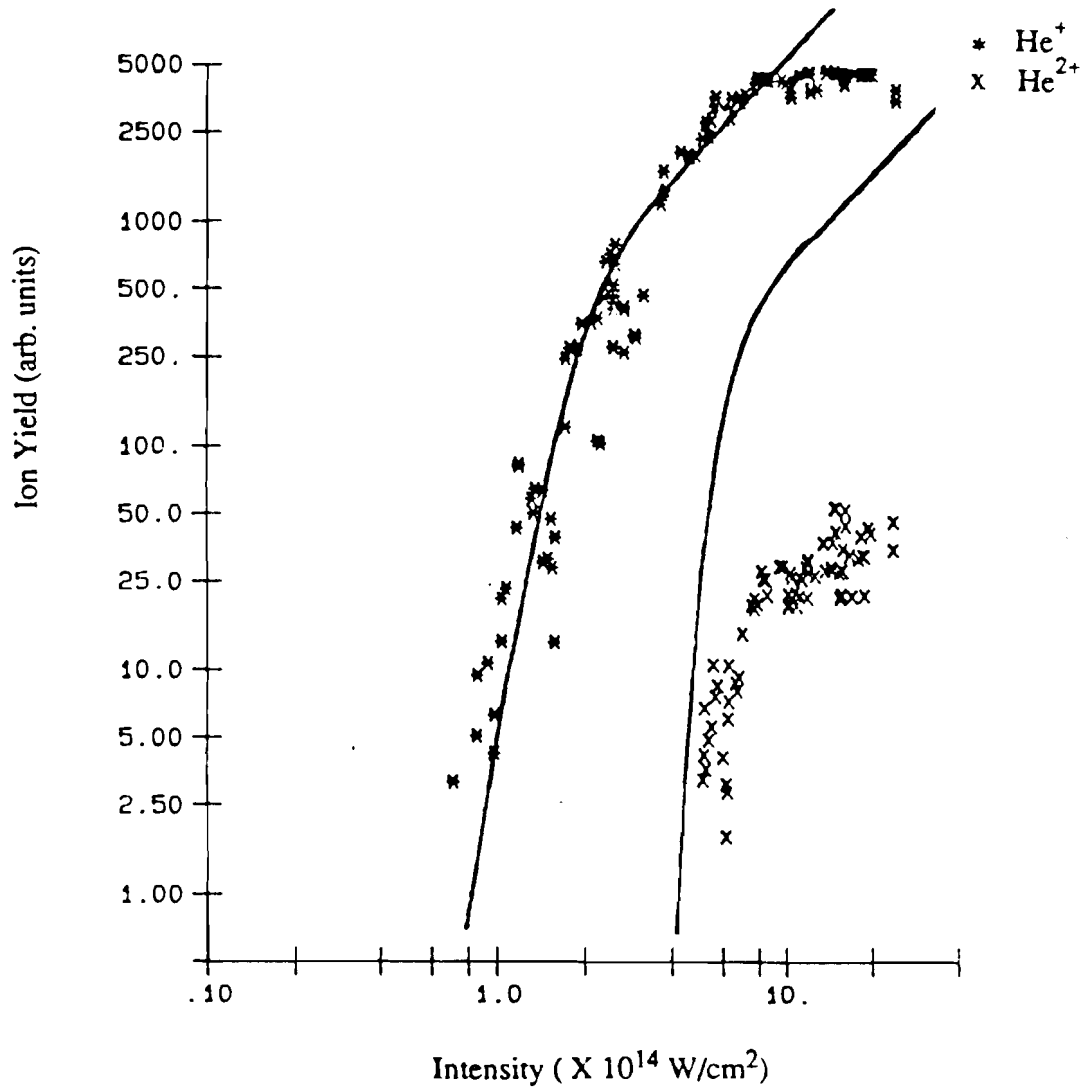


Figure 4 - 7d. Comparison of theoretical and experimental results for helium with green radiation. The experimental intensities have been reduced by a factor of 40 to fit the theory.

It can be seen from the comparison of the data with the theory, that Szöke's modified Keldysh⁵ theory does not accurately describe the ionization process in this wavelength range for short pulse, very intense laser pulses. Even if the intensity of the experimental results is decreased to match the theoretical saturation intensities of the first charge state, the theory fits only the two lowest charge states with any accuracy. The higher charge states deviate strongly.

Milonni has recently shown that the Keldysh approximation may not be valid under the condition of strong ionization.¹³ The Keldysh theory assumes that the probability of removing the electron from its initial state is small, which is not the case for very intense pulses. Javanainen and Eberly have solved for the electron wavefunctions of a model atom that is ionized by an intense field, by first principles.¹⁴ The ion yield is determined by solving the Schrödinger equation with a realistic quantum mechanical potential. Their numerical results also show a quantitative disagreement with the results calculated by the Keldysh approximation. New theories are needed to describe the ionization of an atom to high charge states by the interaction with very intense laser fields.

References

1. A L'Huillier, L A Lompré, G Mainfray and C Manus, J. Phys. B: At. Mol. Phys. 16, 1363 (1983)
2. A. L'Huillier, L. A. Lompré, G Mainfray and C Manus, Phys. Rev. A 27, 2503 (1983)
3. L. A. Lompré, a. L'Huillier, G. Mainfray and C. Manus, Phys. Lett. 112A, 319 (1985)
4. A. L'Huillier, L. A. Lompré, G Mainfray and C Manus, J. Physique 44, 1247 (1983)
5. Abraham Szöke, NATO Advanced Research Workshop, Sherbrooke, Ontario, Canada (1987)
6. M. D. Perry, O. D. Landen, A. Szoke, and E. M. Campbell, Phys. Rev. A 37, 747 (1987)
7. L. V. Keldysh, Sov. Phys.-JETP 20 , 1307 (1965)
8. The theoretical curve was calculated by Qi-chang Su.

9. T. S. Luk, U. Johann, H. Egger, H. Pummer, and C. K. Rhodes, Phys. Rev. A 32, 214 (1985)
10. Charles K. Rhodes, Physica Scripta. T17, 193 (1987)
11. H. Barry Bebb and Albert Gold, Phys. Rev. 143, 1 (1966)
12. Howard R. Reiss, Phys. Rev. AD 22, 1786 (1980)
13. P. W. Milonni, Submitted to Phys Rev. A
14. J Javainen and J H Eberly J. Phys. B: At. Mol. Opt. Phys. 21, L93 (1988)

CHAPTER V

CONCLUSIONS

V. A Summary

A novel laser technique has been investigated, which uses a pulse compression technique to achieve both short pulse durations and high energies. The CPA laser is an optical analog to chirped radar. Short pulses are stretched several times their original duration. The long pulses are amplified to the saturation level of the gain medium and then recompressed to their initial pulse widths. With this technique, high energy amplifiers can be used to efficiently amplify short pulses and create extremely high peak powers.

At present, the prototype system has been designed and constructed. The entire laser system sits on two 4x8 foot optical benches and produces picosecond pulses with energies of 0.5 J. A proposal has been put forth by LLNL, to scale a CPA laser to very large energies in the kJ regime. The power of the system would be in the petawatt regime, which to date has not been possible with conventional amplifying techniques. These ultra-high peak powers should open up new fields of study in such areas as positron production, multi-photon optics and plasma physics.

The prototype laser was used in these experiments to investigate multi-photon multiple ionization at intensities up to 10^{17} W/cm² in the near IR region of the spectrum. The experiments produced the highest charge state, Xe¹²⁺, observed to

date. The wavelength dependence was investigated by comparing the ionization at 1.05 μm and the second harmonic frequency. The CPA experiments resulted in consistently higher saturation intensities than the Saclay results taken at the same wavelengths, but with different pulse durations and bandwidths. The CPA experiments showed that the highest charge states are ionized at lower intensities with longer wavelengths. The CPA laser is an ideal laser to study the effects of pulse duration and bandwidth independently. An initial experiment to compare the ionization yields generated with the uncompressed and compressed pulses was performed. The result showed that the ionization process was independent of pulse duration if the bandwidth remained constant.

The multi-photon results were compared to a modified Keldysh theory. The experimental ion yields did not match the yields predicted by the theory. The experimental error cannot account for the entire discrepancy, indicating that new theories must be developed to explain the multi-photon ionization process at very high intensities.

V. B New Laser Developments

V. B. 1 Towards Shorter Pulse Durations

The bandwidth of Nd:glass is sufficient to support 100 fs pulse durations, but the pulse width cannot be reduced to much less than 1 ps in Nd:glass, because of gain narrowing. Chromium-doped solid state amplifying media, such as Alexandrite and titanium-sapphire have broader bandwidths than Nd:glass and still have the large saturation fluence level of $\sim 1 \text{ J/cm}^2$. Alexandrite has a gain bandwidth of 100 nm and titanium-sapphire lases between 700 and 1000 nm. These lasers can support pulse

durations as short as a few femtoseconds

Since a compression system is needed to produce the picosecond pulse duration for the Nd:glass system, the temporal profile will have a background pedestal due to the residual frequency chirp, which cannot be corrected by the grating compressor. In order to achieve a clean temporal profile, the short pulse will have to be produced directly from an oscillator. The short pulse can then be stretched by several orders of magnitude by a grating pair used in an antiparallel configuration, before being amplified in a solid state medium. Pessot and coworkers have constructed such a system.¹ They used a sub-picosecond dye laser to generate a ~ 270 fs seed pulse for an Alexandrite regenerative amplifier. The short dye pulses are stretched to 50 ps by two gratings that have 1800 1/mm grating constant separated by 140 cm. The long pulse is amplified to ~ 2 mJ at a 20 Hz repetition rate and then recompressed, to ~ 300 fs, by a pair of gratings used in a parallel configuration, with the same angle of incidence and spacing as the expander.

At present, in order to achieve pulse durations on the order of 10 fs, the dye pulses have to be shortened by fibre pulse compression. The amplification, of these short pulses in Alexandrite, and in the future titanium-sapphire, will be done in the same manner as the Nd:glass CPA system.

V. B. 2 Towards Petawatt Power Levels

The chirped pulse amplification technique will allow the generation of extremely high power levels. Nd:glass laser systems can presently produce energies at the kJ level. With the CPA technique, single picosecond pulses could be amplified to this energy, generating powers at the Petawatt (10^{15} W) level. Lawrence Livermore National Laboratory (LLNL) has proposed to build a Petawatt laser system using the

CPA technique. They plan to build a front end, which is basically the same as the TTT laser system developed at LLE. In the LLNL system, the pulse will be stretched to ~ 1 ns by the grating expander and a 25 mm amplifier will be added to bring the energy to 4 J. A series of 31.5 mm amplifiers will then be used to amplify the pulse to 2-3 kJ. The amplifiers chain has been designed to maintain the 4 nm bandwidth of injected chirped pulse and keep the beam quality to be better than four times diffraction limited.

The present limitation on the energy that can be achieved with the CPA technique is the damage threshold of the gratings. With the existing grating technology, very large gratings would be required to reach this energy and keep the fluence at the 20 mJ/cm^2 level. The technology of producing gratings with high damage thresholds of $\sim 1 \text{ J/cm}^2$ exists, but, at present these gratings do not have the required dispersion or high efficiency at the $1 \mu\text{m}$ wavelength. The LLNL proposal includes the development and demonstration of high-damage threshold transmission gratings. The laser intensity after the compression stage will be on the order of 0.05 TW/cm^2 over a beam diameter of 50-100 μm . Because of cost considerations, the compression system will have to be outside the vacuum chamber. The high power pulses then must propagate through the chamber window. The B integral for propagation through a 3 cm fused silica window was calculated to be 2.5, which is acceptable for maintaining a reasonable beam quality. In order to avoid further propagation through a nonlinear medium the beam will be focussed by reflecting optics. This laser system should be capable of generating focussed intensities of 10^{21} W/cm^2 , which corresponds to an electric field in excess of $100 e/a_0^2$.

A Petawatt laser system would open a new regime of physics that at present cannot be investigated. An intensity of 10^{21} W/cm^2 would yield a ponderomotive potential of 100 MeV, which would accelerate the electrons to ultra-relativistic speeds.

This laser will have many applications in various fields such as laser-atom interactions, x-ray lasers, nuclear and plasma physics.

V. C Future Multi-photon Experiments

The measurement of the ions only gives partial insight into the interaction of atoms with intense radiation. The interaction process also produces energetic electrons as well as short wavelength radiation. Much work has already been done on studying the electron spectra produced by Above Threshold Ionization, (ATI).^{2,3,4} In ATI processes, the electrons have energies corresponding to a multiple number of photons minus the ionization potential, such that the electron energy spectrum appears to be spikes separated by one photon in energy. The first electron peak corresponds to the energy of the minimum number of photons required to ionize. The electron spectra has clearly shown the process of channel closing. When the intensity is increased to the point that the ponderomotive potential equals one photon energy, the first ionization peak disappears.

Recently, very high order harmonic generation has been observed for the interaction of high density gas and 1.06 μm radiation, at intensities in the 10^{13} - 10^{14} W/cm^2 range.⁵ Harmonics were observed to the 33rd order, in this experiment, whereas only the seventeenth harmonic has been observed for UV fundamental wavelengths at an intensity of $\sim 10^{16}$ W/cm^2 ,⁶ indicating that the harmonic generation process is much stronger for long wavelength radiation. The Nd:glass CPA laser system is then an ideal source to study the harmonic generation process because it produces the long wavelengths at intensities that otherwise could not be achieved.

In the Saclay experiment, the intensity of the harmonic orders fell sharply from the third to the seventh order as expected, but, the ninth to the twenty-seventh order

had comparable conversion efficiencies, for argon gas. These results are still not understood, but, a connection to the ATI electron peaks is expected. Unfortunately, the harmonics are generated with such low efficiencies, they can only be measured for high densities, where the electron spectrum would be altered by space charge effects.

Also, harmonics were only observed for laser intensities sufficient to produce multi-photon ionization. The Saclay group could not observe harmonics with neon gas. Multi-photon ionization requires a laser intensity of 3×10^{14} W/cm², for neon atoms, which is above the maximum intensity used in the experiment. A CPA laser should then produce harmonics in neon. Harmonic generation experiments using the CPA laser system are planned for the future.

References

1. Maurice Pessot, Jeff Squier, Philippe Bado, and Gerard Mourou, to be published in IEEE J. Quantum Electron. June 1988
2. P. Agostini, F. Fabre, G. Mainfray, G. Petite, and N. K. Rahman, Phys. Rev. Lett. 42, 1127 (1979)
3. P. Kruit, J. Kimman, H. G. Muller, and M. J. van der Wiel, Phys Rev. A 28, 248 (1983)
4. T. J. McIlrath, P. H. Bucksbaum, R. R. Freeman, and M. Bashkansky, Phys Rev. A 35, 4611 (1987)
5. M Ferray, A L'Huillier, X F Li, L A Lompré, G Mainfray and C Manus, J. Phys. B: At Mol. Opt. Phys. 21, L31 (1988)
6. Charles K. Rhodes, Physica Scripta. T17, 193 (1987)

APPENDIX

It can be shown analytically, that the stored energy in an amplifier can only be efficiently extracted, if the input intensity is sufficient to completely saturate the gain. The complete analytical solution can be found in Lasers by Siegman.¹ The main equations will be given here. The rate equations governing the change in pulse intensity and population of the gain medium are as follows:

$$\frac{\partial I(z,t)}{\partial z} = \sigma N(z,t) I(z,t) \quad (\text{A - 1})$$

$$\frac{\partial N(z,t)}{\partial t} = - \left[\frac{\sigma}{h\nu} \right] N(z,t) I(z,t) \quad (\text{A - 2})$$

where $I(z,t)$ and $N(z,t)$ are the intensity and inversion, respectively, in a coordinate system that moves with the pulse. σ is the stimulated-transition cross section, h is Planck's constant, ν is the laser frequency. These equations assume that the lower lasing level decays in a time less than the pulse duration. If this is not the case, the right hand side of Eqn. A-2 is multiplied by 2.

The rate equations can be integrated to give the output intensity I_{out} as a function of the input intensity, I_{in} :

$$I_{\text{out}}(t) = I_{\text{in}}(t) \exp [\sigma N_{\text{Tot}}(t)] \equiv G(t) I_{\text{in}}(t), \quad (\text{A - 3})$$

where $G(t)$ is the time dependent gain and N_{Tot} is the population inversion integrated along the length of the gain medium. The initial gain, G_0 , is given by:

$$G_0 \equiv \exp[\sigma N_0], \quad (\text{A - 4})$$

where N_0 is the initial population inversion.

The input and output energy fluence, U_{in} and U_{out} , respectively, are determined by integrating the pulse intensities in time from the beginning of the pulse, t_0 , to a normalized time, t . A saturation fluence, U_{sat} can be defined as the input fluence required to reduce the initial inversion by half. The saturation fluence is given by :

$$U_{sat} \equiv \frac{h\nu}{\sigma}. \quad (\text{A - 5})$$

The input fluence can be written as a function of the saturation fluence and gain as:

$$U_{in}(t) = U_{sat} \ln \left[\frac{1 - 1/G_0}{1 - 1/G(t)} \right], \quad (\text{A - 6})$$

which for $G_0 \gg 1$, can be simplified to give:

$$U_{in}(t) = U_{sat} \ln \left[\frac{1}{1 - 1/G(t)} \right]. \quad (\text{A - 7})$$

The extracted energy fluence, U_{ext} , is the difference between the output and input fluence and can be determined by solving the preceding equations to give:

$$U_{\text{ext}} \equiv U_{\text{out}} - U_{\text{in}} = U_{\text{sat}} \ln \left[\frac{G_0}{G(t)} \right]. \quad (\text{A} - 8)$$

It can be seen from this equation that the extracted energy increases as the gain decreases to value of one. As $G(t) \rightarrow 1$:

$$G(t) = 1 + \epsilon(t) \quad (\text{A} - 9)$$

$$U_{\text{in}} = U_{\text{sat}} \ln \left[\frac{1}{\epsilon(t)} \right] \quad (\text{A} - 10)$$

where $\epsilon(t)$ is a number less than one. For an $\epsilon(t)$ value of 0.5,

$$U_{\text{in}} \sim U_{\text{sat}}. \quad (\text{A} - 11)$$

Therefore, the energy is only efficiently extracted for input fluence levels that are approximately equivalent to the saturation fluence.

References

1. Anthony E. Siegman, *Lasers*, (University Science Books, Mill Valley, California, 1986) pp. 362 - 373